Laser-Based Broad-Band Spatially Dense Automated Data Acquisition System

by

Monty Moshier

Thesis submitted to the Faculty of the
Virginia Polytechnic Institute and State University
in partial fulfillment of the requirements for the degree of

MASTER OF SCIENCE

in

Mechanical Engineering

APPROVED:

Robert L. West, Chairman

William R. Saunders

A. L. Wicks

LASER-BASED BROAD-BAND SPATIALLY DENSE AUTOMATED DATA ACQUISITION SYSTEM

by

Monty Moshier

Robert L. West, Chairman

Mechanical Engineering

(ABSTRACT)

The scanning laser Doppler vibrometer (SLDV) provides the capability necessary for collecting a broad-band spatially dense data set. A laser-based broad-band spatially dense automated data acquisition system is presented and verified. The motivation for such a system is to provide vibration data at many frequencies and spatial locations to allow a more complete dynamic characterization of a structure.

The acquisition system interfaces an SLDV to a frequency analyzer and a Silicon Graphics Crimson workstation. The system allows the user to specify the frequency range, scanning area, and spatial density. The system moves the laser beam, collects and downloads data for the specified area and spatial density. The system post-processes the data compensating the measurements for calibrations and then computes the complex-valued Frequency Response Function (FRF), and

coherence plots. The data acquisition system is used to collect FRF data for a beam hanging with simulated free-free boundary conditions. Examples of the FRFs are presented and the data verified by extracting the natural frequencies, damping, and mode shapes of the system.

The experimental natural frequencies were compared with those predicted by Euler-Bernoulli beam theory. The comparison yielded less than an 8% difference for the first seven transverse bending modes extracted. The mode shapes were compared by the Modal Assurance Criterion to show the orthogonality of the modes and a comparison with theory. In each of the cases above, the comparisons yielded results that indicated the modes were both orthogonal and close to theory. The overall conclusion based on the above verification was that the system can be used to collect spatially dense broad-band vibration data that can be used to characterize structures.

Dedicated To Kelly, Pierie, Kameron and Konner

Acknowledgments

A great philosopher said, when men are learned they think they are wise supposing they know for themselves, wherefore, their wisdom is foolishness and profit them not. As I have extended my studies and learned from those around me, I have realized how little wisdom I have and how much knowledge there is to be gained. Completing this degree has taught me many lessons, but most of all I have learned that it would not have been possible without the strength and wisdom of many.

I would like to thank those who gave me help and encouragement as I completed this degree. To begin, I would like to thank Professor West for helping me through this Masters and supporting me all the way to the hectic end. Thanks to Professor Saunders for his help and willingness to accommodate last minute changes. Thanks to Professor Wicks for his signal processing advice as well as ME4005 discussions. Thanks to Professor Burdisso for filling in at the last minute. Thanks to David Coe for his encouragement and help. I would also like to thank Jon and Marti Blotter for providing me with a place to stay and chauffeur service while my wife and mother-in-law moved our family to Indiana.

This degree as well as my bachelor's degree would never have been completed if it were not for family. Thanks to my parents and in-laws for the words of encouragement and financial support during rough times. A special thanks to my mother-in-law Bonnie Hart for helping us with a difficult move, a new baby, and this thesis. I especially want to thank my beautiful wife Kelly for taking care of the family and household responsibilities during my many hours of absence. Kelly's sincere support and encouragement kept me trying when I felt like giving up. I could not have done it with out her. I also want my children Pierie, Kameron, and Konner to know of my love for them and how much I appreciated their patience with me while completing this thesis.

Thanks in the end goes to my Heavenly Father for giving me the talents, strength and inspiration to have come this far in school.

CONTENTS

CHAPTER 1 INTRODUCTION **1**

1.1 DYNAMIC RESPONSE MEASUREMENTS 4

1.2 FREQUENCY DOMAIN TESTING 7

1.3 NEED STATEMENT 10

1.4 THESIS GOAL 11

1.5 HYPOTHESIS 12

1.6 OBJECTIVES 12

1.7 SCOPE OF THE THESIS 13

1.8 ORGANIZATION OF THESIS 14

CHAPTER 2 LITERATURE REVIEW **16**

2.1 SPATIALLY DENSE MEASUREMENTS 16

2.2 DATA ACQUISITION USING AN SLDV 18

2.3 LITERATURE REVIEW SUMMARY 22

CHAPTER 3 INSTRUMENTATION **24**

3.1 GPIB 25

3.2 SGI CRIMSON WORKSTATION/GPIB CONTROLLER 27

3.2.1 SGI WORKSTATION 27

3.2.2 GPIB CONTROLLER 28

3.3 DIGITAL TO ANALOG CONVERTER 29

3.4 SIGNAL ANALYZER AND SOURCE CONTROL 31

3.4.1 BASIC CONCEPTS IN SIGNAL PROCESSING 34

3.5 ADDITIONAL EQUIPMENT 37

3.6 BASIC CONNECTIONS 38

CHAPTER 4 SCANNING LASER DOPPLER VIBROMETER 39

4.1 FREQUENCY RESPONSE OF THE LASER 40

4.2 SIGNAL-TO-NOISE RATIO 46

4.2.1 AVERAGING 48

4.2.2 DYNAMIC RANGE 48

4.3 POSITIONING THE LASER BEAM 50

4.4 MEASUREMENT LOCATION 51

CHAPTER 5 EXPERIMENTAL SETUP & DATA ACQUISITION PROCESS 52

5.1 MARKING REGISTRATION POINTS 53

5.2 EXPERIMENTAL HARDWARE SETUP 55

5.3 REGISTRATION 56

5.4 SCAN AREA 60

5.5 ANALYZER SETUP 62

5.6 CREATING THE IBIC SCRIPT FILE 63

5.7 DATA ACQUISITION 66

5.8 POST PROCESSING 68

CHAPTER 6 RESULTS OF DATA ACQUISITION AND VALIDATION 71

6.1 FREQUENCY RESPONSE OF THE SLDV. 73

6.2 FRF AND COHERENCE PLOTS 79

6.3 BASIC CONCEPTS OF MODAL ANALYSIS 82

6.4 RESULTS OF MODAL EXTRACTION 92

6.5 SPATIAL ALIASING 99

CHAPTER 7 CONCLUSIONS 102

7.1 RESEARCH SUMMARY 102

7.2 SUMMARY OF CONCLUSIONS 104

7.3 RECOMMENDATIONS 107

REFERENCES 109

APPENDIX A PROGRAM CODE 111

APPENDIX B USERS MANUAL 129

VITA 134

List Of Figures

FIGURE 3-1 INSTRUMENTATION OF THE DATA ACQUISITION SYSTEM. 25

FIGURE 3-2 INPUT/OUTPUT RELATIONSHIP OF A TYPICAL TIME DOMAIN SIGNAL.....35

FIGURE 4-1 EXAMPLE OF THE FREQUENCY RESPONSE OF THE LASER.....43

FIGURE 4-2 EXAMPLE OF FILE "FILTFRF".....44

FIGURE 5-1 EXPERIMENTAL AND DATA ACQUISITION PROCESS DIAGRAM. 52

FIGURE 5-2 LAY OUT COORDINATE SYSTEM AND MARK SPECIFIC REGISTRATION POINTS. .53

FIGURE 5-3 LOCATION OF REGISTRATION POINTS.....54

FIGURE 5-4 EXPERIMENTAL SETUP.....55

FIGURE 5-5 REGISTRATION PROCESS. 57

FIGURE 5-6 REGISTRATION POINTS.....58

FIGURE 5-7 REGISTRATION FILE BEAM.MEAS. 59

FIGURE 5-8 DEFINING THE SCAN AREA. 60

FIGURE 5-9 DEFINITION OF THE SCAN AREA.....61

FIGURE 5-10 ENTER ANALYZER FUNCTIONS. 62

FIGURE 5-11 IBIC SCRIPT FILE CREATION. 64

FIGURE 5-12 DATA ACQUISITION PROCESS. 66

FIGURE 5-13 POST PROCESSING OF RAW FREQUENCY DATA. 68

FIGURE 6-1 EXPERIMENTAL SETUP.....72

FIGURE 6-2 FREQUENCY RESPONSE OF THE LASER. 75

FIGURE 6-3 VARIANCE OF THE RESIDUALS PLOTTED 76

FIGURE 6-4 FOURTH ORDER POLYNOMIAL FIT COMPARED WITH ACTUAL. 77

FIGURE 6-5 COMPARISON OF AN UNCORRECTED AND A CORRECTED FRF 78

FIGURE 6-6 FRF WITH GOOD COHERENCE. 80

FIGURE 6-7 FRF WITH POOR COHERENCE. 81

FIGURE 6-8 COMPARISON OF THE MEASURED AND SIMULATED FRFS FOR LOCATION 2. 89

FIGURE 6-9 PLOT OF FRF AND COHERENCE FOR LOCATION 2 90

FIGURE 6-10 COMPARISON OF MEASURED AND SIMULATED FRFS FOR LOCATION 31. 91

FIGURE 6-11 PLOT OF FRF AND COHERENCE FOR LOCATION 31 92

FIGURE 6-12 FIRST FOUR EXTRACTED MODE SHAPES. 94

FIGURE 6-13 BEAM SAMPLING POINTS. 99

FIGURE 6-14 DEMONSTRATION OF SPATIAL ALIASING. 101

LIST OF TABLES

TABLE 4-1 BASIC PROCEDURE FOR DETERMINING THE FRF OF THE SLDV. 45

TABLE 6-1 NATURAL FREQUENCIES AND DAMPING.....93

TABLE 6-2 MAC TABLE COMPARING ORTHOGONALITY OF EXTRACTED MODES. 97

TABLE 6-3 MAC TABLE COMPARING EXPERIMENTAL MODES WITH THEORETICAL.....97

Chapter 1
Introduction

Insight and invention clearly play a paramount role in the development of new machines and structures. These mechanical systems are often built on intuition and a trial and error process. However, as these systems fail or do not perform to expectation, knowledge is gained as well as experience to further refine their development. The acquisition and use of experimental data become an important element adding to our understanding of the behavior and the development of mechanical systems.

It has long been realized that experimental data can be used to update analytical models, characterize the dynamic behavior of a structure, or as a diagnostic tool. Each of these purposes requires varied amounts of data at different locations in the structure over a range of operating frequencies. A broad-band spatially dense data set can be used in each technique. Spatially dense data refers to data that is collected at locations more numerous than practically possible with

accelerometers and which can have thousands of spatial locations, providing a better spatial representation of the structure. Since a broad-band spatially dense data set contains both spatially dense and broad-band frequency information, it provides the foundation for a more complete investigation into the behavior of dynamic systems. The different areas of investigation and the usefulness of broad-band spatially dense data are described below.

Experimentally updated models incorporate information from actual tests in an effort to develop high fidelity models of real systems. Finite element models typically use thousands of nodes to describe a structure. Because finite element models are spatial models, spatially dense experimental data can provide the information needed for developing a better model.

Experimental data can also be used for creating an experimentally derived model. Typically the experimentally derived dynamics models are characterized by modal parameters. The three modal parameters which can be determined from experimental data are natural frequency, damping, and mode shape. These parameters are estimated from data acquired by making a number of measurements at a finite number of spatial locations over a structure. The location and quality of the data acquired at these spatial locations on the structure determine the quality of the estimated modal parameters. If measurements are made at nodal lines, locations of zero response, or the number of measurements is insufficient to

describe the spatial response, data necessary to characterize the structure is missed, and therefore spatial aliasing can occur. Optimizing the number and location of response measurements, to avoid missing response data, is an ongoing area of research and concern. An alternate solution is to make spatially dense measurements over the area of interest on the structure such that the spatial response measurements are adequate to support analyses.

Experimental techniques are also used as diagnostic tools. Currently, single and broad-band frequency inputs are used to excite the structure. The hope is that the structure response can be determined by making measurements at select locations at specific frequencies or over a range of frequencies. Experimental work of this type is a highly refined skill that requires the knowledge of an experienced engineer to make the appropriate measurements at the right locations.

The ability to make broad-band spatially dense measurements provides a tool to acquire data which will allow the investigation of both the spatial and frequency dependent nature of the structure under test.

Whether experimental measurements are used as a diagnostic tool or for updating or creating models, spatially dense measurements provide data for use in understanding the spatial nature of the dynamic system. The practical limitations in making spatially dense vibration measurements on vibrating structures are associated with the transducers themselves. Two transducers that are typically

used for making such vibration measurements are the accelerometer and the scanning laser Doppler vibrometer.

1.1 Dynamic Response Measurements

Typically, modal analysis procedures use accelerometers to collect vibration data. Accelerometers are placed directly on the structure and are used to sense structural accelerations due to excitations. Typical accelerometer measurements are made at spatial resolution of 125 mm or more apart in order to minimize the number of data points and reduce the time of data acquisition, yet obtain some spatial resolution.[1] Whether or not the measurements are used for diagnosing problems or model updating, the number of points is limited by time and equipment required to make measurements. Structural responses are measured in two different ways: point by point using one accelerometer, or using a large number of accelerometers to measure the structure response at all locations simultaneously. Each of the methods has its disadvantages. When using a single accelerometer it is very time consuming to change the experimental setup for each location. On the other hand, using multiple accelerometers requires more equipment setup, as well as more time for completing calibration and checkout of

the system. Both methods described above add mass to the structure possibly changing the structure behavior by modifying the structure's mass and stiffness. It is easy to see why using accelerometers for making hundreds of measurements has disadvantages. This is why a great deal of research has been applied to efficiently making a few measurements. Another relatively new transducer available for making vibration measurements is the scanning laser Doppler vibrometer (SLDV). The scanning feature of the SLDV makes it practical to make spatially dense measurements. A scanning laser Doppler vibrometer (SLDV) senses velocity along the line of sight of the laser beam. Mirrors are used to deflect the laser beam to each location for measurement on the structure. The mirrors make it possible to easily and quickly position the laser beam. Point to point measurements using the SLDV can be .15 mm apart with a practical point to point spatial measurement ratio of the SLDV compared to the accelerometer being 830:1.[1] The time required for collection of data at a single point is no different from the SLDV than it is for the accelerometer. The time savings is directly related to the ease and speed of deflecting the SLDV laser beam and the calibration and setup of a single transducer. Additionally, the SLDV provides the capability of a non-contact test. Non-contact testing eliminates the mass loading of the transducer and possible localized stiffness change that is introduced when using an accelerometer.

Three issues associated with the use of SLDV that must be dealt with are the signal-to-noise ratio of the SLDV, the ability to place the measurements on the structure, and the frequency response of the SLDV.

Because the SLDV is a relatively new transducer and does not make measurements by direct contact, the signal-to-noise ratio is approximately one-tenth that of the accelerometer. This signal-to-noise ratio must be considered when the tests are being designed. Typically the SLDV is less able to detect small responses than the more developed accelerometer. This limitation is associated with the development of the laser and the physics associated with the measurement. The laser has had much less time to evolve into a measuring device than the accelerometer. Also, the acceleration measured with the accelerometer is greater than the velocity measured with the SLDV by a factor of ω, as is shown in Eq. 1-1.

$$\begin{aligned} \dot{x} &= j\omega e^{j\omega t} \\ \ddot{x} &= -\omega^2 e^{j\omega t} \\ \dot{x} j\omega &= \ddot{x} \end{aligned} \tag{1-1}$$

Thus the response measured by the accelerometer is larger and more likely measurable than the response measured using the SLDV. In addition, because the demodulation process used to determine the velocity involves filtering, a

frequency dependent phase shift can be introduced. The phase shift and amplitude attenuation can be compensated for by calibrating the laser's output to an accepted reference.

Associated with any non-contact test is the need to place the location of the measurements back on the structure. When a structure is scanned, the measurement coordinates on the structure are unknown and must be determined from the relative position and orientation of the laser relative to the structure and mirror angles. The advantage of using an SLDV instead of an accelerometer is typically decided upon when the benefits of a non-contacting transducer and/or spatially dense measurements outweigh the problems associated with the signal to noise ratio, the frequency response of the SLDV and the effort required to place measurements back on the structure.

1.2 Frequency Domain Testing

Besides understanding a system spatially, it is often important to understand dynamic systems over a range of frequencies. In real world applications mechanical systems and structures are rarely excited by single frequency sources. Mechanical systems and structures are most often exposed to excitation with

multiple frequencies or over a range of frequencies. When structures are excited near natural frequencies they experience large amplitude vibrations. Knowing the natural frequencies and the modes of vibration of a system is an important representation of the dynamic behavior. Because a system contains an infinite number of natural frequencies and modes, it is necessary to understand mechanical systems at multiple frequencies or over broad ranges of frequencies. Understanding mechanical systems over ranges of frequencies provides insight into the system behavior that can be missed if only single frequency measurements are made.

In order to determine dynamic behavior, structure responses are acquired by measuring the responses to known inputs. There are several different types of inputs that can be used to test structures. These tests can be broken down into three basic types of tests. The first test is referred to as a sine-dwell test. The sine-dwell test uses a single frequency input to excite the structure. Measurements are usually done with the single frequency set close to a natural frequency. The other two tests are aimed at getting information over a range of frequencies. The stepped sine-dwell test is basically the sine-dwell test performed over a range of frequencies starting at the lower frequency bound and indexing a set frequency increment, stopping at the upper frequency bound. The third test involves exciting the structure with a source that provides all the frequencies at once. Some of the

sources that are available for this type of test include random, burst random, periodic chirp, and burst chirp signals.

Sine-dwell and broad-band tests each have their advantages and disadvantages. Sine-dwell tests provide a quick method for collecting data at specific frequencies. Stepped sine-dwell tests provide a method for making a set of measurements at specified frequencies and frequency density. However, as the number of frequencies increases, the data collection process becomes very time consuming. Time is required to change frequencies as well as to allow the structure to reach steady state. Broad-band testing provides a method for inputting a range of frequencies into a structure simultaneously. Using this method provides information on vibration behavior across a frequency range. However, the frequency information available over this range depends on the ability to get sufficient energy into the structure over the frequency range of interest as well as the frequency analyzer's resolution capabilities. Typically, frequency analyzers provide 400 spectral lines of information. Whether a large or narrow frequency range is investigated, data collection is limited to 400 spectral lines. The frequency resolution is determined by taking the frequency range and dividing it by the 400 spectral lines. If the range of the frequency investigated is large, the spectral lines will be widely spaced leading to lower frequency resolution. When small ranges of frequency are investigated the frequency resolution is high; however, the time to

acquire the data is increased since the collection time for one block of data is the inverse of the frequency resolution. Thus the excitation of choice depends on the vibration information that is needed.

1.3 Need Statement

One paradigm for structural analysis builds from the idea that having frequency information over certain spatial locations is sufficient for characterizing structures. This idea works well as long as the investigator knows where to measure and how many locations are needed to correctly describe the system. This requires the investigator to know a great deal about the structure. Without this knowledge it is likely that data critical to the model will be missed or the quality of the data will be compromised.

Another paradigm spatially describes structures at a few frequencies. This method works as long as the investigator knows what frequencies to investigate. Without knowing which frequencies are important, making spatial measurements can only give information that is incomplete. Important resonances might therefore be missed or may not necessarily be usable. Fortunately, in most cases it is relatively easy to obtain the frequencies of interest.

Making high spatial density measurements over a broad range of frequencies addresses the concerns associated with each of the above-mentioned methods. As previously discussed, spatially dense measurements at more than just one frequency are useful for providing a more complete dynamic characterization of a structure. This premise provides the foundation for realizing the need for a broad-band high spatial density measuring capability. Combining these capabilities into one test will provide both spatial and frequency dense information at the same time leading to a better characterization of the structure's response.

1.4 Thesis Goal

A data acquisition system capable of broad-band spatially dense measurements is to be developed using the SLDV and a signal analyzer. The system will scan rectangular cross sections collecting data at a user-specified grid density. Frequency response function (mobility function) data are acquired and downloaded to a computer for post-processing and viewing. Corrections to the laser scan angle, measurement locations, and placing the measurements on the structure are accomplished by incorporating previously coded algorithms. Frequency response corrections of the laser are characterized and corrected.

It is the goal of this thesis to develop the test capability of measuring spatially dense broad-band frequency data by exploiting the high spatial density measuring capabilities of the SLDV.

1.5 Hypothesis

Spatially dense vibration response measurement data over a broad-band of frequencies is useful for gaining an understanding of the dynamic behavior of mechanical systems. High spatial density vibration response data over a broad-band of frequencies can be acquired using the SLDV and instrumentation capable of providing a excitation source and signal processing of two input (reference and response) channels. The SLDV and a dynamic signal analyzer can be interfaced, providing an automated vibration response data acquisition system.

1.6 Objectives

The research objectives for supporting the research goal and hypothesis of this thesis are generalized in the following key steps:

- Characterize the frequency response of the laser and use the characterization to compensate for phase shift and amplitude attenuation of the SLDV.
- Locate the laser measurements in the structure coordinate system.
- Develop a program to control the position of the laser.
- Develop a program to setup and control an HP 35665A analyzer.
- Develop a programming sequence to interface the SLDV, the frequency analyzer, and a Silicon Graphics Crimson workstation.
- Post process the raw data from the FFT analyzer, correcting the data for laser beam deflection angle, phase shift, and calibration constants.
- Create Mobility FRFs for plotting and FRF data for implementation into a FRF curve fitting routine.
- Set up an experiment to collect FRF data.
- Demonstrate the developed capability by collecting FRF data and curve fit the data to extract, natural frequencies, damping and mode shapes.

1.7 Scope of the Thesis

A scanning laser Doppler vibrometer is used to develop a data acquisition system to allow collection of spatially dense data over a broad range of

frequencies. The raw frequency data will be downloaded to a computer and saved for post processing. Post processing of the raw data will include angle corrections, laser frequency response correction, and calibration constants. Additionally, the location of the measurement points will be placed in the structure coordinate system. Mobility, phase, and coherence plots will be created from the downloaded data as well as the post processed data prepared for implementation into an FRF curve fitting routine. The data acquisition system development will be limited to rectangular areas. Using periodic chirp as the excitation source, FRF data will be collected for a bungee cord/beam setup simulating a free-free boundary condition. Natural frequencies, damping, and mode shapes will be extracted using a FRF curve fitting routine.

1.8 Organization of Thesis

This thesis describes an effort to exploit the advantages of making spatially dense broad-band frequency measurements and a data acquisition program for completing such tests. Chapter 2 reviews some of the current methods used for making measurements with the SLDV. Chapter 3 introduces the instrumentation required for developing the data acquisition system. Chapter 4 introduces the

SLDV and how it can be used to practically acquire spatially dense measurements over a broad range of frequencies. Chapter 5 presents the experimental setup and data acquisition process. With the data acquisition system, data from a free-free beam test are acquired and the resulting mobility, phase, and coherence plots are presented in Chapter 6. Chapter 6 also includes results from the FRF curve fitting routine as well as the extracted natural frequencies, damping, and mode shapes. Chapter 7 discusses the conclusions that are reached through the development and implementation of a spatially dense broad-band frequency acquisition system.

Chapter 2
Literature Review

The primary emphasis of this literature review is to identify work already completed in the area of broad-band spatially dense data as well as identify some of the uses for spatially dense measurements and techniques for acquiring spatially dense data over broad frequency ranges.

2.1 Spatially Dense Measurements

Spatially dense measurements acquired using the SLDV have advantages. The SLDV can be used to practically measure responses at many spatial locations and can be done without mass loading the structure. Wicks, Kochersberger, and Mitchell[1] highlight these advantages the laser has over accelerometers. Additionally they speculate the usefulness of spatially dense measurements for

updating finite element models. Agee, Kelly, and Mitchell[2] present information for updating finite element models of a reciprocating compressor. The paper notes the time, 3-5 days, for obtaining 65-100 points of experimental data using accelerometers. The resulting data still has relatively low spatial resolution. The possibility of spatial aliasing is great since the finite element model has 3000-5000 spatial degrees of freedom and the data collected using the accelerometer only represents a few spatial degrees of freedom. Using the SLDV and single frequency inputs, over 100,000 mobility data points were made on the compressor. The results demonstrated the usefulness of the resulting images from spatially dense measurements to correlate the mode shapes of the finite element model. This paper demonstrates the usefulness the SLDV has for measuring structure responses. The SLDV has promise for use in structure characterizations, both for verifying and updating finite element models as well as providing spatially dense response data that can be used to better describe structures spatially.

Sririam, Hanagud, and Craig[3] present an experimental method using the laser and a frequency analyzer to measure the second mode shape of a light-weight cantilever beam. The paper notes the advantages of the non-contact measurement and spatially-dense measuring capability of the laser. The non-contact measurement eliminates mass loading of the structure caused by the use of accelerometers. Additionally, because the laser beam can be quickly and easily

positioned for multiple response measurements it is now practical for spatially dense measurements. Results of tests on the lightweight cantilever beam showed good correlation between beam theory and the experimental data collected using a laser. This paper concludes that the SLDV provides a good tool for making non-contact measurements at multiple points. The paper also notes the need for further testing of the laser's capabilities and the development needed to further exploit the full benefits of the laser.

2.2 Data Acquisition Using an SLDV

Mitchell, Kochersberger, and West[4] detailed the process of using the SLDV for measuring one dimensional mobility. Angle corrections, phase shift corrections, and errors associated with in-plane measurements were investigated. The presentation shows how error due to in-plane motion can result in as much as a 20 percent error in the out-of-plane measurements. The percent error in the out-of-plane velocity when in-plane velocities are negligible and angle corrections are not applied is less than five percent for the plus or minus 12.5 degree angle range of the laser mirrors. It is also noted that when FRF data is taken and referenced to

another transducer, the frequency response characteristics of the laser must be corrected or erroneous FRF data is measured.

The work above shows that the laser can be used to collect one dimensional mobilities. However, caution needs to be exercised when using the SLDV for this purpose. In order to obtain accurate mobility plots angle corrections and the frequency response of the laser need to be included.

Kochersberger[5] demonstrates a method for determining modal residues. The procedure involves accurately measuring a structure FRF at one location using step-sine excitation. The global parameters of the structure are then extracted from this FRF. The structural responses are scanned by using the SLDV at the frequencies determined with the initial FRF. Time savings results from eliminating the need to measure entire FRFs at each structural point. Instead, the measurement procedure is done at only selected frequencies.

The procedure above assumed that the mode shapes were well separated and that frequencies of the system were well known. This approach expanded the one dimensional mobility work of Mitchell et. al.[4] by combining several single frequencies to obtain an FRF with less than sixteen specific frequencies and thousands of spatial points. This approach is very effective for spatial modal analysis for structures with well separated modes. This method will have to be developed further to accommodate structures with high modal density.

Mitchell, Agee, West and Wicks[6] present the development of a laser-based data acquisition system to acquire mobility data. The acquisition system is developed around the Ometron[a] SLDV, Zonic System 7000[b], and I-DEAS[c] modeling package. The basic procedure involves building an I-DEAS Finite Element (FE) model of the structure from which a scan grid is defined. With the I-DEAS FE model the laser position and scan points are determined. A scan list is created for each node of the I-DEAS model and the mobility data is acquired. The mobility data is then used to update the FE model. The paper concludes that an automated system capable of acquiring mobility data can save time and man hours associated with gathering mobility data for modal analysis. An additional advantage is the non-contact measuring capability of the SLDV. The investigation also reported, however, that the coherence functions were lower at anti-nodes and suggested additional averaging of the data.

Polytec has a system that uses an SLDV and an FFT signal processing card in a personal computer.[7] The system allows scanning of full areas, but only allows the viewing of information at eight spectral lines for full scans. Polytec's system claims to provide an available 512 spectral lines. Polytec's PSV-100[d] Class II He-

---

[a] Ometron VPI 9000 Scanning Laser Doppler Vibrometer, Ometron Inc., Sterling, Virginia.

[b] Zonic System 7000, Zonic Corporation, Milfred, Ohio.

[c] I-DEAS is a registered trademark of SDRC of Milfred, Ohio.

[d] Polytec, PSV-100 Scanning Laser Vibrometer, Polytec PI, Inc., Auburn, MA.

Ne SLDV transducer claims the capability of measuring velocities anywhere from .16 μm/s to 10 m/s. The transducer is claimed usable up to 20 MHz. The position of the laser beam can be moved ±20 degrees in both x and y directions. The specifications also state the phase response of the laser to be -1.3 °/kHz to -1.8°/kHz.

Ometron also has a system which has a similar capability to Polytec.[8] The promotional literature available from Ometron points out the advantage of having the ability to do broad-band structural responses. It also points out the error involved if FRFs are measured without averaging. The literature concludes that at least 16 averages are necessary, but note that the time for data collection at each point is escalated by each additional average. Ometron alleviates some of the time problems by processing a user specified thirty two spectral lines for viewing per scan. Ometron's VPI 4000 sensor Class II He-Ne transducer is capable of measuring velocities anywhere from .001 mm/s to 1000 mm/s. It is claimed that the transducer is usable up to 250 kHz. The position of the laser beam can be moved ± 12.5 degrees in both x and y directions.

2.3 Literature Review Summary

The literature review has shown that the SLDV is an appropriate device for making high spatial density measurements. High spatial density measurements have been found to be beneficial for correlating finite element models with experimental work as well as eliminating problems dealing with spatial aliasing. The SLDV has successfully been used in the past to acquire mobility data and it has been shown that the data is viable for predicting dynamic responses. Data acquisition systems involving the laser for broad-band frequency methods are available commercially and have also been investigated previously at Virginia Tech by Mitchell, Agee, West and Wicks.

Virginia Tech's previous laser-based data acquisition system was based on a finite element package and required the building of a finite element model before data could be acquired. The system was based on the signal processing capabilities of the Zonic System 7000.

The work by Mitchell[4] and Kochersberger[5] can be used as the basis for developing a broad-band spatially dense data acquisition system. The commercial systems provide a step in this direction but only provide up to 32 spectral lines of data. The lack of more complete frequency data leads to models with important

data being missed. Although a broad-band spatially dense system was developed using the SLDV, Zonic 7000, and I-DEAS modeling package the system relied on a Finite Element mesh, providing nodes, rather than including the actual geometry of the structure. Additionally, this system was designed for only one dimensional investigations.

Chapter 3
Instrumentation

Collecting broad-band spatially dense data provides a data set containing a more complete spatial representation of dynamic systems for the understanding of their dynamic behavior. Unfortunately, this can be time consuming. The majority of this time is used by moving accelerometers and the time needed by the frequency analyzer to analyze the data. Though the time used by the frequency analyzer cannot be minimized, the time for the setup of the analyzer at each point and the movement of the measurement location can. Automating the data acquisition process provides an efficient time-saving method for completing repetitive sequences. The SLDV and an automated data acquisition system provide an efficient method for collecting broad-band spatially dense data, leading to an informative investigation of vibrating structures.

This chapter introduces the instruments of the data acquisition system shown in Figure 3-1. Figure 3-1 shows the instrumentation used to collect

vibration data for a beam hung under simulated free-free boundary conditions. The following sections of this chapter cover the General Purpose Interface Bus (GPIB), SGI Crimson Workstation, the digital to analog converter (DAC), HP 35665A signal analyzer, and the other equipment related to the experimental setup.

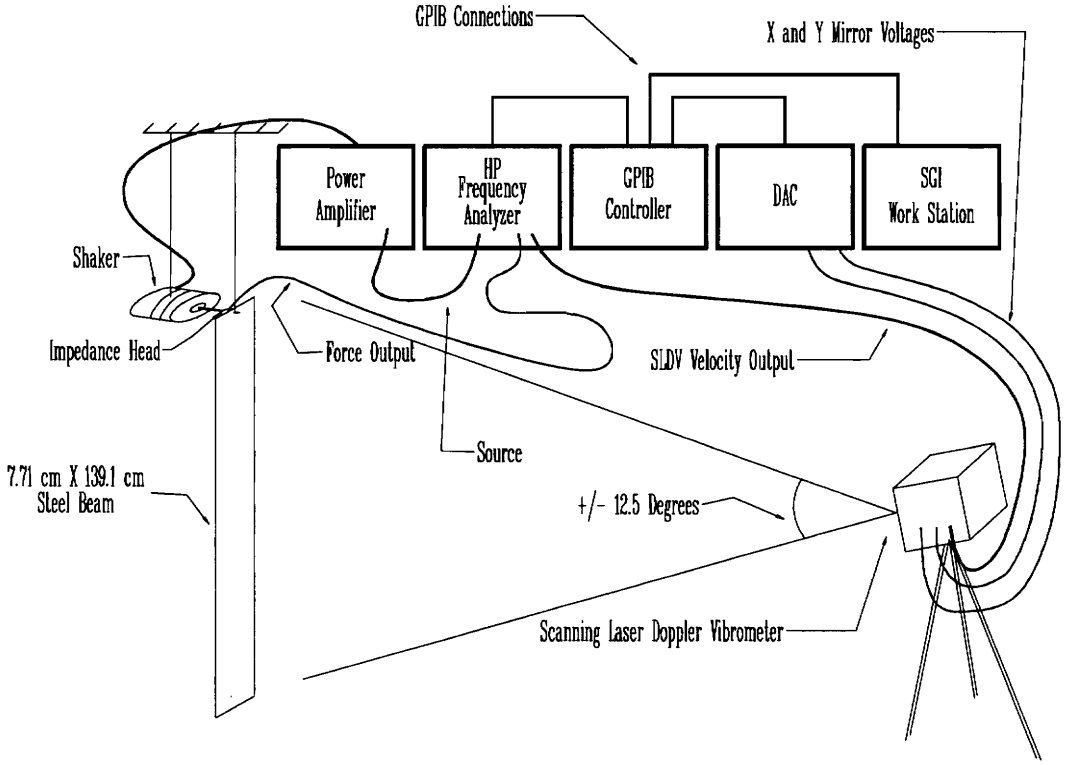

Figure 3-1 Instrumentation of the Data Acquisition System.

3.1 GPIB

The General Purpose Interface Bus, GPIB, is a high performance bus that

provides capabilities for building integrated test systems from individual instruments and computers. The bus and its associated operations are defined by IEEE 488.2 standard, Digital Interface for Programmable Instrumentation. All the instruments used will be connected, using GPIB implementation of the IEEE 488 standard. The IEEE 488 standard provides an electrical and mechanical description for interconnecting electronic measurement devices. Because each of the instruments may be manufactured by different companies, the IEEE standard provides the basic foundation for interfacing each instrument.

The devices in a GPIB system function in at least one of three capacities: talker, listener, or controller. The controller becomes the central communication center between all other devices. Programs are written so the controller sends commands to other devices, controlling each instrument's functions. The controller also has the ability to listen, thus providing complete interaction between the devices.

National Instruments has developed IBIC[e], Interface Bus Interactive Control Program, which can be used to develop, program, debug, and run application programs involving GPIB commands. IBIC uses the IEEE 488 protocol but alleviates the necessity of the programmer learning low level commands. IBIC

---

[e] IBIC, National Instruments, Austin, Texas.

programs can be converted to any standard programming language such as C, FORTRAN, or Basic.

IBIC uses keywords to send commands to each device. Two types of commands exist, as follows:

- Commands to control the GPIB interface which are common to all GPIB devices.
- Device commands, which are used to send commands to the different components of the system and are specific to each instrument.

Instruments based on the GPIB standard can be combined together creating a system of instruments providing a specific capability. GPIB provides the necessary foundation for interfacing the SLDV and a dynamic signal analyzer enabling the development of an automated laser-based broad band data acquisition system.

3.2 SGI Crimson Workstation/GPIB Controller

3.2.1 SGI Workstation

The Silicon Graphics Crimson workstation is used as the user to instrument interface. The data acquisition system and control of the laser beam position are

carried out using the Silicon Graphics workstation. The Silicon Graphics Crimson workstation is used to run the IBIC (Interface Bus Interactive Control) software. The IBIC software controls the GPIB controller through a Small Computer System Interface (SCSI). The National Instruments GPIB controller is an 8-bit microcomputer that operates as a full function IEEE 488/SCSI Controller. It can turn any computer with a SCSI port into a GPIB Talker/Listener/Controller or it can make any device on the SCSI bus look like a GPIB device. In this particular setup the SGI is designated as the controller. In addition to being used as the controller, the SGI Crimson workstation serves the purpose of a data storage device for the data processed by the frequency analyzer.

3.2.2 GPIB Controller

Controller interface commands set the address of each instrument so that the specific instrument can be called at later times. Interface commands also include commands to clear the controller, send specific device commands, and time-out commands. A short list of typical controller interface commands is shown below.

- ibfind dev1 *: Set the name of the 1st instrument to dev1*
- ibpad 11 *: Set the address of a device to 11*
- ibclr *: Clear the bit stream of the controller*

- ibwrtf"filename" *: Execute, "filename", a string of executable commands*
- ibwrt "command" *: Execute device command*
- ibwait rqs timo *: Wait for request of service or time-out*
- ibrsp *: request the serial poll status*

Device commands are specific to each instrument and are defined by the respective manufacturer using the IEEE 488 standard. A device must be IEEE 488 compatible to be able to be connected and interfaced to the controller. An example of a specific device command would be a command that would tell a signal analyzer to start collecting data. These commands are usually in an abbreviated keyword format. The device specific commands of each of the instruments is described below.

3.3 Digital to Analog Converter

An IOtech DAC488/4[f] digital to analog converter will be used to provide the voltage inputs to the SLDV laser beam deflection mirrors. The DAC488/4 is a multiple output, digital to analog converter (DAC) interface for the IEEE 488 bus. Each port uses a 12 bit ±sign D/A converter. Voltages can be specified in bits or

[f] DAC488/4, Digital To Analog Converter, IOtech, Inc., Cleveland, Ohio

voltages with resolutions of 250 μvolts/bit, 1.25 mv/bit, and 2.5 mv/bit respectively.[9] Each port can be programmed for full scale output of ±1 volt, ±5 volt, and ±10 volt nominally.

The DAC has four modes of operation: (1) Direct Mode, (2) Indirect Mode, (3) Stepped Mode, and (4) Waveform mode. The direct mode is used for controlling the SLDV deflection mirrors because it allows specific voltages to be sent at specific times. The other modes of operation allow less control of the DAC output and are not appropriate for controlling the SLDV mirror deflection system. Direct control is accomplished by selecting the DAC port, range, output voltage, and sending an execute command. The example below gives an example of the syntax.

Command String ⟶ *"c0 p1 a0 r2 v-3x"*

- c0 *: Direct Control Mode*
- p1 *: Selects Port1*
- a0 *: Disables Autorange*
- r2 *: Set Range to ±5 volts*
- v-3*x* *: Send -3 volts*

Laser beam positioning will be controlled using port 1 to send the x voltage and port 3 to send the y voltage. Port 2 is not used because it currently does not

meet calibration specifications. The voltages that are sent from the DAC to the SLDV are determined by the scan area and grid density specified in the data acquisition program.

3.4 Signal Analyzer and Source Control

A Hewlett-Packard 35665A signal analyzer with IEEE 488 interface was used to analyze the data in the frequency domain as well as provide the excitation source. The analyzer is a two channel FFT spectrum analyzer with a frequency range that extends from .09 Hz to 51.2 kHz when it is used in two channel mode. The analyzer has a built-in source providing random, burst random, periodic chirp, burst chirp, and fixed sine sources. The analyzer provides the option of representing the signal by 100, 200, 400, and 800 spectral lines. In addition, the analyzer provides a noise floor of -130 dBVrms when operated below 1.28 kHz and a cross talk between channel 1 and 2 and the source of -121 dBVrms.

All analyzer commands can be controlled by the SGI/SCSI controller. The acquisition program uses an initial setup file to configure the analyzer for each test, such as window type, coupling, display, source type, trigger, and so forth.

During the data acquisition process a file is used to setup the analyzer's available functions. The complete setup file, "frs", is shown below with each of the commands explained.

- CAL:AUTO OFF: *Turns the calibration procedure off to prevent interruption of other analyzer commands*
- INP2 ON: *Activates the two channel mode of the analyzer*
- DISP:FORM ULOW: *Sets up the display to an upper and lower screen for viewing two measurements at once*
- WIND UNIF : *Sets the windowing function to uniform (none)*
- FREQ:SPAN 800 HZ : *Sets the analyzer frequency span to 800 Hz*
- INP1:COUP AC : *Turns on AC coupling for channel 1*
- INP1:LOW GRO : *Grounds the input shields of channel 1*
- INP1:BIAS ON : *Turns on the ICP (Integrated Circuit Piezoelectric) power for channel 1*
- INP2:COUP : *AC Turn on AC coupling for channel 2*
- INP2:LOW GRO : *Grounds the input shields of channel 1*
- CALC1:FEED 'XFR:POW:RAT 2,1';MATH:STAT OFF;*WAI : *Sets the upper display to show the frequency response of channel 2/channel 1*
- AVER ON : *Turn the averaging function on*
- INIT:CONT OFF; *WAI : *Pauses the averager*
- AVER:COUN 50 : *Sets the number of averages to 50*
- AVER:TYPE RMS : *Set the type of average to RMS*

- CALC2:FEED 'XFR:POW:COH 1,2';MATH:STAT OFF;*WAI : *Sets the lower display to show the coherence function resulting from the FRF data*
- CALC1:FORM MLIN;:DISP:WIND1:TRAC:Y:SPAC LOG;*WAI : *Sets the scale of the upper display to a Log scale*
- CALC2:FORM REAL;*WAI *: Sets the scale of the lower display to linear and real*
- TRIG:SOUR INT1 : *Sets the trigger to trigger on the internal source*
- TRIG:LEV 5 PCT : *Sets the trigger level to 5 percent*
- DISP:WIND1:TRAC:Y:AUTO ON : *Autoscales the display in channel one*
- DISP:WIND2:TRAC:Y:AUTO ON : *Autoscales the display in channel two*
- SOUR:FUNC PCH : *Sets the source type to periodic chirp*
- SOUR:VOLT 0.034 Vrms : *Sets the amplitude of the source*
- OUTP ON;*WAI : *Turn the source on*
- VOLT1:RANG:AUTO ON : *Autorange channel 1*
- VOLT2:RANG:AUTO ON : *Autorange channel 2*
- FORM:DATA ASCII,7 : *Set the form of the data that will be downloaded*
- *WAI : *Commands the analyzer to wait until the setup is complete before it continues any other process*

All commands available from the front panel of the analyzer have corresponding GPIB commands and can be implemented remotely. The signal analyzer provides the signal processing and signal generator needed to collect mobility type frequency response functions on structures.

3.4.1 Basic Concepts in Signal Processing

Frequency response estimators H1 and H2, and the coherence function are introduced in order to develop a better understanding for the functions of the frequency analyzer.

Frequency response functions, FRF, are a response characterization of a device or structure to an input. Determining an accurate FRF function then provides a linear relationship between the input and output resulting in a linear prediction of the output model. The FRF is a system response characterization that provides the basic knowledge needed to understand the system. The FRF represents the system response as a frequency dependent transfer function. This transfer function provides magnitude and phase information for the system at each frequency.

Accurate FRF estimation then becomes important for determining accurate characterizations of systems. H1 and H2 are the two most common FRF estimators of the FRF. A schematic of the input/output relationship of the time domain signals with uncorrelated noise on the input and output is presented in Fig. 3-2. The estimated input signal, $\hat{x}(t)$, is equal to the true input signal, x(t), plus, m(t),

the uncorrelated signal on the input. The estimated output signal, $\hat{y}(t)$,is equal to the true output signal, y(t), plus, n(t), the uncorrelated signal on the output.

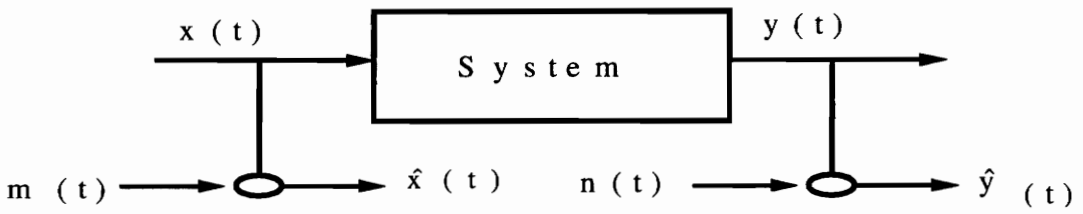

Figure 3-2 Input/Output relationship of a typical time domain signal with uncorrelated noise on the input and the output.[10]

The true FRF ($H1_{True}$) is defined below in Eq. 3-1, where G_{xy} and G_{xx} are the input cross spectrum and autospectrum of the time domain signals, respectively.[10]

$$H1_{True} = \frac{G_{xy}}{G_{xx}} \tag{3-1}$$

The FRF estimator (H_1), shown in Eq. 3-2, however, contains uncorrelated noise (G_{mm}) on the input leading to a bias estimator. H_1 is always lower than the true FRF. It is noted, however, that if G_{mm} =0 then an unbiased estimator results.

$$H_1 = \frac{G_{xy}}{G_{xx} + G_{mm}} = \frac{G_{\hat{x}\hat{y}}}{G_{\hat{x}\hat{x}}} \tag{3-2}$$

Another estimator for the FRF, H_2, assumes that the uncorrelated noise is on the output measurement.[10] H2 always estimates the FRF high. It is also noted as in H_1 that if $G_{nn}=0$ then H_2 becomes the true FRF.

$$H_2 = \frac{G_{yy} + G_{nn}}{G_{yx}} = \frac{G_{\hat{y}\hat{y}}}{G_{\hat{y}\hat{x}}} \tag{3-3}$$

The quality of the estimator is determined by the coherence function. The coherence function is defined as H_1 over H_2 as shown in Eq. 3-4.

$$\gamma_{xy}^2 = \frac{H_1}{H_2} = \frac{G_{\hat{x}\hat{y}} G_{\hat{y}\hat{x}}}{\left(G_{xx} + G_{mm}\right)\left(G_{yy} + G_{nn}\right)} \tag{3-4}$$

Recall from the previous discussions that H_1 estimates the FRF low and H_2 estimates the FRF high. However, if there is not any noise presence both H_1 and H_2 become H_{True} and the coherence function becomes equal to unity. Because H_1 is always lower than H_2, the coherence function is always less than or equal to unity. As can be seen from Eq. 3-4 the coherence decreases towards zero with the presence of any noise and approaches unity as the noise terms decrease.

The HP 35665A signal analyzer uses H_1 for collecting FRFs. Both H_1 and the coherence function are computed at each spectral line. The information is then displayed and/or saved.

3.5 Additional Equipment

In addition to the instrumentation mentioned in the other sections of this chapter, the experimental set up requires a power amplifier, shaker, impedance head, and SLDV.

The power amplifier used to boost the signal from the frequency generator to the shaker is a harman/kardon hk770 twin toroidal ultrawideband DC amplifier. The amplifier has a signal-to-noise ratio of 123 dB. The frequency range of the power amplifier is 8Hz to 100 kHz. Each channel has an available 65 watts into 8 ohms.

The shaker used for excitations was a B&K mini-shaker type4810 SN293657 with an impedance of 3.5 ohms. The shaker has a maximum stroke of ± 3 mm. The maximum rated power input is 15VA.

The impedance head used in this study was a PCB 288A11 SN328. The rated frequency range of the impedance head is 5 to 5000 Hz. The force gage of the impedance head can measure forces from -5 lb to +5 lb. The mass of the head is 45 gm and the mass used to sense the force(uncompensated mass) is 2.7 g. The accelerometer part of the head can measure from -50 g to + 50 g. The force gage is used as the input side of the FRFs and the accelerometer is used to measure the response of the structure for driving point measurements. The SLDV will be discussed in the next chapter.

3.6 Basic Connections

The frequency analyzer, GPIB controller, and DAC are connected together using GPIB connectors. The SGI Work station and GPIB controller are connected with the appropriate SCSI cable and software. Channels one and three of the DAC are connected to the x and y deflection mirrors of the SLDV, respectively. Channels one and two of the frequency analyzer are connected to the force transducer and SLDV velocity output, respectively. The excitation source of the frequency analyzer is connected to the power amplifier and then routed to the shaker.

Chapter 4 Scanning Laser Doppler Vibrometer

The Doppler shift is a phenomenon due to the motion of a source relative to a receiver. The Doppler shift is applicable to all types of electromagnetic radiation, including light.[11] The technique using the Doppler shift of laser light to determine velocities in fluid flows was first introduced in 1964[12]. Today the scanning laser Doppler vibrometer can be used to measure surface vibrations.

The fundamental Doppler shift equation is shown in Equation 3.1. The equation relates the fractional frequency change to the velocity, where c is the wave velocity, Δf is the change in frequency due to relative motion between the source and receiver, and θ is the angle between the wave normal line and the velocity, v.

$$\frac{\Delta f}{f} = \frac{v\mathrm{Cos}\theta}{c} \tag{4-1}$$

As can be seen from the equation above, the true normal velocity is measured when the angle θ is zero. To measure velocities normal to the surface of a structure (assuming the velocity is out of plane), the laser beam has to be normal to the

measuring surface or angle corrections must be used to compensate for the angle difference. Without correcting for angles, a -4% error in the velocity exists.[4]

The Doppler shift is measured by using two beams, one as the reference beam and one as the measuring beam. The reference beam stays inside the laser unit and is combined with the measurement beam producing destructive and constructive interference at a frequency equal to the difference between the reference beam and the Doppler shifted beam.[11] This difference is electronically demodulated to determine the magnitude and direction of the velocity.

The following sections in this Chapter introduce limitations associated with using the SLDV for vibration testing over a broad range of frequencies and suggested solutions for overcoming them. Limitations to be presented here include frequency response of the laser, signal-to-noise ratio, laser positioning and measurement location.

4.1 Frequency Response of the Laser

Frequency response functions are determined by measuring the ratio of output to input over a range of frequencies. Unfortunately, the post processing demodulation filter on most Doppler processing units has a varying phase shift

across the frequency spectrum.[4] In addition to the post demodulation filters, the internal optics and electronics of the SLDV affect the laser response. When the laser is used with a force transducer to measure frequency response functions, the phase shift of the laser must be corrected. The correction must be made since the force transducer does not experience this phase shift over the frequency range of interest. Without correcting the laser, the relative phase of the output to the input in the FRFs is inaccurate.

The frequency response of the laser can be measured by using an accelerometer as a reference. The process involves mounting an accelerometer to the top of a shaker. The shaker is excited while the SLDV is used to measure the velocity of the top of the accelerometer and the accelerometer is used to measure the corresponding acceleration. The frequency response function is formed by using the accelerometer as the input and the laser as the output. Integrating the acceleration, the ratio becomes velocity measured by the laser over the velocity measured by the accelerometer. Figure 4-1 shows an example of the phase and magnitude of the frequency response of the SLDV. Fitting a complex function to the measured FRF and assuming the integration of the accelerometer measurement gives the true velocity; a compensation curve can be determined to correct the laser measurement. The compensation curve corrects for both the magnitude and phase since the FRF of the laser is a complex function. Equation 4-2 below shows the FRF as the ratio of the velocity measured by the SLDV over the velocity determined from the

accelerometer measurement. Assuming the velocity determined by the accelerometer

$$FRF_{laser}(\omega) = \frac{V_{laser}(\omega)}{V_{accel}(\omega)} = \frac{V_{laser}(\omega)}{V_{True}(\omega)} \tag{4-2}$$

is the true velocity, the true velocity can be solved as a function of the laser measurement and the FRF of the laser, as seen in Eq. 4-2. Because both the velocity and the FRF are complex numbers they can written in the form shown in Eq. 4-3, where V and θ are the magnitude and phase of the laser velocity and where X_L and θ_L are the magnitude and phase of the laser's FRF. It is clear from Eq. 4-3 that if the magnitude of the laser FRF, X_L, is less than unity, as is the case for part of Fig. 4-1, it will properly increase the magnitude of the measured velocity. Similarly, Eq. 4-3 shows if the phase of the laser FRF, θ_L, is negative θ_L is added to the phase measured by the laser, correctly shifting the phase upward.

$$V_{True}(\omega) = \frac{V_{laser}(\omega)}{FRF_{laser}(\omega)} = \frac{V(\omega)e^{i\theta}}{X_L(\omega)e^{i\theta_L}} = \frac{V}{X_L}(\omega)e^{i(\theta-\theta_L)} \tag{4-3}$$

The complex polynomial representation of the FRF is determined using a Mathematica program which reads in the FRF file saved from the laser characterization. The FRF file is saved directly to the HP analyzer's internal floppy disk and later converted to ASCII format using HP's Standard Data Format utility software.

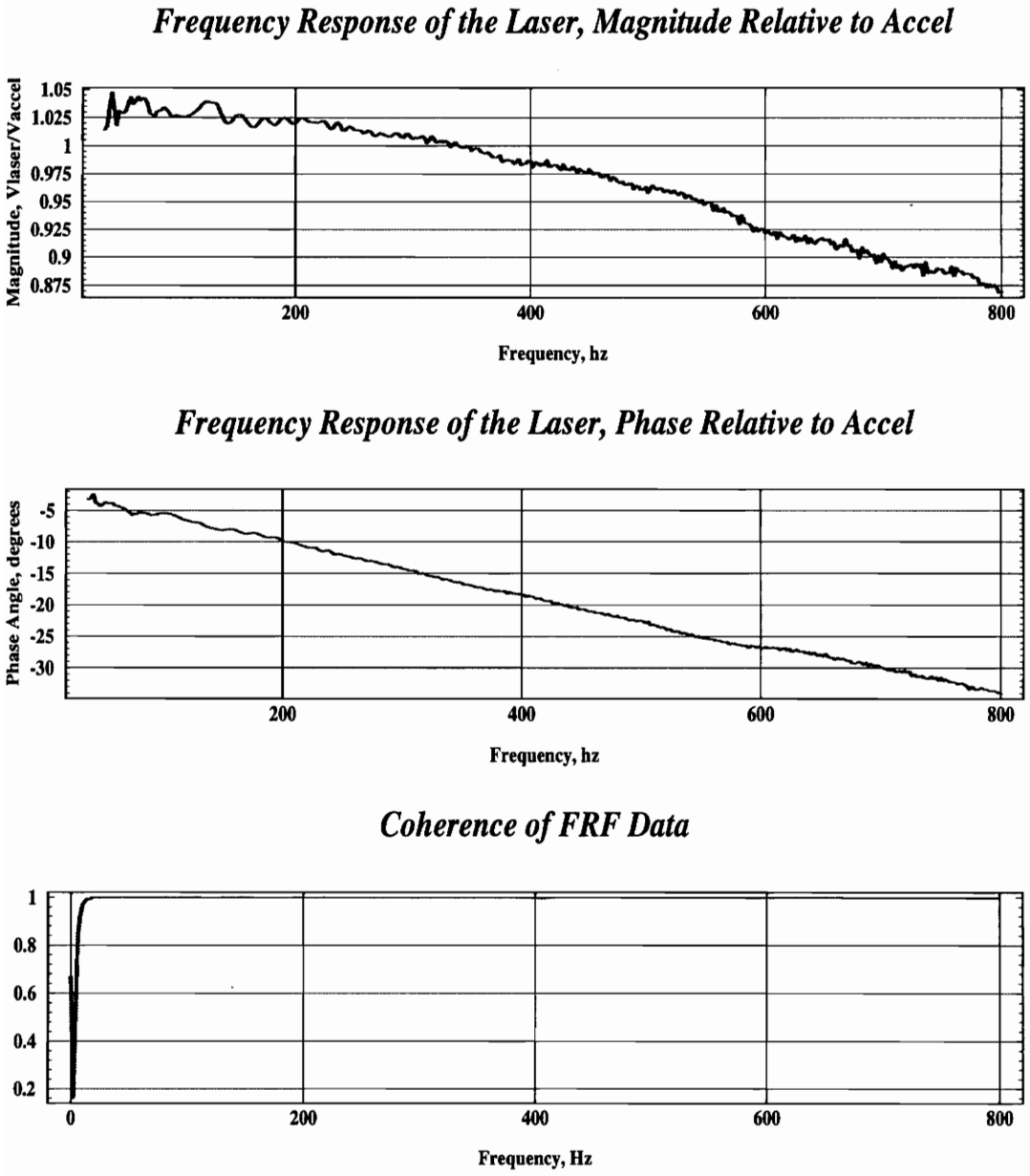

Figure 4-1 Example of the frequency response of the laser.

Small section of FILTFRF

Frequency	Real	Imaginary
0.000000e+000	1.553855e+002	0.000000e+000
2.000000e+000	-3.226952e+000	-5.362724e+001
4.000000e+000	-1.000191e+002	-2.345485e+002
6.000000e+000	-3.421627e+001	-3.346652e+002

Figure 4-2 Example of file "FILTFRF".

An example of a section of a converted file is shown below in Fig. 4-2, where the first column of data is the frequency in Hz and the second and third columns of data correspond to the real and imaginary parts of the FRF, volts/volts, respectively. The pseudocode for the Mathematica code "correction" included in Appendix A is shown below:

Correction: *- Determine the best complex polynomial fit of the laser's frequency response characterization.*

Begin Program Correction

Read FRF data- "FILTFRF"

Apply calibration factors to FRFs

Do for each polynomial order up to 4

Fit Complex polynomial to current FRF data

Compute residuals

Calculate the mean residual, variance of resid. Ans Sig. to Noise ratio

Plot computed FRF and Actual FRF

Plot the residuals

End Do

Create postscript files of plots (filenames - LFIX1, LFIX2, LFIX3, LFIX4)

Create plot of polynomial order versus variance of the residuals

Create a post script file of the above plot (filename - ORD1)

End Program Correction

Table 4-1 outlines the basic procedure for determining the frequency response of the SLDV.

Table 4-1 Basic procedure for determining the frequency response of the SLDV.

1.	Mount an accelerometer to a shaker.
2.	Put a piece of reflective tape on the end of the accelerometer.
3.	Using a two channel frequency analyzer equipped with a source. Connect the output of the accelerometer and SLDV two channels one and two, respectively so that the FRF forms the ratio of SLDV output over the accelerometer output. Also connect the source connection to the shaker via an amplifier.
4.	Set up the analyzer. Choose the corresponding source, frequency span, and frequency resolution that will be used for tests.
5.	Enter the calibration constants for the accelerometer and laser into the analyzer. Use the math functions of the frequency analyzer to integrate the acceleration. Setup the display to display the FRF, SLDV output over the integrated acceleration.
6.	Turn on all instrumentation. Start the excitation source and collect 1000 averages, triggering on the input channel.
7.	Save the data to disk. Note: If HP analyzers are used, the data saved to disk is in the Standard Data Format form and must be converted to ASCII using the HP provided program for completing this conversion.

In addition to the frequency response correction, the signal-to-noise ratio of the laser must be monitored in order for the laser to properly measure the velocity.

4.2 Signal-to-noise Ratio

The signal-to-noise ratio for the SLDV is lower than that of the accelerometer.[1] Two reasons are associated with the signal-to-noise ratio of the SLDV being lower than that of the accelerometer. The signal the accelerometer produces has less noise than the signal produced by the non-contacting measurement of the SLDV. Because the accelerometer makes direct contact with the test piece, noises associated with the test environment are less likely to be introduced. On the other hand, because the SLDV measurement is made without direct contact it includes both the velocity and noises introduced between the interface of the laser and the test piece. Another reason for the difference between the accelerometer and SLDV signal to noise ratio is technology. The development of the SLDV is still in its early years of evolution, whereas the accelerometer has had thirty years to develop.

The signal-to-noise ratio of the scanning laser Doppler vibrometer for this series of tests is defined as the ratio of the peak signal to the noise floor. The noise floor is defined as the output of the laser at zero velocity across all frequencies of interest.

In order to investigate the signal-to-noise ratio of the SLDV, it was

necessary to determine the SLDV's noise floor. For this specific experiment an accelerometer was attached to the wall of the laboratory and the motion of the wall was measured with both the accelerometer and the SLDV. The SLDV was placed about 3.3 meters away from the wall corresponding to the same distance used to gather FRF data for the beam. Additionally, the frequency range investigated for the signal-to-noise ratio also corresponded to the 800 Hz bandwidth used in the beam test.

It was assumed that the laboratory wall was stationary and that the corresponding measurements would correspond to the noise floors of the transducers. An HP 35665A frequency analyzer was used to collect one thousand averages of the autospectrum of the Ometron VPI 9000 SLDV and a PCB 307A SN996 accelerometer. The noise floor of the HP analyzer was specified to be -130 dB Vrms. The noise floor of the SLDV and the accelerometer was measured to be -60 dB Vrms and -95 dB Vrms, respectively, at a range of approximately 3.3m.

In order to use the SLDV for measurements, the majority of all measurements must be above the noise floor of the laser. It was observed that the coherence of FRF data falls off at the measurement location where the velocity approaches zero. The reason for this poor coherence is due to the signal-to-noise ratio problem. Two things can be done to help improve the accuracy of the data: (1) averaging and (2) utilization of the full dynamic range.

4.2.1 Averaging

Averaging the FRF data helps to reduce the noise present in the FRF (H1). Averaging is the process of acquiring multiple blocks of data and averaging the set of data spectral line by spectral line. By averaging in this way, random noise that is present approaches the noise floor of the laser. What results from the averaging process is the ability to resolve measurements to the noise floor of the laser without additional random noise present from other sources. Because measurements in the noise floor make it more difficult to extract quality estimates of signal parameters, a better parameter estimate will result if measurements can be raised above the noise floor. This can be done by optimizing the dynamic range of the measurement.

4.2.2 Dynamic Range

The SLDV has three available dynamic range settings - low, medium and, high. The particular setting is determined by the amplitude of the velocity which is being measured. Utilizing the full dynamic range within one of these settings is

important. Velocities which are measured on the lower end of each of these dynamic ranges are often buried in the noise floor of the SLDV.

Fewer measurements are likely to be buried in the noise floor when the SLDV dynamic range has been optimized. One can optimize the dynamic range when scanning a structure by first selecting one of the three laser settings and then forcing the structure within each laser setting with sufficient power to maximize the dynamic range. Dynamic range maximization should be done at a location of peak response so all other measurements produce levels of response lower than the dynamic range. The maximum peak response is difficult to find. However, by quickly surveying the structure with the laser one can find a location that has a higher response compared to the other points in the survey. With the peak measurement from the survey the input excitation power level can be set equal to 80-90 percent of the full dynamic range. Setting power at this level leaves 20-10 percent of the dynamic range for those points with a higher response which were not found through the surveying process. With the dynamic range optimized, the laser signals at lower velocities have a better chance of being above the noise floor.

Using these procedures improves the quality of the data, but not the signal-to-noise ratio. However, knowing the limit of the signal-to-noise ratio of the SLDV helps one set up the data acquisition equipment appropriately. For this particular

test the laser was used in the low setting with sufficient power to provide at least 90 percent usage of the full dynamic range.

4.3 Positioning the Laser Beam

The position of the laser beam can be manipulated by positioning two mirrors. The first mirror controls the vertical reflection of the laser beam relative to the laser head and the second mirror controls the horizontal reflection of the laser beam relative to the laser head.

The range of deflection angles for the Ometron VPI Sensor is $\pm 12.5^{\circ}$ for both mirrors. The voltage to angle relationship for the mirror deflection angles has been calibrated and found to follow a linear model. The mirror angles can be controlled by x and y voltage inputs with full deflection of the mirrors corresponding to a nominal input of ± 5 Volts. The x and y voltages can be provided using a computer with digital to analog converter (DAC) outputs. The angular step size available depends on the DAC step size. The DAC step size depends on the number bits of the D/A converter and the voltage range selected. For the IOtech DAC488/4 the voltage resolution for the ± 5 Volts range is

1.25mv/bit which corresponds to .003125 degrees, assuming the SLDV deflection mirrors are within calibration.

4.4 Measurement Location

Determining the measurement location on the structure is taken care by two processes. The first process is referred to as a registration process. The registration process is basically the process of determining the location of the structure in the SLDV coordinate system. The registration process is described in Chapter 5.3. The next step in determining the position of the measurement points is done using a program called ConvertScans. ConvertScans uses the structure location determined by the registration process and calculates the position of each measurement. The use of ConvertScans is discussed in Chapter 5.8.

Chapter 5
Experimental Setup and Data Acquisition Process

This chapter demonstrates the data acquisition process. The sections in this chapter describe the components of the flow diagram, presented in Fig. 5-1.

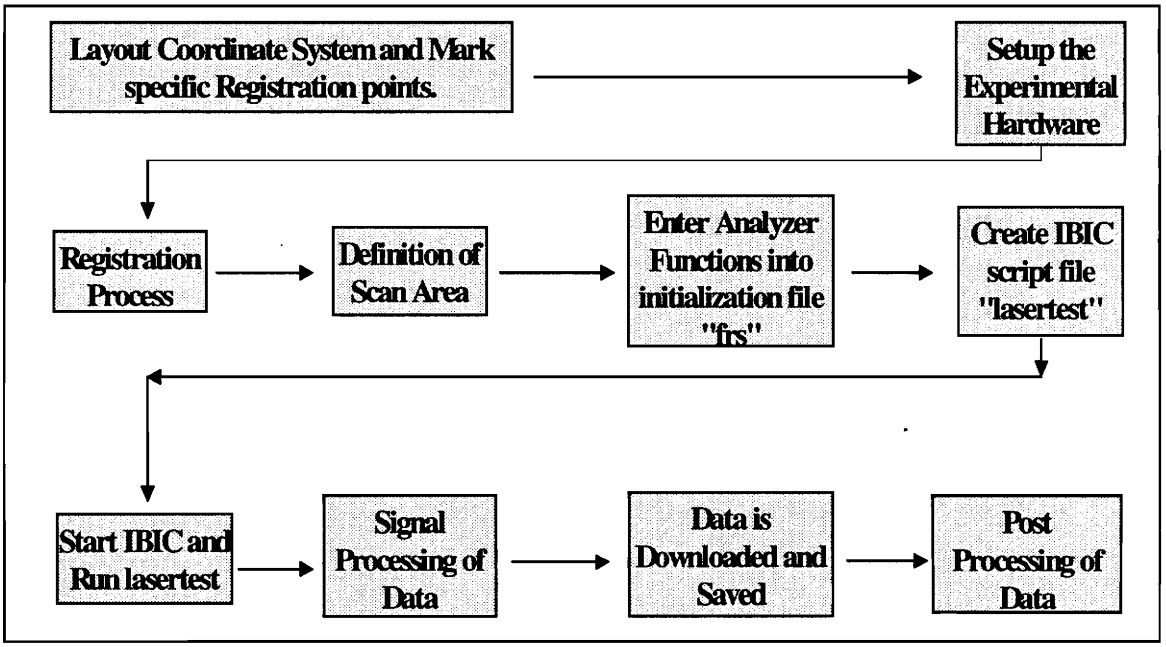

Figure 5-1 Experimental and data acquisition process diagram.

5.1 Marking Registration Points

Deciding on a coordinate system and points for the test structure is the first important step in the registration process.

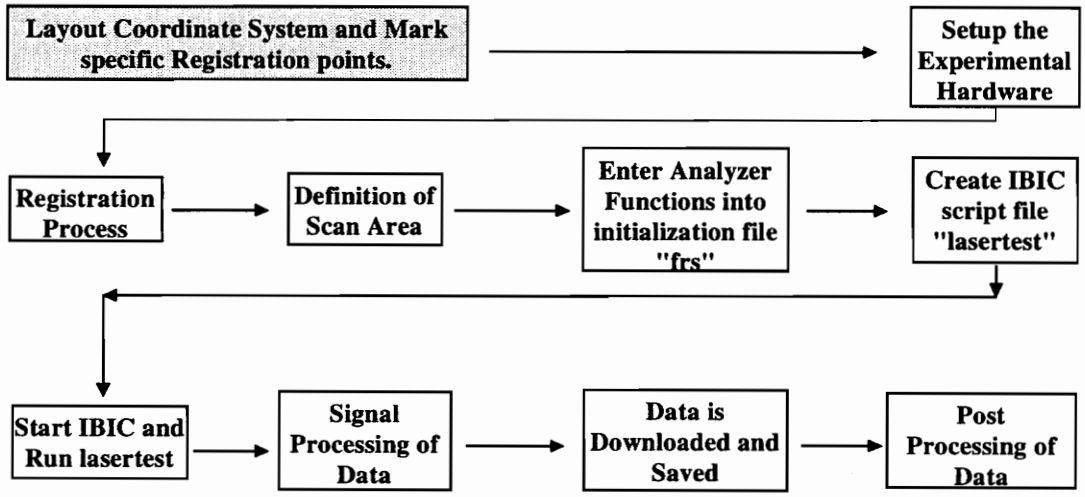

Figure 5-2 Lay out coordinate System and mark specific registration points.

The points that are marked should be measured as accurately as possible. The points should be laid out in such a fashion so that a wide foot print of the structure is represented. The number of points used to perform the registration process must be at least four, preferably more. More of the information on the structure is incorporated into the solution when more points are used during the registration.

The disadvantage with using too many points is the time associated with laying out each of the points and the time needed to register each point.

For this particular test, the registration points and origin of the beam structure are shown in Figure Fig. 5-3.

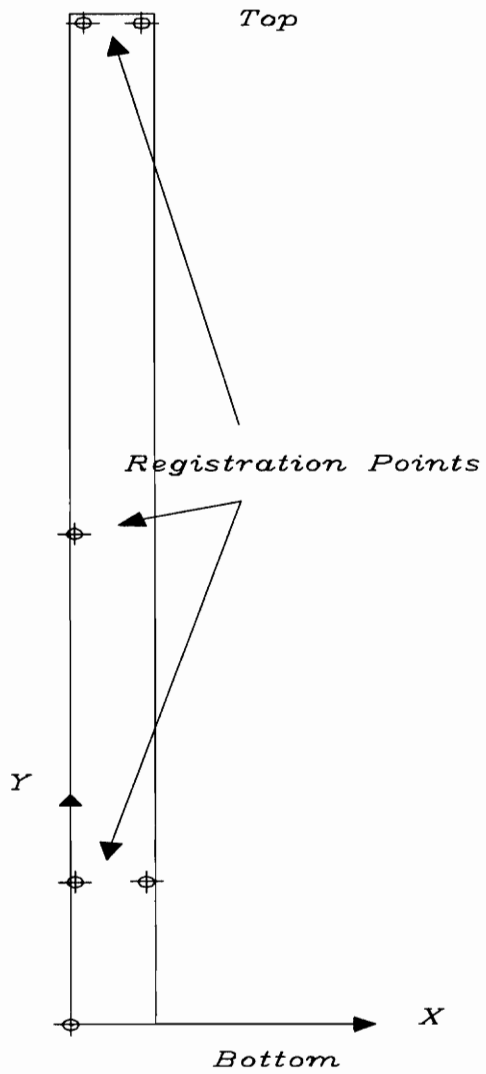

Figure 5-3 Location of registration points.

5.2 Experimental Hardware Setup

The purpose of setting up an experiment is to learn more about the structure being tested. In order to avoid introducing the effects of the support system cautions must be exercised during setup.

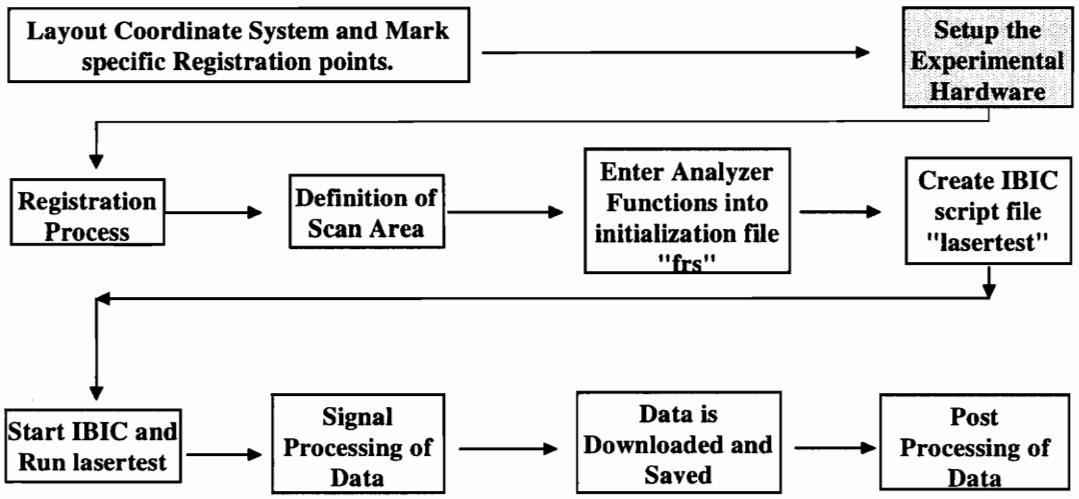

Figure 5-4 Experimental setup.

The idea behind a suspension used to set up the structure is to minimize the influence of the boundary conditions in the test. This is accomplished in some cases by trying to achieve a free-free condition with a test suspension system. The concept is to use soft springs to reduce the stiffness of the suspension system by using a bungee cord of surgical tubing. By making the suspension system soft, the

natural frequency of the suspension system is lowered so that it is much less than that of the structure being tested. The test suspension should also reduce external mass by building the suspension system from a bungee cord and monofilament. Hardware used to attach the filament and bungee cord should be placed high above the test to reduce the pendulum motion. Taking these precautions will help to reduce the pendulum frequency to as low as possible to try and avoid the lowest natural frequency of the test structure by about 1/10.

The shaker should be attached in such a way that the direction of excitation is limited to one direction. To eliminate the transmission of moments into the structure a stinger made of material possessing high axial stiffness and low bending stiffness can be used as the junction between the shaker and test structure.

5.3 Registration

The laser beam position on the structure is unknown in the structure coordinate system. However, if the location of the structure coordinate system is known, and if the location and orientation of the laser, and the mirror deflection angles of the laser are known, all laser velocity measurements can be transferred back to the structure coordinate system.

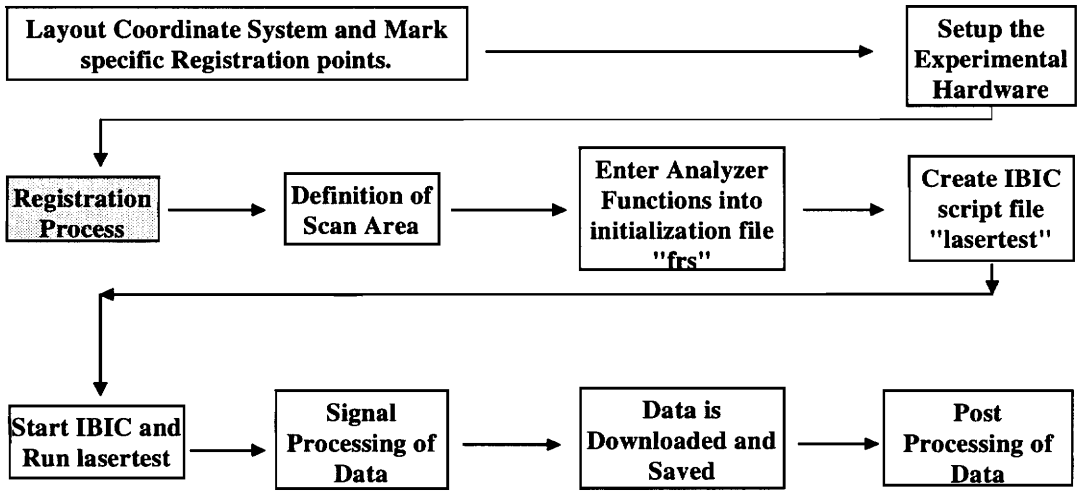

Figure 5-5 Registration process.

With a registration procedure developed by Montgomery,[13] the relative position and orientation of the laser relative to the structure is determined. The position and orientation of the laser relative to the structure is used to determine a laser to structure transformation matrix. The transformation matrix is used to convert mirror deflection angles into structure coordinates, given the geometry of the structure in the structure coordinate system.

The registration procedure requires choosing a coordinate system on the structure and marking points with precise coordinates; these points are referred to as the registration points. Four or more points must be used in order to provide sufficient data for the algorithm to solve for the position and orientation of the laser in the structure coordinate system. Figure 5-6 shows the six registration

points that were chosen for testing the beam. Once the registration points are marked and their coordinates determined in the structure coordinate system, the structure can be positioned in the experimental setup. Registration of the laser with the structure is performed by using program ESDM. ESDM is used to manipulate the laser beam position, aligning the laser beam by sight with the registration points. The laser beam is steered to each registration point on the structure where the mirror deflection voltages and coordinate information are recorded. After ESDM is done it creates a file that contains structure coordinates and mirror angles for each registration point that will be used later to determine the laser to structure and structure to laser transformations.

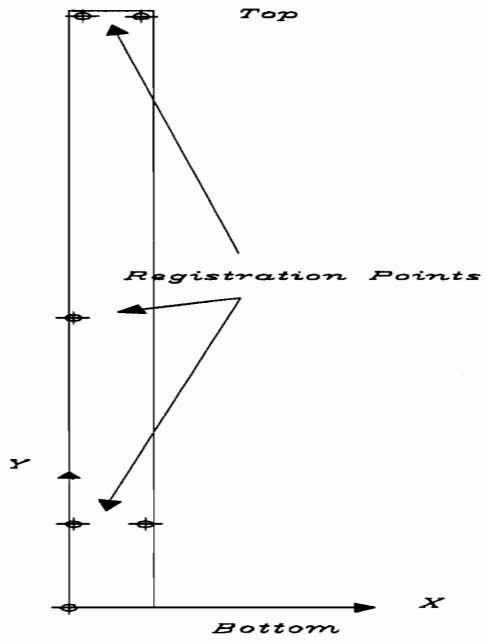

Figure 5-6 Registration points.

The ESDM program procedure is outlined below with pseudocode.

ESDM: - Controls to manipulate the laser beam and both input the coordinates and record the mirror angles of the each registration point and save to a file.

Begin Program ESDM

Do for each registration point

Move x and y sliders to position laser beam to the current registration point

Enter the previously noted coordinates of the current registration point

Record mirror deflection angle and coordinate for the current registration point

End Do

Press Done - Saves registration into file name of the users choice

The registration files can be saved to any file name; an example of the registration file beam.meas is shown below.

```
NUMREG 7
UNITS   m
DISTGUESS  3.35
REGPOINT 1 0.012700 1.379000 0.000000 -10.695897  0.561545
REGPOINT 2 0.065900 1.378500 0.000000 -10.687098  -0.430539
REGPOINT 3 0.074000 0.785500 0.000000 -0.831100  -0.561844
REGPOINT 4 0.0040000 0.675000 0.000000 1.098100  0.726197
REGPOINT 5 0.0039700 0.195500 0.000000 8.765697  0.705772
REGPOINT 6 0.069100 0.196000 0.000000 8.739298  -0.475974
REGPOINT 7 0.000000 0.000000 0.000000 11.753697  0.745372
```

Figure 5-7 Registration file beam.meas.

Lines 1-3 give the number of registration points used, units that are used for the coordinate system, and an initial distance guess for the laser to the test structure. The next lines give information about each of the registration points. Spatially, the x, y, and z coordinates of each registration point measured in the structure

coordinate system is followed by the corresponding x and y mirror deflection angles.

The mirror deflection angles that are recorded in the registration process are determined by using an analog to digital converter (ADC) to read the actual voltage received by the laser. After the voltages are recorded they are converted to mirror angles using a calibration factor.

5.4 Scan Area

The scan area is defined using ESDM (laser movement/registering program) and four points.

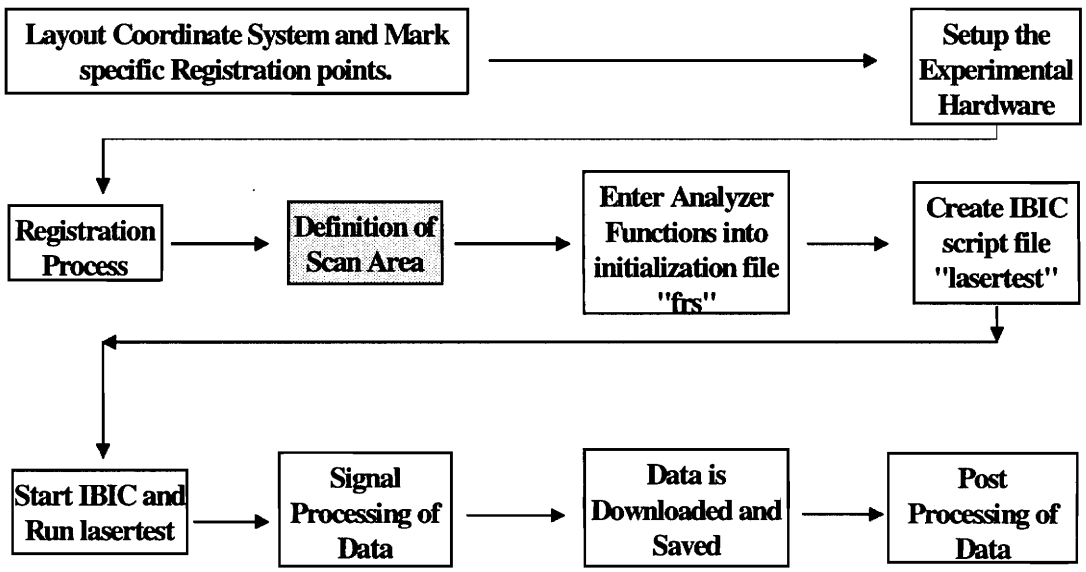

Figure 5-8 Defining the scan area.

The four points can be used to define any rectangular area; however, the order the points are selected is important because of the way the acquisition system defines the area. The points must be defined as top to bottom on the left side and top to bottom on the right side as shown in Figure 5-9.

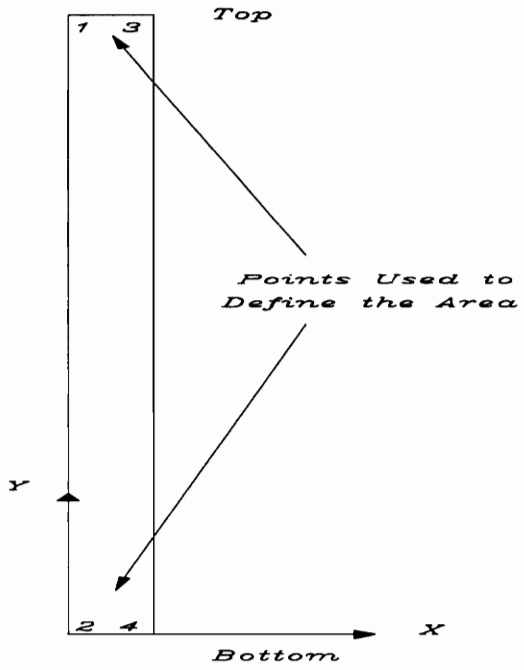

Figure 5-9 Definition of the scan area.

The steps are outlined using a procedure similar to the registration.

ESDM: - Controls to manipulate the laser beam and record the mirror angles of the each point defining the area and save to file, "scanarea".

Begin Program ESDM

Do for each point.

Move x and y sliders to position laser beam to the (1st,2nd,3rd,4th) point.

Complete each of the above steps defining the area as shown in Figure 5-9.

Record mirror deflection angle and coordinate for the current registration point

End Do

Press Done - Saves file to "scanarea".

The file name "scanarea" is important because the program uses this specific filename for the definition of the scan area. The scan area file looks identical to the registration file except that it has only four points and all the x, y, and z coordinate information is defined to be zeros. The program uses only the mirror angles for definition of the scan area and scan grid.

5.5 Analyzer Setup

As discussed in Section 3.4 the setup of the analyzer is accomplished by writing all the desired settings into the text file "frs".

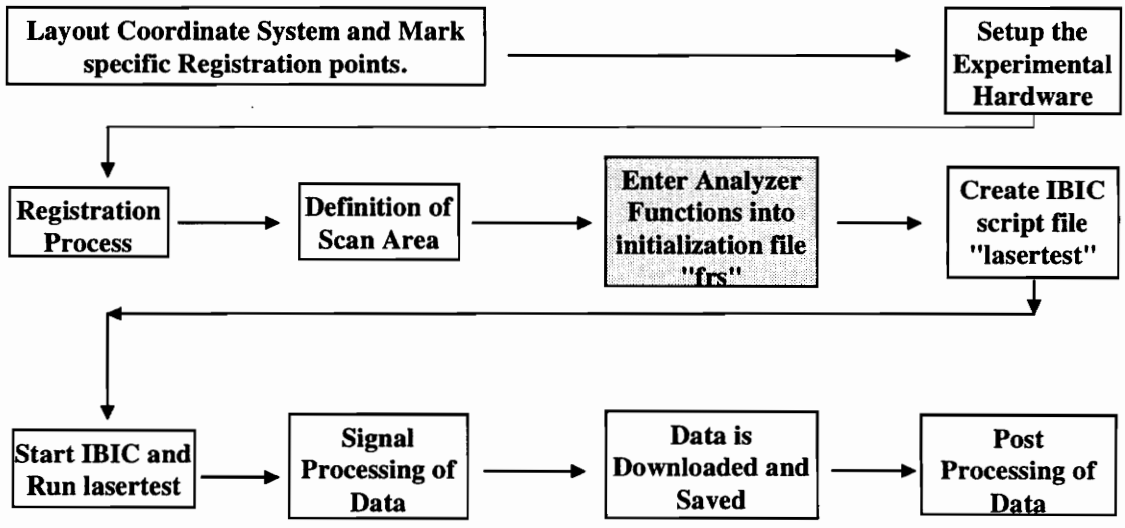

Figure 5-10 Enter analyzer functions.

The filename "frs" is also important to the program structure and must be named accordingly. A note of caution here about setting up the source level. The desired source level to the shaker should be investigated before a value is entered into the setup file "frs". Selecting any value for the source level, within the "frs" setup file, may damage the shaker. Currently, the signal source is automatically turned on during the start up of the data acquisition program and the user has no way to react fast enough to save the shaker from damage if the value entered into the "frs" setup file is too high.

5.6 Creating the IBIC Script File

The IBIC script file is created using the scan area information and a Mathematica program, "ibicrun". "ibicrun" uses all of the controller commands and device commands discussed in Chapter 3 to control the analyzer and position the laser beam, as well as downloading the data at each point. The pseudocode for "ibicrun" is included here, the actual program appears in Appendix A.

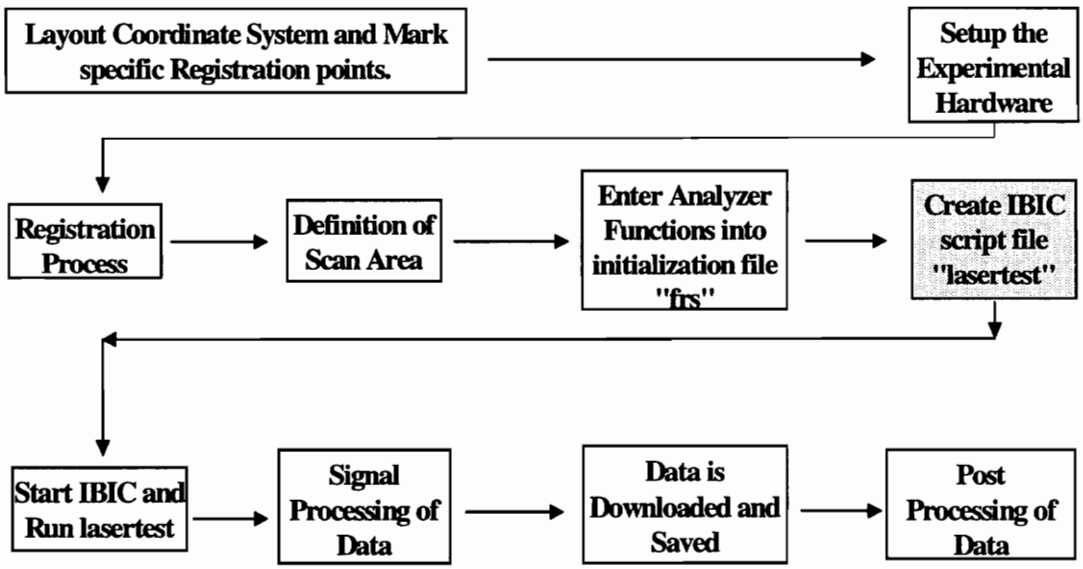

Figure 5-11 IBIC script file creation.

"ibicrun": - *Used to create an IBIC script file "lasertest".*

Begin Program "ibicrun"

Read the file "scanarea" which contains mirror angle data defining the scan area

Convert the mirror angles to voltages

Divide the scan area (defined by voltages) into a rectangular pattern of mxn points.

Save voltage coordinates of each point into a specially formatted file called "scanvoltages"

Scanvoltages will be used later with "ConvertScans"

Create data file names used to store FRF, Coherence and Frequency information

Open a file called "lasertest"

Write the command to define the name of and the address of the signal analyzer

Write the command to run the analyzer setup file name, "frs"

Write the command to define the name and address of the DAC

Do for each scan position

Write the command to change communication to the DAC

Write the DAC command for the x and y voltages defined previously

Write commands to change communication to the signal analyzer

Write the commands to Auto range channels 1 and 2

Write the command to start the signal analyzer averaging

Write the command to pause until the data is collected

Write the command to download FRF, Coherence, and corresponding x axis frequency information to the previously defined file names

End Do

Close file "lasertest"

End Program ibicrun

A portion of the file "lasertest" created by ibicrun is shown below.

ibfind dev1 : Defines the name of the signal analyzer.
ibpad 11 : Defines the address of the signal analyzer.
ibclr : Clear the communication lines.
ibwrtf "frs" : Runs the analyzer setup file.
ibfind dev2 : Defines the name of the DAC.
ibpad 9 : Defines the address of the DAC.
set dev2 : Change communications to the DAC.
ibwrt "c0 p1 a0 r2 v-0.304152x" : Send -.304152 volts to out port 1 of the DAC. This moves the x deflection mirrors.
ibwrt "c0 p3 a0 r2 v4.52476x" : Send 4.52476 volts to output port 3 of the DAC. This moves the y deflection mirrors.
set dev1 : Change communications to the signal analyzer.
*ibwrt "VOLT1:RANG:AUTO ON;*WAI" : Send command to the analyzer to autorange channel 1.*
*ibwrt "VOLT2:RANG:AUTO ON;*WAI" : Send command to the analyzer to autorange channel2.*
ibwait rqs timo: Wait for the analyzer to Autorange.
*ibwrt "ABOR;:INIT;*WAI" : Start collecting 50 averages of the FRF data for this position.*
ibwait rqs timo : Wait until averaging is complete.
ibwrt "TRAC:DATA D1, TRAC1" : Save FRF data shown in the upper display to data register #1.
ibwrt "TRAC:DATA D2, TRAC2" : Save coherence data shown in the lower display to data register #2.
ibwrt "TRAC? D1" : send the FRF data in the 1st data register down line.
ibrdf "p1.dat" : save the FRF for location number 1 to p1.dat.
ibwrt "TRAC? D2" : send the coherence data in the 2nd data register down line.
ibrdf "c1.dat" : save the coherence for location number 1 to c1.dat
ibwrt "TRAC:X? TRAC1" : send the x axis, frequency information corresponding to the spectral lines of data collected in both the FRF and coherence files, down line.
ibrdf "x1.dat" : save the frequency information for the first location as x1.dat.

set dev2 : Change communication to the DAC.
ibwrt "c0 p1 a0 r2 v-0.13151x" : Send -0.13151 volts out port 1, new x position.
ibwrt "c0 p3 a0 r2 v4.52476x" : Send 4.52476 volts out port 3, new y position

The file continues with the same commands, except the voltages change, for all points in the defined grid.

5.7 Data Acquisition

Using the SGI workstation the IBIC program is launched. Once IBIC is started the script file "lasertest" can be started from the IBIC prompt by typing "$ lasertest".

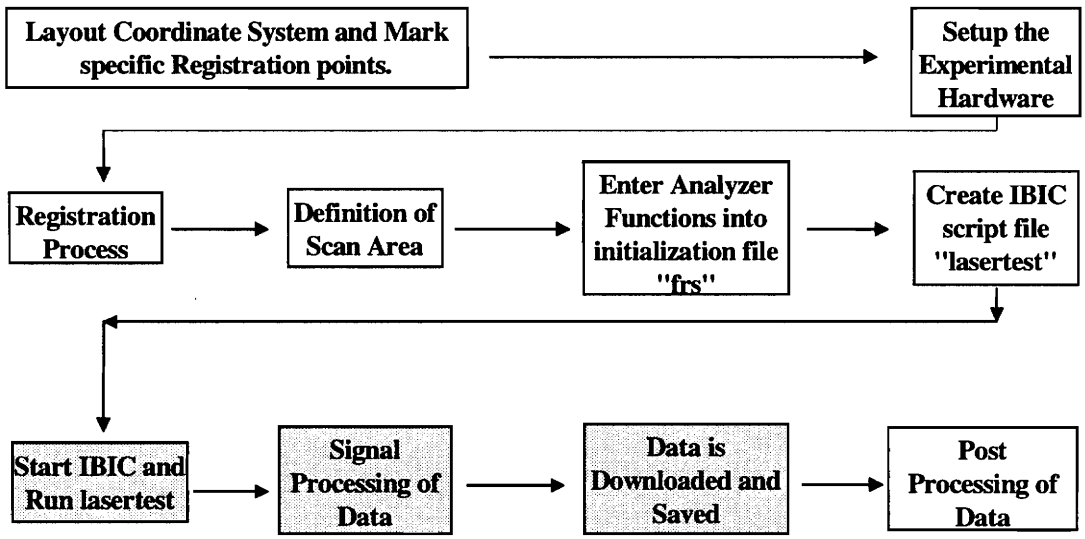

Figure 5-12 Data acquisition process.

The program immediately starts setting up the analyzer and turns on the shaker source. The laser beam is moved to the first position and data is collected and

downloaded to the SGI Crimson Workstation. This process continues for each location in the scanning grid. The output files are recorded as voltages. An example of the output files which are saved is shown below.

FRF data file p1.dat

Real part of FRF | Imaginary part of FRF | Real part of FRF | Imaginary part of FRF

-1.369015E+001,+0.000000E+000,-2.057158E+002,1.377316E+002, ...

Every two numbers of the file represent the real and imaginary numbers for the FRF at the spectral lines corresponding to the frequency file.

Coherence data file c1.dat

Coherence for the 1st spectral line | Coherence for the 2nd spectral line | Coherence for the 3rd spectral line

8.683056E-001,+9.843400E-001,+9.467295E-001 ...

Every number in the file represents the coherence of the FRF corresponding to the spectral lines in the frequency file.

Frequency Data File x1.dat

Frequency of the 1st spectral line | Frequency of the 2nd spectral line | Frequency of the 3rd spectral line

+0.000000E+000,+2.000000E+000,+4.000000E+000, ...

Every number of the file represents the frequency corresponding to the spectral lines.

5.8 Post Processing

The binding of the FRF and coherence data with the angle correction and laser calibrations is done using the Mathematica Notebook "ibicprocess". The "ibicprocess" is broken down into two sections. Before "ibicprocess" can be run and angle corrections done the angles of incidence of the laser beam with respect to the structure coordinate system must determined by using ConvertScans.

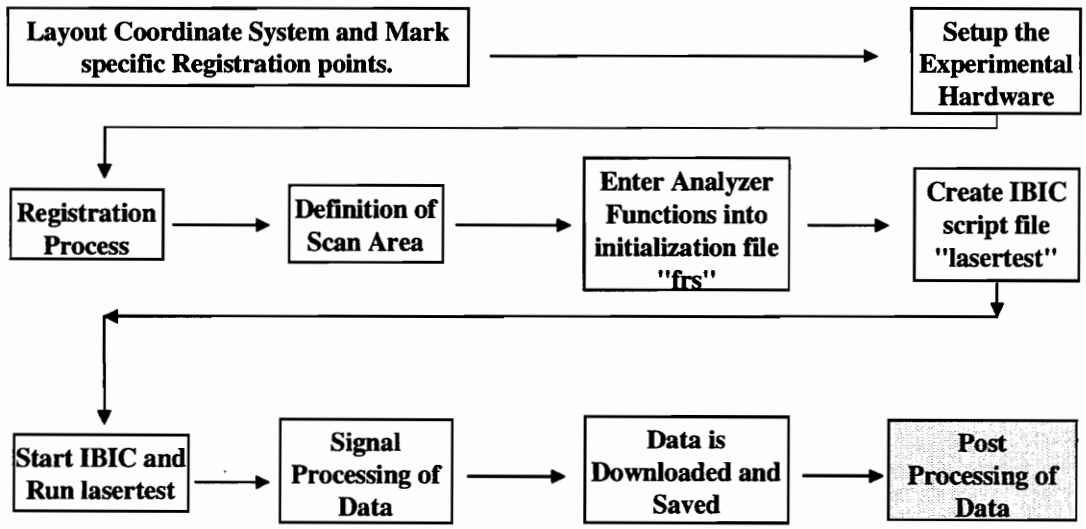

Figure 5-13 Post processing of raw frequency data.

"ConvertScans" uses the information in the registration file and scanvoltages file to create a file that includes both the angle correction needed for the velocity as well as the location of the beam measurements locations. A section of the output file "ConvertScans" is shown below.

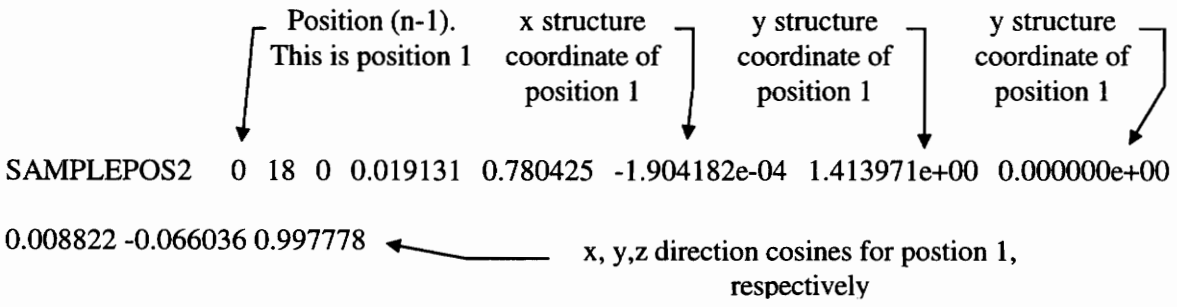

Section I of the Mathematica notebook "ibicprocess" uses information in the file created by "ConvertScans" to correct the velocity and then create FRF, magnitude and phase plots, and coherence plots. In addition, the plots are corrected for the laser characterization problem as well as applying calibration constants of the laser and impedance head. Section II creates magnitude, phase and coherence plots for each of the sets of FRF data and saves the plots to a postscript file for printing and/or viewing through a postscript viewer. The pseudocode for the "ibicprocess is included below with the actual program appearing in Appendix A.

ibicprocess *- Post processes data acquired using laser test*

Begin ibicprocess

Data Processing section I

Define names of the data files

Read in FRF data

Read in Coherence Data

Read in Frequency Data

Create an array of the Frequency, FRF, Coherence data for each set of position data

Using the equation from the FRF of the laser's frequency response characterization

create an array of discrete values corresponding to the frequency information in the data files.

Read in the z direction cosines from "beamnov4.meas"

Correct the FRF for each point based on the z-direction cosines

Calculate the FRF for each position using the correction based on the laser characterization

Apply the calibration constants of the laser and Force gage to the FRF for each position
Export the FRF data into four files FrfR(real values of FRF),Frfl(imaginary values of FRF), Frfcohe(coherence values),Freq(the frequency lines) for the Modhan curve fitting Routine

Data processing section II

Create magnitude, phase and coherence plots for each position in the scan grid

Create postscript files for each scan grid location containing magnitude, phase, and coherence plots and saving them to file, (Plot1, Plot2 ,Plot3 ...)

End ibicprocess

The process results in mxn plot files corresponding to each of the measurement locations. The plot files include magnitude, phase angle, and coherence for each FRF at each location.

Chapter 6
Results of Data Acquisition and Validation

This chapter presents the data acquired during the testing of a beam suspended in a simulated free-free boundary condition. The frequency response of the laser system and the calibration curve of the laser response are presented. FRF and coherence plots resulting from post processing the acquired data are shown and discussed. Validation of the data is accomplished by curve fitting the experimentally measured FRFs and by extracting the modal properties of a suspension system approximating a free-free beam. The extracted mode shapes and frequencies are compared with theory. In addition, a demonstration of the value of spatially dense data is presented.

The beam tested is 139.1 cm long and 7.7 cm wide. It was suspended from the ceiling with a 0.5 m of bungee cord and 1.5 m of filament, which reduced the suspension mass and placed it high above the test structure in an effort to reduce the pendulum motion and provide a low swing frequency. The low pendulum

frequency would not affect the measurement of the lower natural frequencies of the beam. A PCB Model 288A11 SN328 impedance head with sensitivities of 970 mv/lb and 96.6 mv/g for force and acceleration, respectively, is attached to the upper midpoint of the beam. A shaker is hung from the ceiling by bungee cords. The impedance head is attached to the shaker through a stinger made of material possessing high axial stiffness and low bending stiffness in order to eliminate the transmission of moments into the structure. The result of this reduction in transmission of moments is to produce primarily transverse point loading with minimal participation of the shaker and suspension system. Additionally, the instruments described in Chapters 3 and 4 and shown in Fig. 6-1 are all connected with the appropriate connections.

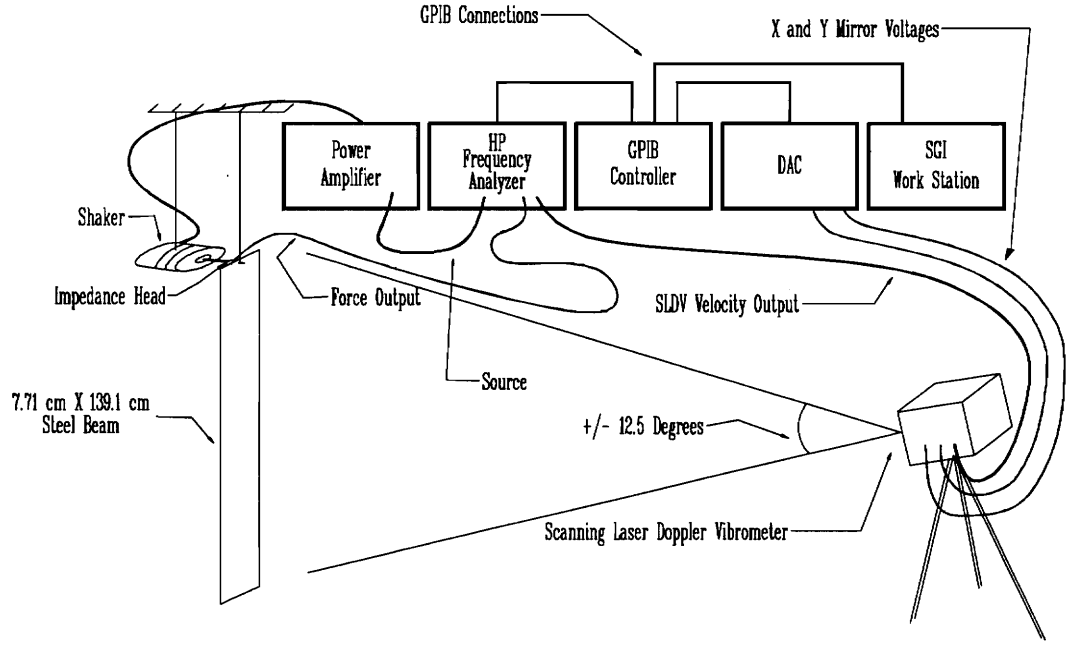

Figure 6-1 Experimental setup.

6.1 Frequency Response of the SLDV.

Using the SLDV to collect data over a broad-band of frequency ranges requires a correction based on the frequency response of the laser. This limitation, previously discussed in Chapter 4, is due to the frequency response of the laser which is influenced by the electronics and optics used to determine the velocity. The suspect components involved are the demodulation filters and the optics; however, to analyze this problem further would require some disassembly of the laser. These components introduce error into the phase and the magnitude of the velocity when the laser is referenced to an accelerometer or force transducer. This frequency response of the laser depends on the setting - low, medium or high - used while data are collected. The tests in this study use the laser's low setting. For this analysis it was sufficient to characterize the response of the laser and use it to correct the measurements. Because the experiments in this study were restricted from 0 to 800 Hz, the laser characterization and correction are also limited to this range with the laser's low setting.

With periodic chirp as the source, FRF data of the laser referenced to a PCB 307A SN996 accelerometer was collected with the procedure outlined in Section 4.1. Additionally, one thousand averages of the FRF data were taken in

order to reduce the noise content. The resulting frequency response of the laser relative to the reference accelerometer is shown in Fig. 6-2.

If both the SLDV and the reference accelerometer were measuring the same response, it would be expected that the FRF of the laser would be flat and it would therefore be measuring the correct velocity over the entire spectrum. However this was not the case since both transducers were not affected by the filters internal to the laser. The frequency response of the SLDV produces errors in the phase and magnitude of the measured velocity over the frequency range. These errors can be seen in Fig. 6-2 and are as large as 13% and 35 degrees for the magnitude and phase, respectively.

In order to calibrate out the frequency response of the laser, the FRF of the laser is used to correct the measured velocity as was demonstrated in Chapter 4, and shown again in Eq. 6-1.

$$V_{True} = \frac{V_{laser}}{FRF_{laser}} = \frac{Ve^{i\theta}}{X_L e^{i\theta_L}} = \frac{V}{X_L} e^{i(\theta-\theta_L)} \tag{6-1}$$

To obtain a mathematical representation of the laser FRF, a complex polynomial of the form given in Eq. 6-2 was fit to the laser FRF data.

$$C_4 f^4 + C_3 f^3 + C_2 f^2 + C_1 f + C_0 \tag{6-2}$$

where the constants C are complex numbers and f is the frequency.

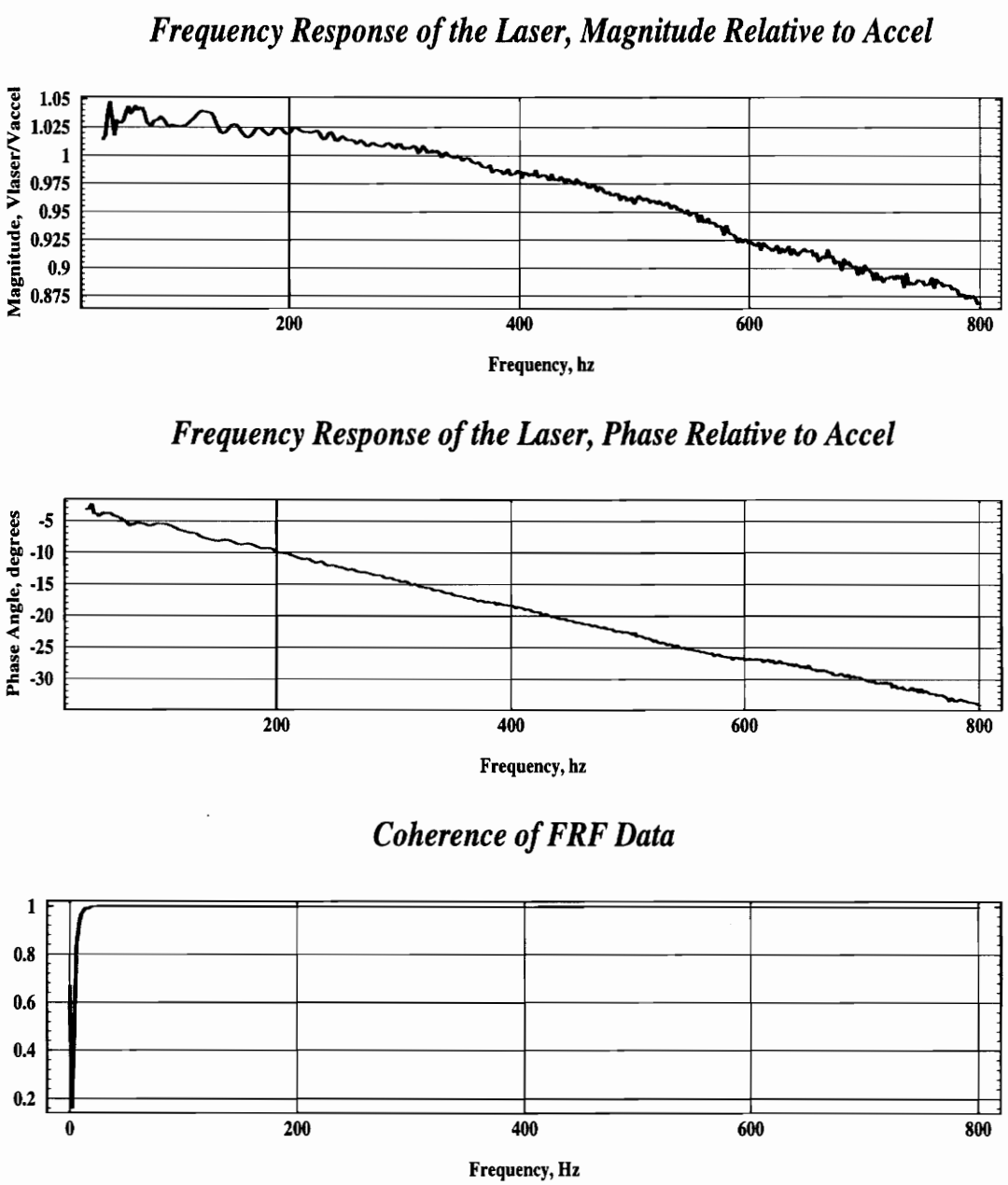

Figure 6-2 Frequency response of the laser.

A fourth order polynomial was chosen based on the decrease of the variance of the residual error. The residual error is defined as the actual data minus the curve fit evaluated at the corresponding frequency. The resulting variance has both real and imaginary components due to the complex polynomial representation. The magnitude of the variance of the residuals is plotted as a function of polynomial order in Fig. 6-3. As can be seen in Fig. 6-3 little improvement is gained when the polynomial order is greater than four.

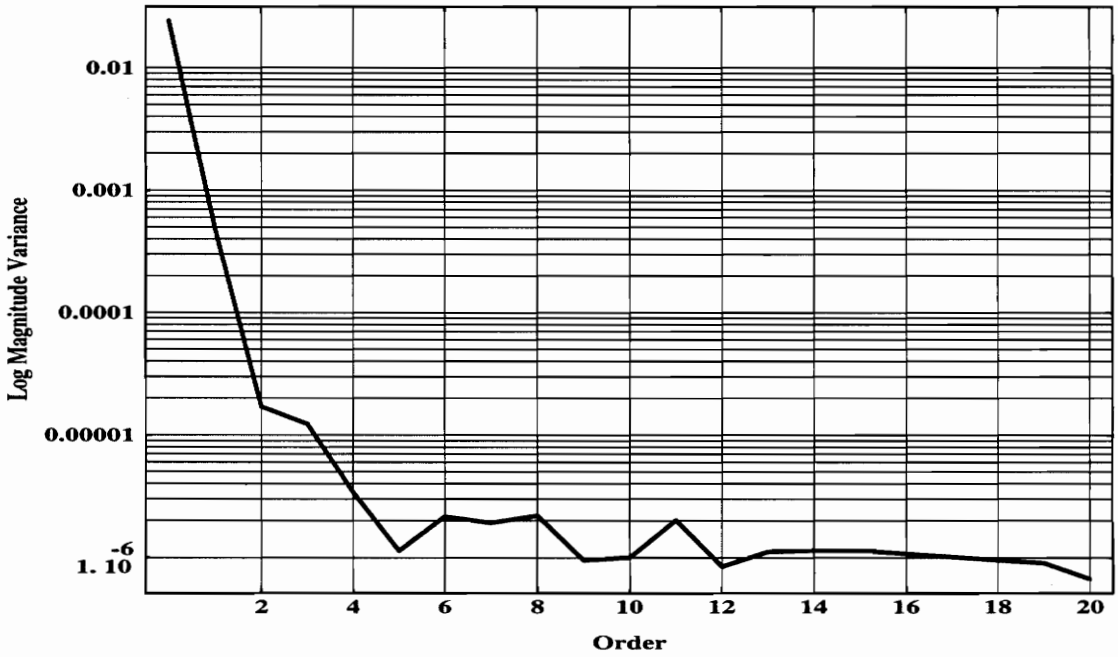

Figure 6-3 Variance of the residuals plotted as a function of order of polynomial used to fit the data.

Figure 6-4 shows the fourth order fit and compares the fit to the actual data points. Additional verification of the fit was done by ensuring that the mean of the residuals was close to zero. The mean of the residual for the complex 4th order

polynomial was -1.9 10^{-15} + i 7.2 10^{-15}. The variance of the residuals was -3.4 10^{-6} + i 2.8 10^{-7}. Additional verification was done by examining the residual for any significant deterministic content. As can be seen in Fig 6-4, no significant deterministic content exists. The signal-to-noise ratio of this fit is defined as the peak magnitude divided by the standard deviation of the residual error. The signal-to-noise ratio for this model is 561. The resulting fourth order complex polynomial was used as the basis to correct FRF data collected using the SLDV.

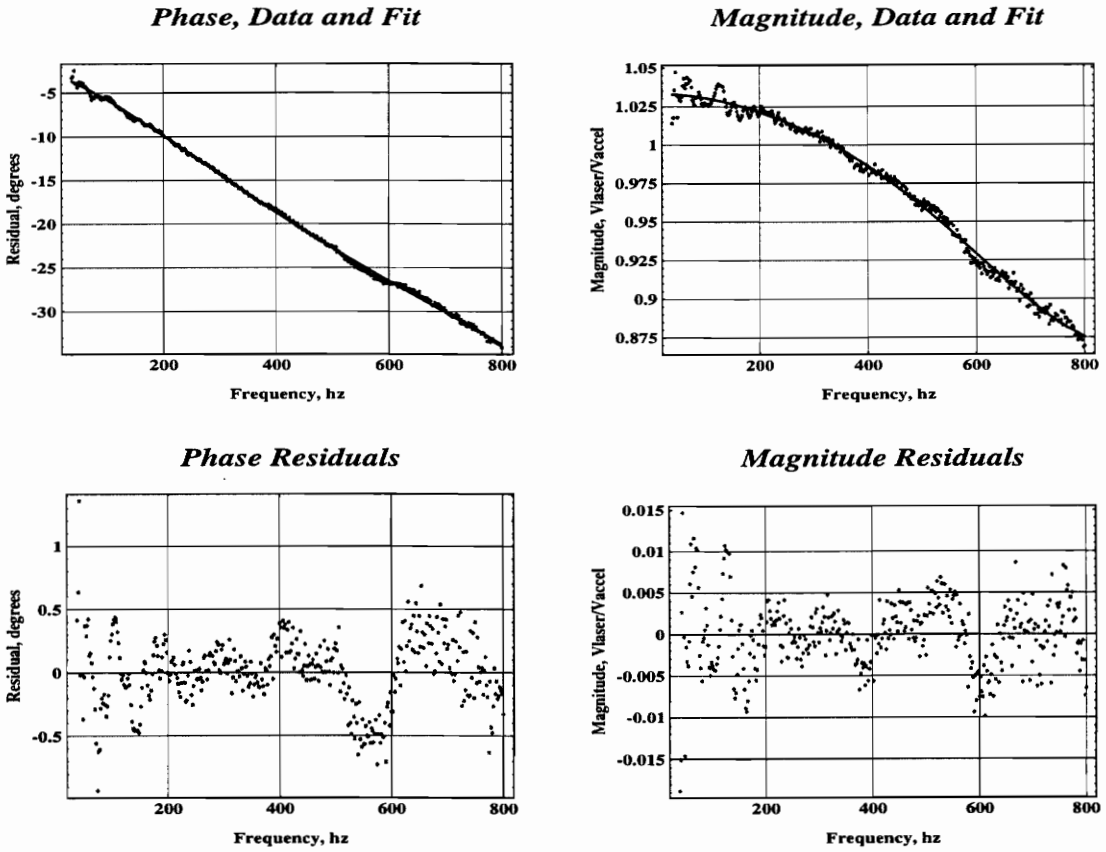

Figure 6-4 Fourth order polynomial fit compared with actual data and residuals.

Figure 6-5 shows an example of a comparison of the corrected (black) and the uncorrected (red) FRFs acquired using the SLDV. The corrected phase and magnitude are apparent in this figure. With this correction, FRF data collected by the SLDV can be calibrated over a range of frequencies and used in subsequent analysis.

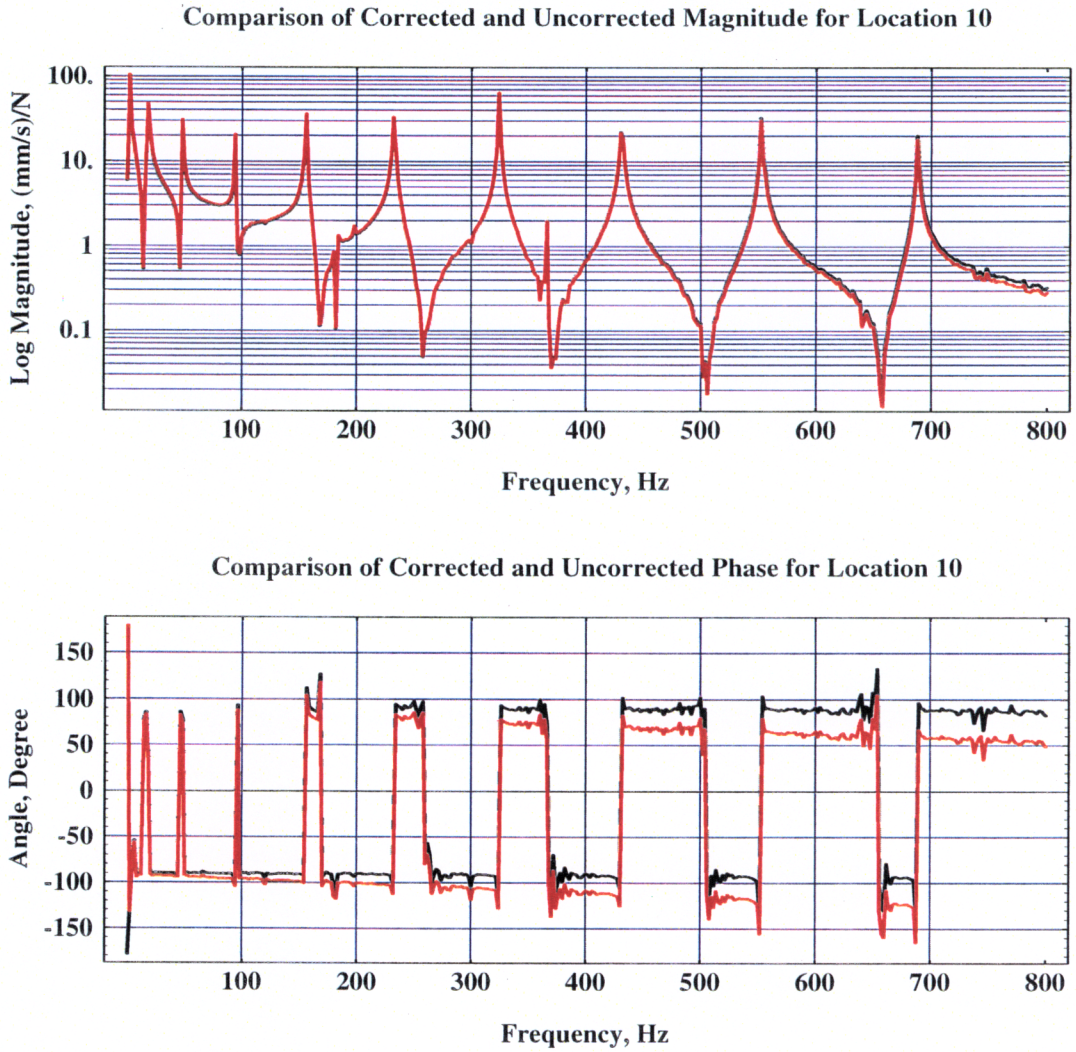

Figure 6-5 Comparison of an uncorrected and a corrected FRF.

6.2 FRF and Coherence Plots

With the developed data acquisition system, FRF and coherence data was collected for each point defined in the scanning grid. For this particular test, eighty FRFs were collected with the corresponding coherence data. The HP 35665A frequency analyzer uses the H_1 FRF estimator described in section 3.3.1 of Chapter 3.

The quality of the collected FRF data varied depending on the location from which the data was collected. Points of low coherence occurred in two different situations. The first situation occurred at anti-resonances where the velocity approached zero. The second case occurred at resonances when the output of the force transducer approached zero. Examining the autospectrum of each signal revealed poor signal quality at anti-resonances for the laser and poor signal quality at resonances for the force. Equation 6-3 can be used to explain the reasons for poor coherence in both of these cases.

$$\gamma_{xy}^2 = \frac{H_1}{H_2} = \frac{G_{\hat{x}\hat{y}} G_{\hat{y}\hat{x}}}{(G_{xx} + G_{mm})(G_{yy} + G_{nn})} \tag{6-3}$$

At anti-resonances or locations of zero velocity G_{yy} approaches zero and the noise, G_{nn}, becomes the dominant part of the denominator. Additionally, when the noise G_{nn} is not correlated with the input, Gxy is small. This results in dividing a small

$G_{\hat{x}\hat{y}}$ by a larger $G_{nn,}$ thus producing a low coherence. A similar occurrence happens at locations of peak response or resonance frequencies. At resonance the autospectrum of the force signal, $G_{xx,}$ approaches zero forcing the noise, $G_{mm,}$ to become the dominant signal. Once again G_{mm} in the denominator becomes the dominant forcing term, which results in a low coherence.

Figure 6-6 shows a FRF for a measurement location with a strong response and overall good coherence. The "Coherence FRF Overlay" plot of Fig. 6-6 overlays coherence onto a log scale making the coherence appear to start at 10; however this, actually is unity. Again this plot shows the low coherence coincident with the resonances and anti-resonances.

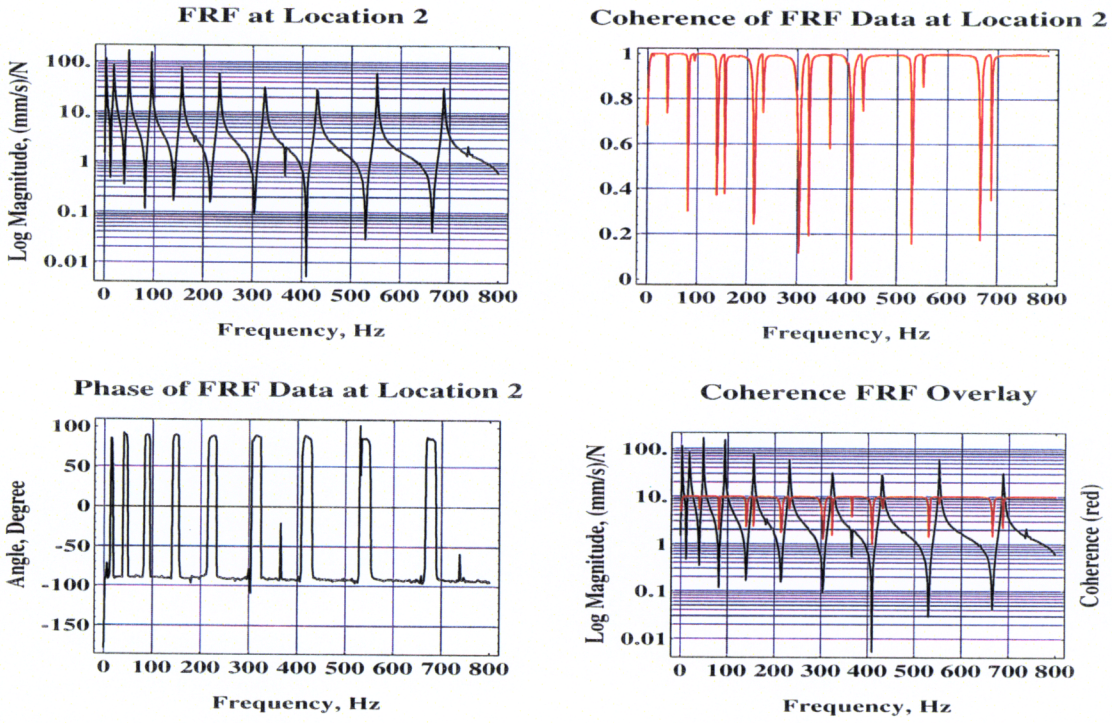

Figure 6-6 FRF with good coherence.

Figure 6-7 presents an FRF at a location with less response and poorer overall coherence than Fig. 6-6. The lower coherence occurs mostly near anti-resonances and can be attributed to the SLDV signal being close to the noise floor.

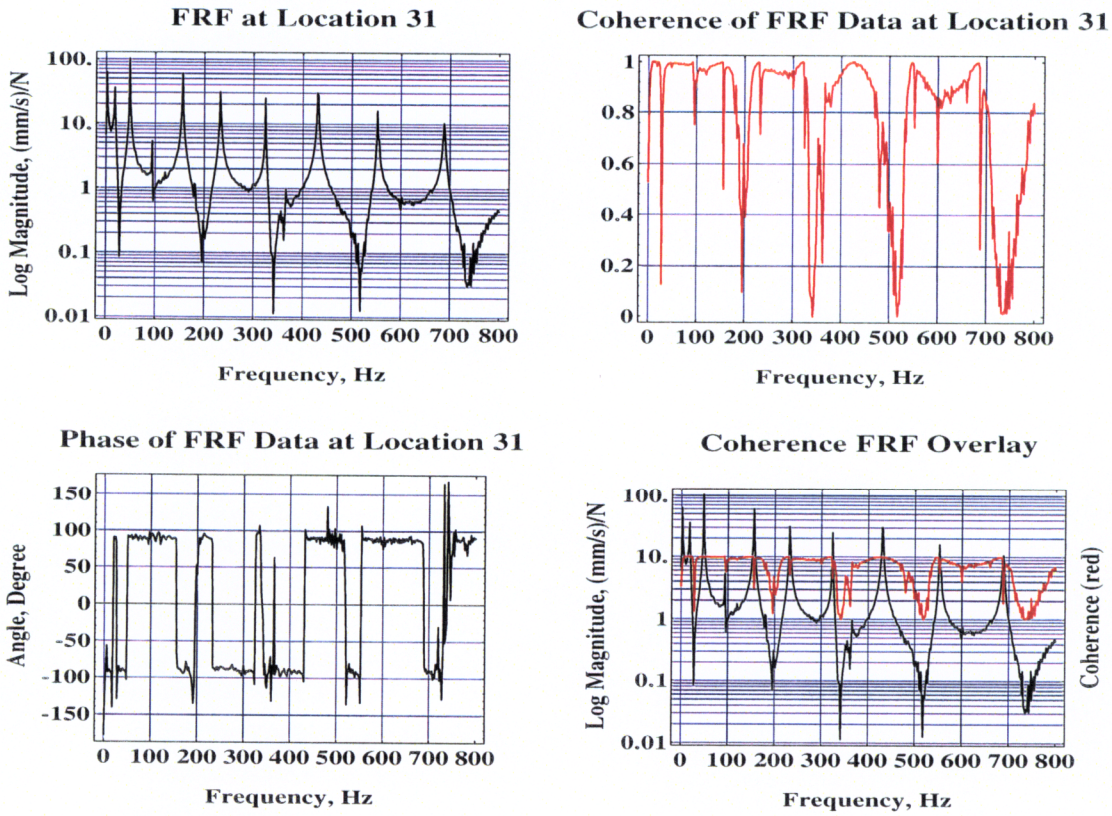

Figure 6-7 FRF with poor coherence.

The next section of this chapter validates that the data acquisition system can be used to obtain useful data. Which can be used to determine the natural frequencies, damping, and mode shapes of the suspended system simulating a

beam with free-free boundary conditions. The basic concepts of modal analysis and FRF curve fitting used to extract modal parameters will be presented, along with the results of the FRF curve fit and modal extraction. Additionally, the extracted mode shapes will be compared to those predicted by Euler-Bernoulli theory for a free-free beam. A presentation showing spatial aliasing and the benefits of spatially dense data also follows.

6.3 Basic Concepts of Modal Analysis

Modal analysis is a method for investigating vibrating structures. Modal analysis involves the application of a modal transformation which uncouples the differential equations of motion to obtain equivalent single degree of freedom equations to facilitate the characterization and analysis of multiple degree-of-freedom systems. The basic differential equations for a multiple degree of freedom system are given in Eq. 6-4, where M is the mass matrix, C is the damping matrix, K is the stiffness matrix, and where x, $\dot{x}$, $\ddot{x}$,and F represent column vectors of the displacement, velocity, acceleration, and force, respectively.

$$M\ddot{x} + C\dot{x} + Kx = F \tag{6-4}$$

The set of differential equations is uncoupled with a linear transformation relationship where ϕ is the modal matrix. Each column of the

$$\begin{aligned} x &= \phi y \\ \dot{x} &= \phi \dot{y} \\ \ddot{x} &= \phi \ddot{y} \end{aligned} \tag{6-5}$$

modal matrix represents the eigenvectors or normal-mode shapes of the system. The y's represent the modal coordinates. Substituting the linear transformation relationship into the original differential equation gives Eq. 6-6.

$$M\phi\ddot{y} + C\phi\dot{y} + K\phi y = F \tag{6-6}$$

Pre-multiplying Eq. 3.2 by ϕ^T the transpose of ϕ gives Eq. 6-7.

$$\phi^T M\phi\ddot{y} + \phi^T C\phi\dot{y} + \phi^T K\phi y = \phi^T F \tag{6-7}$$

Equation 6-7 can be uncoupled by assuming proportional damping. The uncoupled equations of motion that result allow the multi-degree of freedom system to be modeled as a sum of **n** single degree of freedom systems. Equation 6-8 shows the uncoupled independent equations, where the mass, damping, and stiffness matrices are diagonal matrices.[14]

$$\begin{bmatrix} M_r \end{bmatrix}\begin{Bmatrix} \ddot{y}_1 \\ \ddot{y}_2 \\ \cdot \\ \ddot{y}_{n-1} \\ \ddot{y}_n \end{Bmatrix}+\begin{bmatrix} 2\zeta_r \omega_r M_r \end{bmatrix}\begin{Bmatrix} \dot{y}_1 \\ \dot{y}_2 \\ \cdot \\ \dot{y}_{n-1} \\ \dot{y}_n \end{Bmatrix}+\begin{bmatrix} \omega_r M_r \end{bmatrix}\begin{Bmatrix} y_1 \\ y_2 \\ \cdot \\ y_{n-1} \\ y_n \end{Bmatrix}=\phi^T F \quad (6\text{-}8)$$

In general the forcing vector F in Eq. 6-8 can be a column vector with as many forces as degrees of freedom. However, in many cases in modal analysis we are often interested in the dynamic response when excited by one force. The particular case that is investigated in this thesis will be that of a single harmonic force F_1 with all other forces zero. Dividing Eq. 6-8 by the modal mass, M_r, and assuming the forces and response are harmonic produces Eq. 6-9.

$$-\omega_r y+i2\omega_r\varsigma_r\omega+\omega_r y=\frac{\phi^T F}{M_r} \quad (6\text{-}9)$$

Using a singe harmonic force and transferring from modal coordinates back into the spatial coordinates, x, and changing subscripts gives Eq. 6-10, where input is the index for the location of the force and meas is the index for the location of the measured response.

$$\frac{x_{meas.}}{F_{input}}=\frac{\sum_{r=1}^{n} {}_r\phi_{meas}\ {}_r\phi_{input}}{M_r(\omega_r^2-\omega^2+j2\varsigma_r\omega_r\omega)} \quad (6\text{-}10)$$

Equation 6-10 is the solution for the response at position "meas" due to a harmonic input F_{input} at location input. Equation 6-10 also shows that the response at each measured location includes some contribution from each mode. The equation above is the basic form of the frequency response function (FRF). The pole-residue form of the FRF can be written as shown in Eq 6-11, where P_r is the r_{th} system pole, ${}_rA_{meas\ input}$ is the r_{th} system residue at the given response measurement location due to the measured force of the input location. Again, as was seen in Eq. 6-10, Eq. 6-11 shows that the response at each measured position includes a contribution from each mode.

$$\frac{x_{meas.}}{F_{input}} = \sum_{r=1}^{n}\left[\frac{{}_rA_{meas\ input}}{S-P_r} + \frac{{}_rA^{*}_{meas\ input}}{S-P^{*}_r}\right] \tag{6-11}$$

Where

$$P_r = -\varsigma_r\omega_r + j\omega_r\sqrt{1-\varsigma_r^2} \tag{6-12}$$

$${}_rA_{meas\ input} = \frac{{}_r\phi_{meas}\ {}_r\phi_{input}}{j2M_r\omega_r\sqrt{1-\varsigma_r^2}} \tag{6-13}$$

and

$$S=j\omega \tag{6-14}$$

The residue can be used to extract the mode shape. The driving point residue is given in Eq. 6-15, where the input force and measurement location are the same.

$$ {}_{r}A_{(input)(input)} = \frac{{}_{r}\phi_{input} \; {}_{r}\phi_{input}}{j2m_r\omega_r\sqrt{1-\varsigma_r^2}} \tag{6-15} $$

Using the driving point residue, Eq. 6-15, the mass normalized amplitude at the driving point, Eq. 6-16, is found, where the damped natural frequency, $\omega_d=\omega_r\sqrt{1-\varsigma_r^2}$.

$$ \frac{{}_{r}\phi_{(input)}}{\sqrt{M_r}} = \sqrt{{}_{r}A_{(input)(input)}j2\omega_d} \tag{6-16} $$

Substituting Eq. 6-16 into Eq. 6-13 and solving for the mass normalized amplitude at any location, meas, gives Eq. 6-17. Using Eq. 6-17 the mode shapes of any r_{th} mode can be found. The spatial characterization of the system is carried in the mode shape which comes from the numerator of the residue while the denominator of the residue characterizes the global characteristics, ω_r and ς_r.

$$ \frac{{}_{r}u_{meas}}{{}_{r}\sqrt{M_r}} = \frac{{}_{r}A_{meas \; input}\sqrt{j2\omega_d M_r}}{\sqrt{{}_{r}A_{(input)(input)}}} \tag{6-17} $$

To implement this procedure experimentally requires the measured FRFs to be put in a mathematical pole-residue format. A curve fitting routine which minimizes the error between the measured FRFs and the mathematical form of the FRF can be used for this procedure. The MODHAN[15] FRF curve fitting software was used to create FRFs based on the measured FRFs.

MODHAN uses orthogonal polynomials to form the FRF in the form of the ratio of two polynomials. The roots of the denominator are the poles of the system. MODHAN uses an iterative least square approach to determine the best fit of multiple FRF measurements. MODHAN allows the user to choose how the curve fit is to be done based on several different parameters. The coherence options are (1) none, (2) variance, and (3) coherence blanking. The none option uses all the data no matter how poor the coherence. The variance option uses some type of weighting process for using the data. The type of weighting is not documented and therefore unknown. The coherence blanking option allows the user to specify the threshold of the coherence to use in determining which data to throw out. The coherence blanking threshold used in this study was set at 0.95 so that all spectral lines in the FRFs with coherence below 0.95 were not used. Additionally, MODHAN gives one the option of how many FRFs are to be used to determine the poles and residues. This particular study used all 80 SLDV FRFs plus a driving point FRF as data input to the curve fitting process. The two measured and simulated FRFs are compared in Fig. 6-8 and Fig. 6-10. These FRFs are identical to the FRFs presented in Fig. 6-6 and Fig. 6-7. These two graphs were chosen to illustrate that the curve fits were good in the regions where the coherence was above the specified 0.95. Figure 6-8 presents an FRF with relatively good coherence across the spectrum. The residuals for both the magnitude and phase are

close to zero except on the spectral lines in the FRF where the coherence was low. The coherence plot is shown in Fig. 6-9. As can be seen by comparing the coherence and residuals, the high residuals coincide with locations of coherences below 0.95. This is because the curve fitting routine did not use any data with coherences below 0.95. The curve fit near 800 Hz is poor because the participation of adjacent modes above 800 Hz was not considered during the curve fitting process. FRF data above 800 Hz was not collected in this case. The signal-to-noise ratio for the fit is defined as the maximum peak value in the FRF divided by the standard deviation of the error residuals. The error residuals were calculated by taking the measured data and subtracting the value of the fit at the corresponding frequency. Residuals with coherence below 0.95 were not considered in the statistics because the curve fitter did not use them to determine the curve fit. The signal-to-noise ratio for the FRF at location 2 was 116.5. The mean and variance of the residuals was 0.37 and 5.1, respectively.

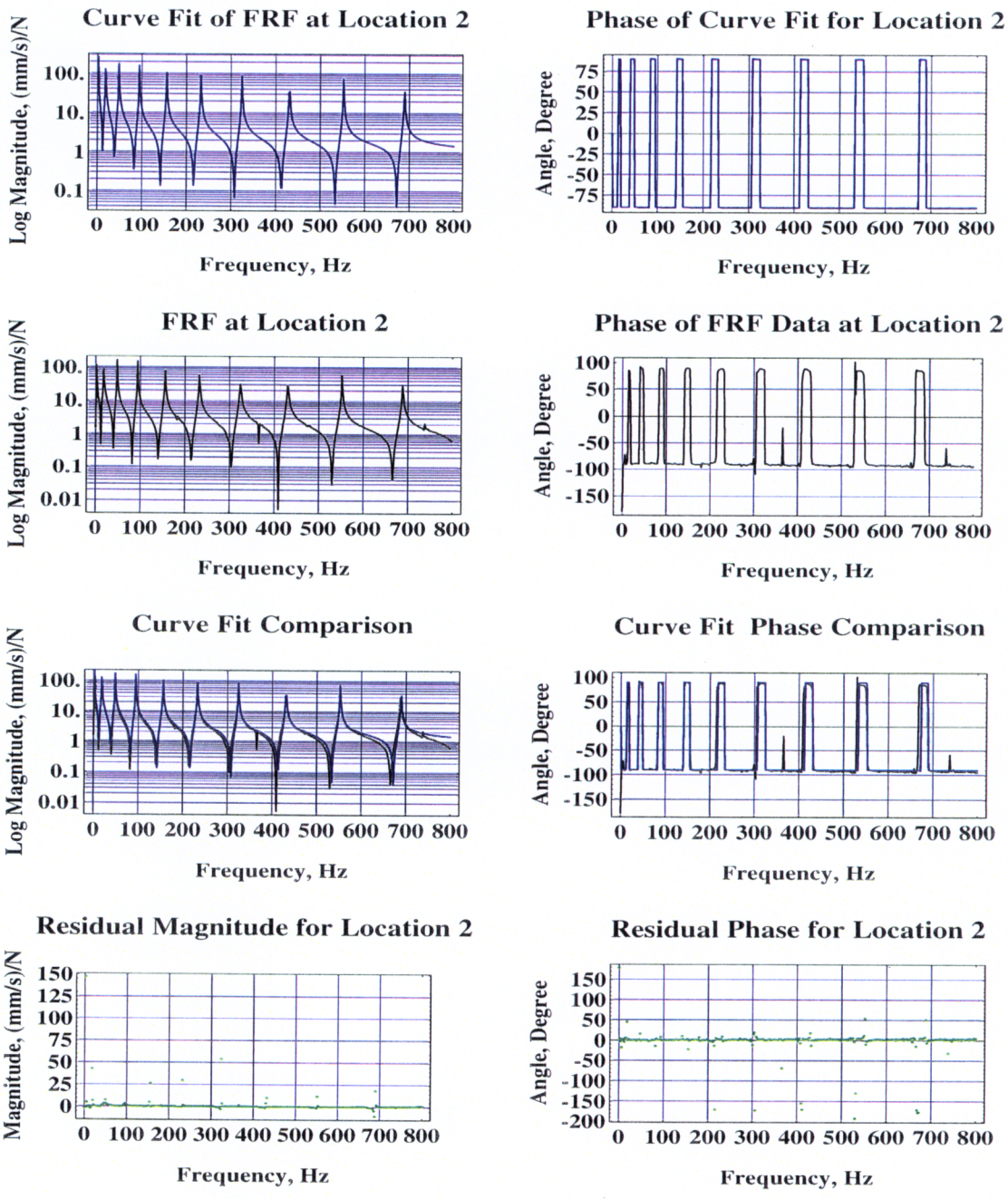

Figure 6-8 Comparison of the measured and simulated FRFs for location 2.

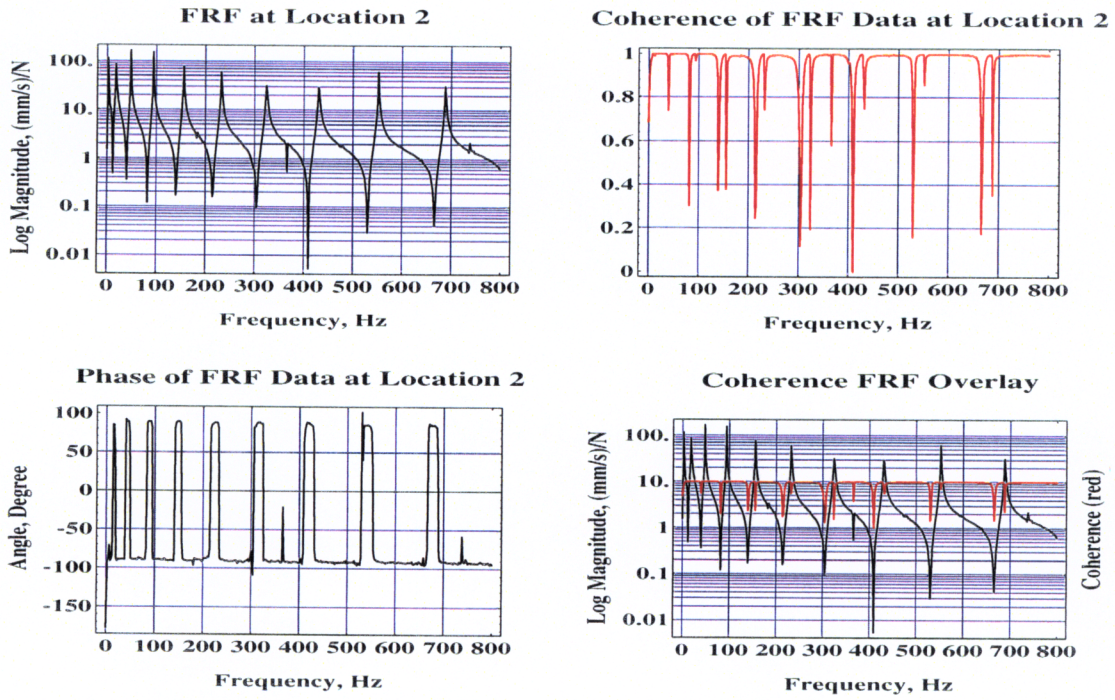

Figure 6-9 Plot of FRF and Coherence for location 2.

The curve fit of the FRF for location 31 is shown in Fig. 6-10 as well as the coherence in Fig. 6-11. The signal-to-noise ratio for the fit at location 31 was 120.2. The mean and variance of the error residuals were 0.06 and 1.1, respectively. It is again noted that the residuals of the curve fit tend to be worse at locations where the coherence was below 0.95. The overall fit of the measured FRFs was good based on the mean and variance of the error residuals and signal to noise ratio. The modal parameters, natural frequency, damping, and mode shape were determined from the poles and residues. The next section in this chapter presents the extracted modal parameters as well as a comparison of the mode shapes to modes predicted by theory.

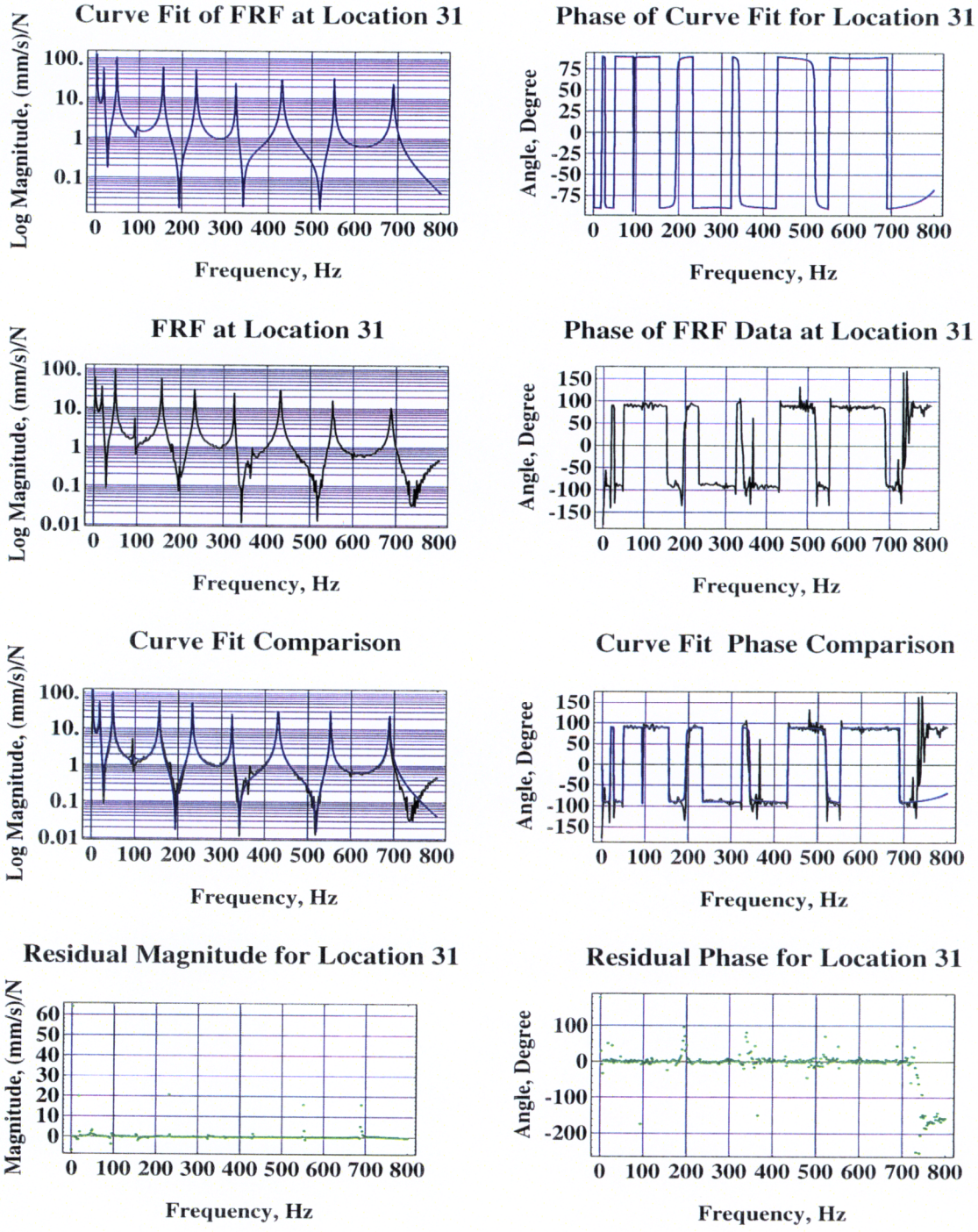

Figure 6-10 Comparison of measured and simulated FRFs for location 31.

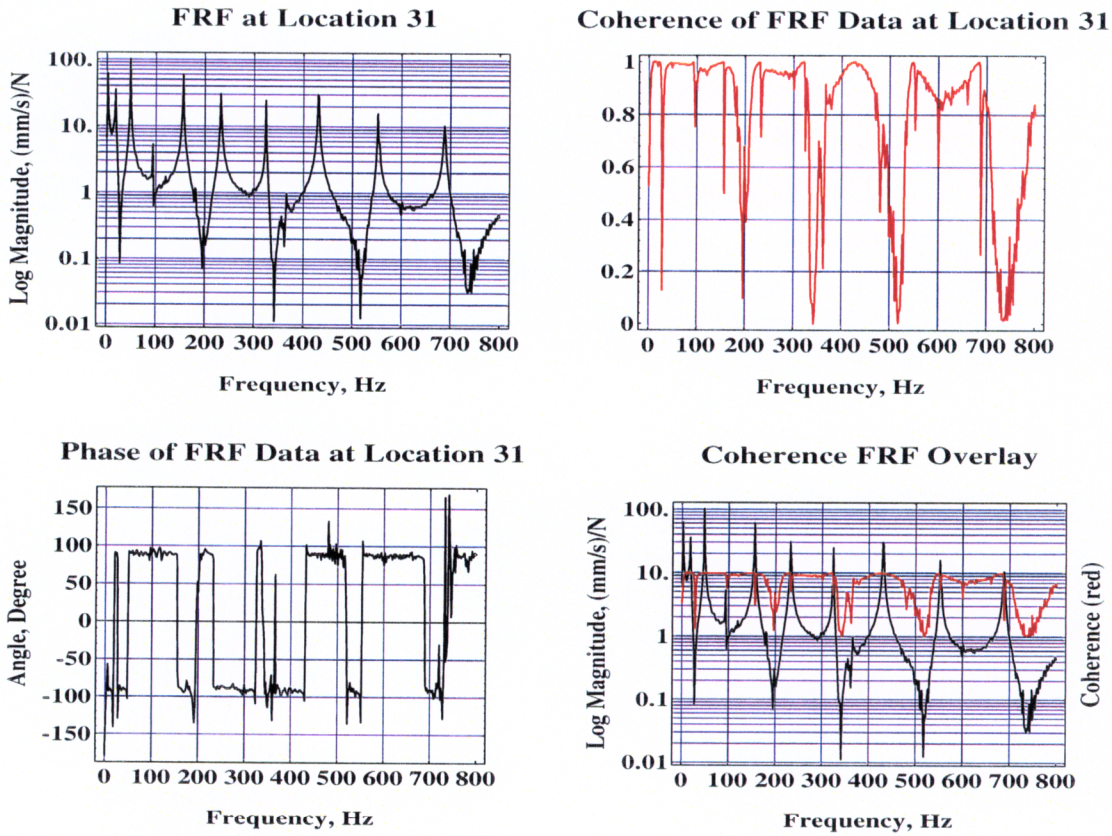

Figure 6-11 Plot of FRF and Coherence for location 31.

6.4 Results of Modal Extraction

The damping and natural frequencies that were extracted from the curve fitting process are shown in Table 6-1. The natural frequencies predicted from theory agree well with experimental natural frequencies. The percent difference between experimental and theory ranges from 2.1% to 7.61 % as can be seen in Table 6-1. The percent difference is defined in Eq. 6-18.

$$\%\,Difference = \frac{Theoretical - Experimental}{Theoretical} * 100 \qquad (6\text{-}18)$$

Table 6-1 Natural frequencies and damping.

		Rigid Body Mode	1st Mode	2nd Mode	3rd Mode	4th Mode	5th Mode	6th Mode	7th Mode
Experimental	f_r, Hz	1.8	18.4	48.3	94.3	155.5	232.5	324.4	431
	ζ_r	.0009	.0003	.00002	$5.2e^{-6}$	$7.6e^{-6}$	$3.5e^{-6}$	$2.8e^{-6}$	$4e^{-6}$
Theoretical	f_r, Hz	1.91	18.8	51.8	101.6	167.9	250.9	350.4	466.5
Natural Frequency % Difference		5.76	2.1	6.76	7.2	7.4	7.3	7.42	7.61

The extracted mode shapes for the free-free beam are shown in Fig 6-12 and Fig. 6-13. The extracted mode shapes are in good agreement, relative to the percent difference, with the shape predicted from Euler-Bernoulli theory for a free-free beam. The rigid body mode natural frequency, pendulum mode frequency, is estimated from the standard simple pendulum frequency equation of $\sqrt{\frac{g}{l}}$.[16] The natural frequency was calculated using the combined length of the monofilament, bungee cord, and half the length of the beam as the length, l. This approximate total length was 2.7 m.

The Modal Assurance Criterion, MAC, can be used to determine how orthogonal modes are within a system. MAC tables can also be used to compare experimental modes with theoretical modes.

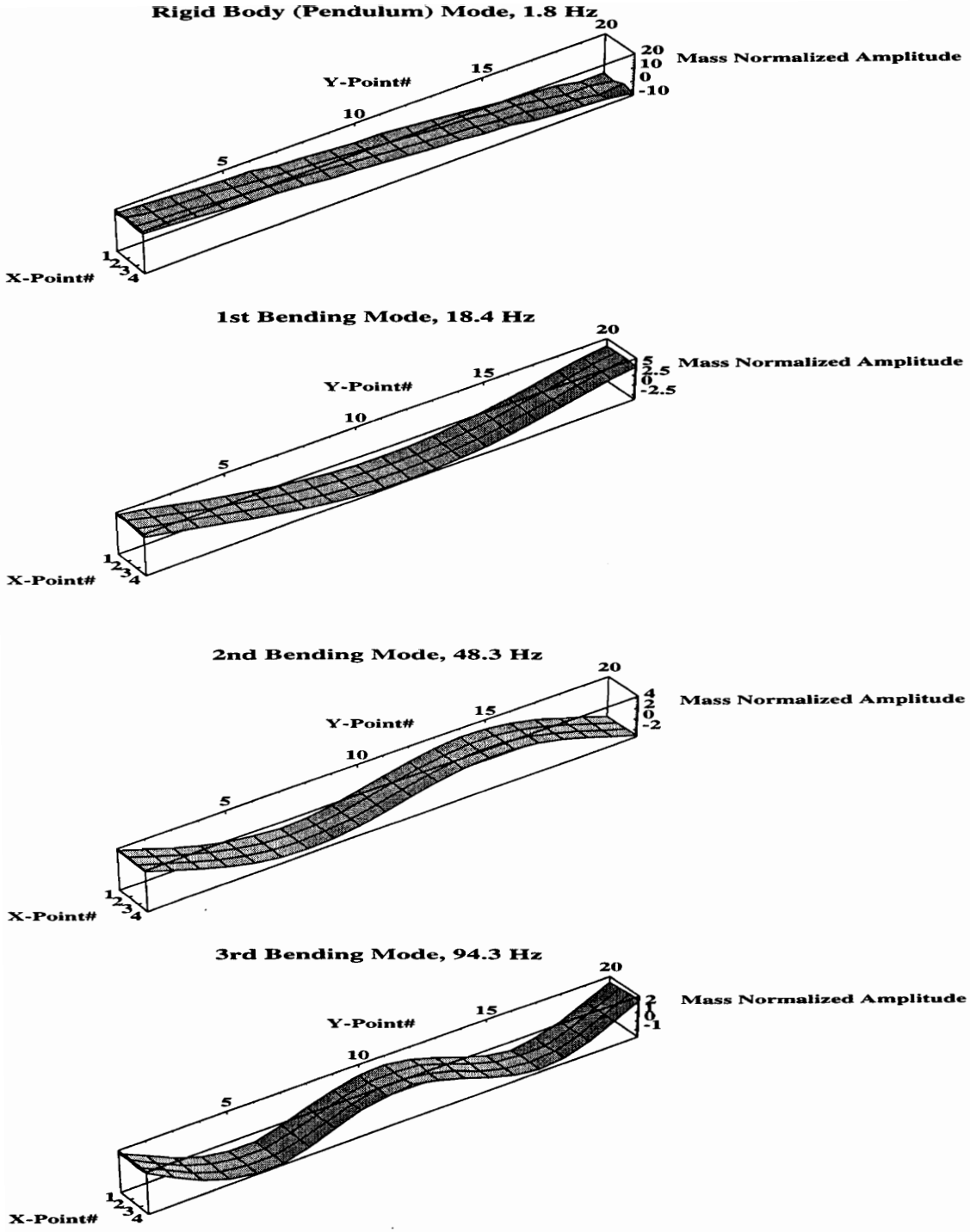

Figure 6-12 First four extracted mode shapes.

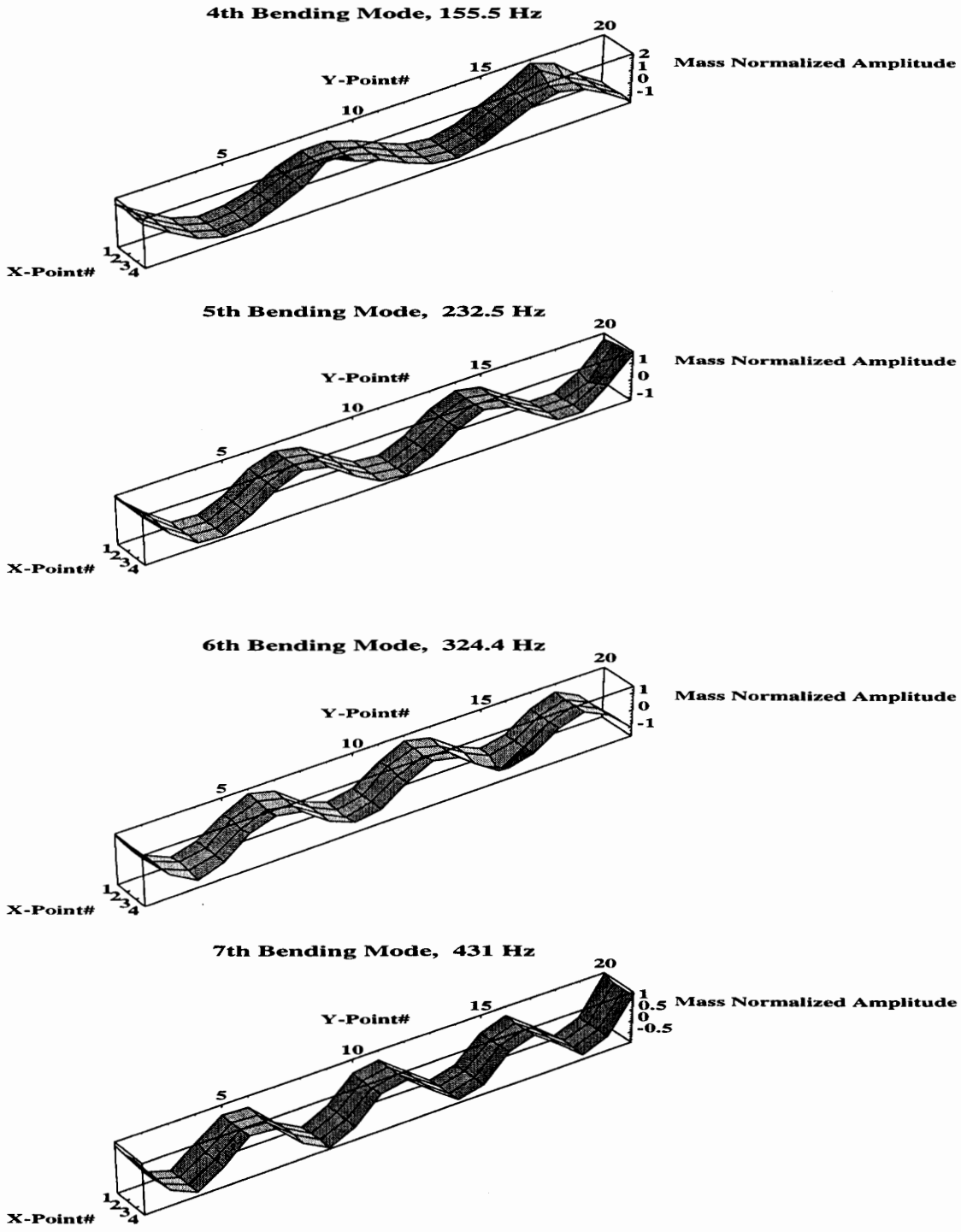

Figure 6-13 Second four extracted mode shapes

Equation 6-18 shows the equation used to compare mode shapes. MAC tables can be created to compare **N** modes by changing a and b, in Eq. 6-18, until all possible

$$MAC(a,b) = \frac{\left(\sum_{r=1}^{n} \phi_a \phi_b\right)^2}{\left(\sum_{r=1}^{n} \phi_a \phi_a^*\right)\left(\sum_{r=1}^{n} \phi_b \phi_b^*\right)} \qquad (6\text{-}18)$$

combinations have been compared. A comparison of like modes should yield unity and a comparison of orthogonal modes should yield zero.

The quality of the extracted mode shapes is determined by the off-diagonal elements of the MAC table. The closer off-diagonal elements are to zero, the closer the extracted modes are to being orthogonal. Theoretically all the modes should be orthogonal to each other and therefore no participation from other modes is present. As can be seen from Table 6-2, the off diagonals are close to zero, representative of both good mode shapes and good data. Table 6-3 shows a comparison of theoretical mode shapes with experimental. When the compared modes are the same or equal the diagonal elements of the MAC table will be equal to one. If the compared modes were exactly the same, all ones would be expected on the diagonal and zeros on the off diagonals. As can be seen in Table 6-3 the diagonals are close to one and the off diagonal elements close to zero indicative of a close experimental to theoretical match.

Table 6-2 MAC table comparing orthogonality of extracted modes.

	Rigid Mode	1st Mode	2nd Mode	3rd Mode	4th Mode	5th Mode	6th Mode
Rigid Mode	1	.0094	.0194	.0048	.0181	$.3e^{-6}$	.021
1st Mode	.0094	1	.0104	.017	.0047	.0104	.000035
2nd Mode	.0194	.0104	1	.00415	.019	$1.9e^{-9}$	.0216
3rd Mode	.0048	.017	.00415	1	.0027	.0103	.00065
4th Mode	.0181	.0047	.019	.0027	1	.00187	.017
5th Mode	$.3e^{-6}$	.0104	$1.9e^{-9}$	.0103	.00187	1	.00141
6th Mode	.021	.000035	.0216	.00065	.017	.00141	1

The first five modes have diagonal values close to unity, indicating good agreement between theoretical and experimental mode shapes.

Table 6-3 MAC table comparing experimental modes with theoretical.

	1st Mode	2nd Mode	3rd Mode	4th Mode	5th Mode	6th Mode	7th Mode
1st Mode	.97	.0069	.031	.0017	.028	.000082	.021
2nd Mode	.00082	.93	.00025	.021	.002	.06	.014
3rd Mode	.012	.00022	.93	.00042	.045	.013	.12
4th Mode	$1.3e^{-7}$	.0063	.0011	.96	.0063	.07	.019
5th Mode	.015	.00025	.014	.000012	.97	.0096	.067
6th Mode	.000043	.019	.00015	.014	.00034	.83	.0005
7th Mode	.04	.0017	.048	.000013	.011	.013	.71

Differences between the theoretical and experimental mode shapes can be attributed to (1) the fact that the system under test was not a beam with completely free-free boundary conditions, (2) the possibility of missing the contribution of a torsional mode, and (3) a possible error involved with placing laser measurements at the correct spatial location on the structure. The perfect free-free boundary

condition was not achieved in this study due to the suspension system used to hang the beam. Previous finite element work on this beam indicated a torsional mode present around 176 Hz between the 4th and 5th bending modes above. Because this structure was excited at the center line, the torsional mode received little excitation. However, referring back to Fig. 6-10 and Fig. 6-12, a possible torsional beam mode might be responsible for the glitch seen in the FRF between 175 and 200 Hz. Because the coherence of this data was below the blanking threshold the FRF curve fitting program did not use this data in the analysis. Therefore, the small participation of this mode may possibly contribute to the difference. Lastly, the registration program used to develop a transformation matrix between the laser and the structure coordinate system may not have resolved the exact locations on the structure where the data was collected. This spatial error introduces error by assigning response values at locations on the structure which are different than where the measurement was actually made. In spite of these possible errors, the experimental modes agree quite well with theory, both qualitatively and with MAC tables.

6.5 Spatial Aliasing

In the same fashion aliasing occurs in temporal signal processing because of an insufficient sampling rate, spatial aliasing occurs when the spatial measurements do not meet Shannon's sampling theorem. In order to prevent aliasing, waveforms must be sampled uniformly with more than two discrete points per wave form. Figure 6-14 shows a 2-D view of the post-processed data (both the black and red combined). The black wave form represents the 6_{th} bending mode

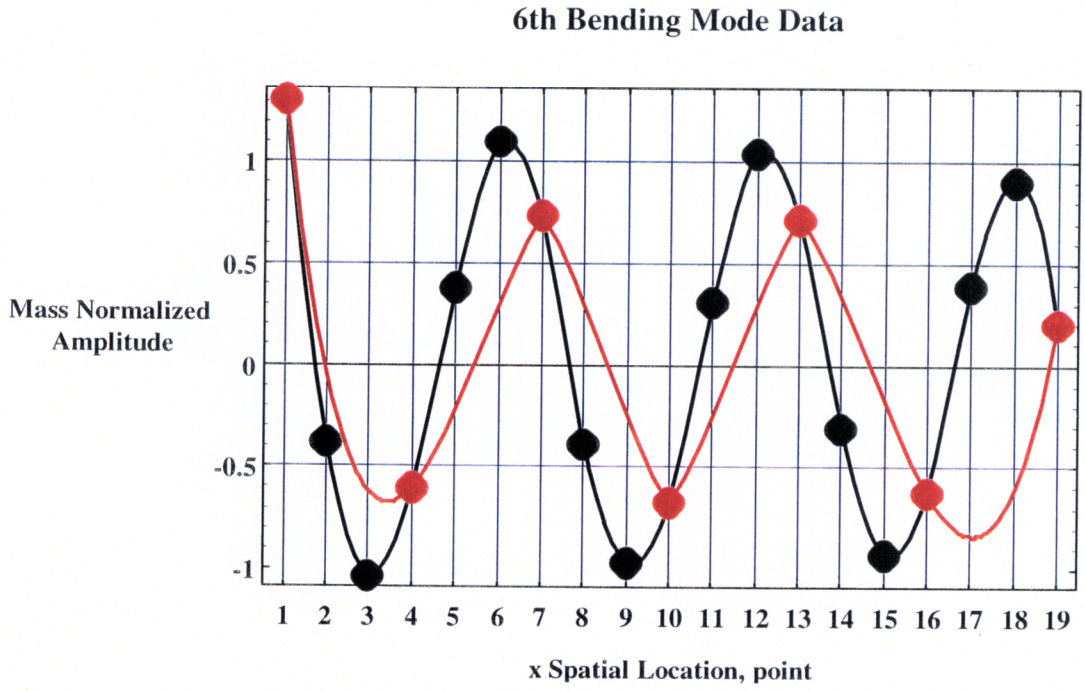

Figure 6-13 Beam Sampling points.

plot of the free-free beam which was uniformly sampled with more than the required two points per wave form. When fewer than two points per wave form are used one can expect aliasing. The red wave form shows the resulting aliased shape that occurs when fewer than the required two points per wave form are sampled. Aliasing causes the data to appear to have frequency content lower than what actually existed. In the case of spatial data, aliasing results in a misrepresentation of the operating shape.

This test used the FRFs at a total of 80 points to characterize the beam: four points along the width by twenty points along the length. If fewer points were used, as would typically be done with accelerometers, the spatial fidelity of the mode shapes would be reduced significantly even for this simple structure. Figure 6-14 shows the 3-D view of the post-processed beam data. The bottom figure is shown with only twenty-eight spatial locations (4 by 7) rather than eighty (4 by 80) used in the top figure. The bottom figure does not give the correct mode shape due to spatial aliasing. As can be seen by this comparison, a lack of spatial measurements can cause incomplete information and lead to erroneous interpretation of the data.

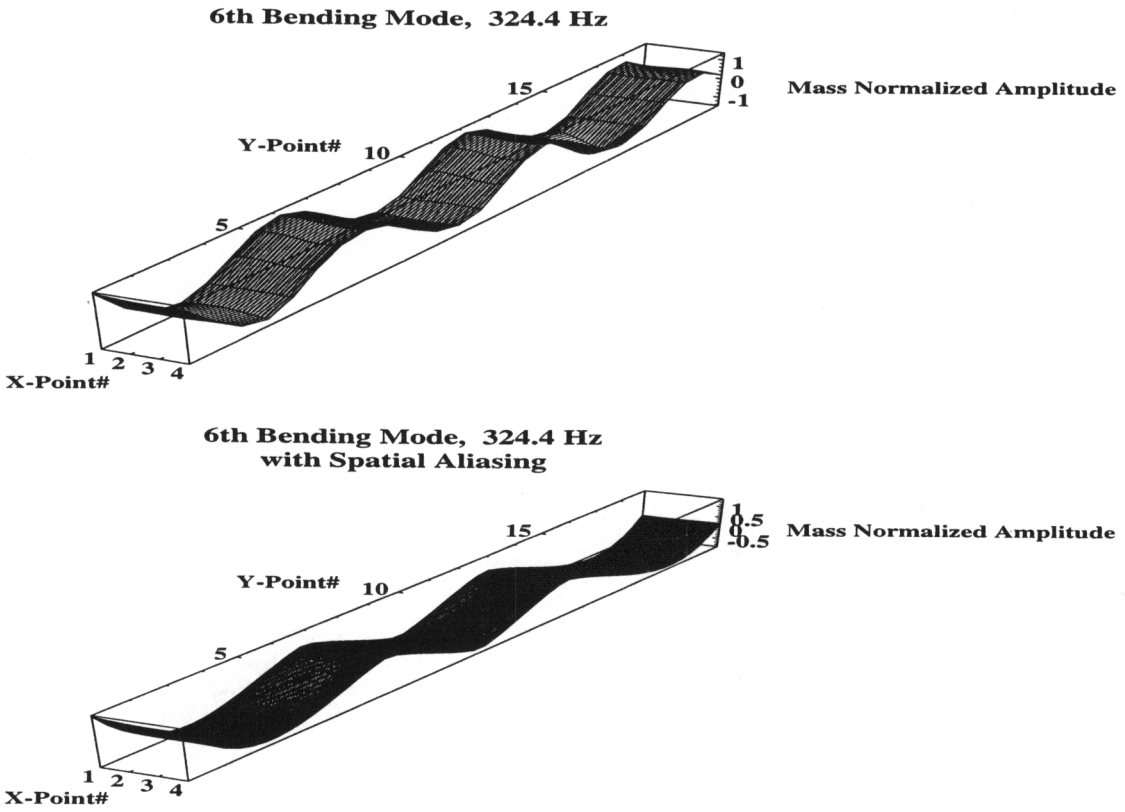

Figure 6-14 Demonstration of spatial aliasing.

Chapter 7
Conclusions

This chapter contains three sections which present the research summary, conclusions, and recommendations The first section summarizes the goal and objectives of this thesis. The second section presents the conclusions drawn from this research evaluated against the goals and objectives of this thesis. The last section outlines recommendations for further research.

7.1 Research Summary

The goal of this thesis was to develop the test capability of measuring spatially dense broad-band frequency data as well as to exploit the high spatial measuring capabilities of the SLDV. This was done by interfacing the SLDV and a HP 35665A frequency analyzer.

In order to use the SLDV over a range of frequencies, the frequency response of the laser had to be characterized. Compensation for phase shift and

magnitude attenuation was performed using the frequency response of the laser relative to a reference accelerometer with the same frequency range and laser setting as used for the corresponding test.

The GPIB interface standard provided the basis for programming and interfacing a Silicon Graphics workstation, digital-to-analog converter (DAC), and a frequency analyzer. Voltages to control the deflection of the laser beam were provided by the DAC. Frequency response function measurements of a structure were collected and analyzed with an HP frequency analyzer. Using the Silicon Graphics workstation as the user to interface instrument controller, a program was written to control both the signal analyzer and the DAC, providing control to deflect the laser beam from one spatial location to another. The collection and downloading of frequency response data from the frequency analyzer was also controlled by the control program.

Post processing of the raw data was performed in order to present accurate mobility plots. The correct mobility plots were calculated by using the laser characterization, angle corrections, and calibration constants.

The developed acquisition system was applied to the testing of a beam/suspension system simulating a beam with free-free boundary conditions. The process of defining registration points and setting up the beam as well as post processing of the data was completed The resulting FRF magnitude and phase

plots along with the corresponding coherence plots were presented.

The FRF and coherence data was imported into the FRF curve-fitting program, MODHAN. The curve-fitting program fit the experimentally gathered FRF data, returning the poles and residues necessary for determining the natural frequencies, damping, and mode shapes.

7.2 Summary of Conclusions

The overall conclusion of this research is that the developed system for collecting broad-band spatially dense data provides a data set with more spatial measurements than typically found in conventional modal testing. The data acquisition system provides data that can be used to explore the characterization of dynamic systems with high spatial density broad-band frequency data. The modal analysis performed showed that the data acquired could be used to predict natural frequencies, damping, and mode shapes. The results from the modal analysis were compared to beam theory and good agreement resulted, demonstrating that the data acquired by this system, when properly acquired, can be used in subsequent analysis.

Use of the laser over a broad-band of frequencies was found to introduce

phase and magnitude errors. A compensation for these errors can be determined and applied to the laser measurements so that the laser can be used to make broad-band frequency vibration measurements. The compensation was achieved by characterizing the laser with an accelerometer as a reference. In the case studied, a fourth-order complex polynomial was sufficient to characterize the laser's calibration curve needed to correct the measured FRFs. This process worked very well and the corrected phase correctly depicted phase measurements expected from structural vibrations.

The GPIB interface standard was successfully used to interface the SLDV and an HP 35665A frequency analyzer. Using IBIC, a test script was automatically generated to carry out automated laser based broad-band spatially dense vibration response measurements of rectangular scan areas. The program creates files for both the FRF and coherence of each point on the structure defined by the scan grid. The program allows the scanning grid to be set by the user. The GPIB interface and script file to command the data acquisition made it possible to prototype the system and complete the acquisition system goals. However, implementing this process with another programming language would combine many of these step by step processes into one. With another programming language the registration process and acquisition of data would be done in sequence rather than by running Mathematica first and then IBIC.

The raw FRF voltage data from the scanning process can be corrected by using the developed post-processing program "ibicprocess". "ConvertScans" is used to acquire the necessary direction cosine angles and positions of the measurements. Once this process is complete, corrections based on the direction cosines, calibration constants of the laser and force gage, and compensation for the laser's frequency response can be made, creating the corrected data needed to create FRF magnitude and phase plots. The creation of the different plots for each location is done in one large process with the end result being a list of plot files that can be viewed with a postscript viewer or printed. This process was very useful especially when changes to the plots were needed. The changes would be made once and then the program would recreate all the plots. "ConvertScans", on the other hand, had difficulty with this beam. The beam was too thin for the registration program to accurately place the measurements. Getting satisfactory results required a great deal of time during the registration process to ensure the registration points were as accurate as possible. However, it still seems that a better approach to solving this problem can be found.

The mobility (FRF) data and coherence data were analyzed with an FRF curve-fitting routine to determine the poles and residues of the system. Natural frequencies, damping, and modes shapes were determined using the poles and residues from the curve fit. Using MAC tables the quality of the extracted modes

was found to be very close to being orthogonal. The experimental mode shapes, when compared to the mode shapes predicted by theory, were found to have good correlation through the fifth bending mode. The natural frequencies also agreed well with theory. This process showed that the data was indeed reliable and useful for extracting modal parameters.

Spatial aliasing was demonstrated using one third the spatial information of the original test case. Modeling the beam with fewer points showed how mode shape information can be misrepresented when too few points are used to describe the spatial domain.

7.3 Recommendations

This thesis provides a tool for acquiring spatially dense broad-band data. The time required to gather data has been reduced by using the SLDV as the transducer. However, additional time can be saved by implementing a procedure that incorporates registration, data collection, and post processing. Combining these methods into an integrated control program will make the process much more cohesive and therefore easier to carry out. Integration of this process will also save the time required to prepare and complete each step.

It was found in this process that the registration procedure was very sensitive to the location of the registration points relative to each other. Because this test involved a long slender beam, the location of the registration from side to side was small and inherently introduced error into the structure to laser transformation. Since it is necessary at times to deal with this type of structure, a way of providing points off the structure in the structure's coordinate system would provide a larger footprint and therefore remove the ill-conditioning of the registration problem for this case. The result is that the registration would be more accurate. The more accurate transformation would then lead to points that were placed back on the structure with less spatial error.

Collecting spatially dense broad-band data on more complex structures and using it to complete both modal analysis and update FE models would provide some quantitative studies for realizing the full benefits and limitations of the system. However, additional testing on other simple structures is needed to determine the advantages and limitations of the spatial and frequency measurements collected by this system.

References

[1]Wicks, A. L., Kochersburger, K., and Mitchell, L. D., "Laser Structural Imaging," *Proceedings of the 2nd USAF/NASA Workshop System Identification and Health Monitoring of Precision Space Structures*, March 27-29, 1990, California Institute of Technology, Pasadena California, pp. 24-42.

[2]Agee, B. L., Kelly, A. D., and Mitchell, L. D., "Finite Element Model Updating Using Laser-Based Experimental Dynamics for Noise Prediction Purposes," Won Noise-Con 91 Student Paper Contest, *Proceedings of Noise-Con 91*, Tarrytown, NY, 14-16 July 1991, pp. 657-666.

[3]Sriram, P., Hanagud, S., and Craig, J.I., "Mode Shape Measurement Using a Scanning Laser Doppler Vibrometer," *International Journal of Analytical and Experimental Modal Analysis*, Vol 7, No 3, July 1992, pp169-178.

[4]Mitchell, L. D., Kochersberger, K., and West, R. L., "Measurement of a One-Dimensional Mobility Using A Laser Doppler Velocimeter," presented at and published in *Proceedings of the society of Experimental Mechanics Spring Conference*, Milwaukee, WI, June 10-13, 1991, pp. 846-853.

[5]Kochersberger, K., *A Method of Determining Modal Residues Using an Improved Residual Model and Least Squares*, Ph.D. dissertation., Virginia Polytechnic Institute & State University, Blacksburg, VA, 1994.

[6]Mitchell, L. D., Agee, B. L, West, .R. L., and Wicks, A. L., "Development of a Laser-Based Automated Structural Mobility Measurement System.," *Proceedings of a the 1992 NSF Structures, Geomechanics, and Building Systems Grantees Conference*, San Juan, Puerto Rico, 10-12 June 1992, pp. 74-76.

[7]Polytec PI, Inc., *Polytec Scanning Vibrometer,*PSV-E-4-9504-2.0.

[8]Ometron Inc., *VPI 4000 Vibration Pattern Imager,* V400/7/695.

[9]IOtech, Inc., *DAC488 Instruction Manual,* Part No. DAC488/4-901,Cleveland,Ohio, 1989.

[10]Wicks, A. L., Class Notes, ME 5714, Signal Processing, Fall 1995.

[11]Drain, L.E., *The Laser Doppler Technique*, John Wiley & Sons Ltd., Chichester, 1980.

[12]Yeh, Y. And Cummins, H. Z., Applied Physics Letters, 4, pp. 176-178. 1964.

[13]Montgomery, D.L., *Modeling and Visualization of Laser-based Three-Dimensional Experimental Spatial Dynamic Response*, Ph.D. dissertation, Virginia Polytechnic Institute & State University, Blacksburg, VA, 1993.

[14]James, M.L., Smith, G. M., Wiford, J. C., and Whaley, P. W., *Vibration of Mechanical and Structural Systems: With Microcomputer Applications*, Harper & Row, Publishers, New York, 1989.

[15]Han, M. C., and Wicks, A. L., "On the Application of Forsythe Orthogonal Polynomials for Global Modal Parameter Estimation," *Proceedings of the seventh International Modal Analysis Conference*, 1989.

[16]Serway, Raymond A., *Physics for Scientists & Engineers,* Saunders College Publishing, Philadelphia, 1986.

Appendix A Program Code

correction -

This Mathematica program reads in the FRF data from the characterization of the laser filters and fits complex polynomials 1st order through 4th order. It also determines the mean residuals, variances and sum square errors. Additionally, it produces postscript plots containing comparisons of the raw and fitted data for magnitude and phase as well as a plot comparing variance as a function of polynomial order up to 20. Calibration constants for the PCB 307A sn 996 accelerometer and low setting constants for the laser have been applied as well as the accelerometer data multiplied by jω to convert to velocity. Plot files are saved as LFIX1 through LFIX4 and ORD1 for magnitude and phase and variance comparison, respectively.

```
<<Statistics`DescriptiveStatistics`
SetDirectory["/disk2/users/monty/BEAMDAT"];
<<LFIX; (*Reads in the file with the Print file names and margins for the postscript file.*)
(*Next lines read in the files FILTCOH and FILTFRF in column format*)
filtcoh = OpenRead["/disk2/users/monty/BEAMDAT/FILTCOH"];
coh = Table[Read[filtcoh,{Number,Number}],{401}];
Close[filtcoh];
filtfrf = OpenRead["/disk2/users/monty/BEAMDAT/FILTFRF"];
frf = Table[Read[filtfrf,{Number,Number,Number}],{401}];
Close[filtfrf];
reim=Table[{frf[[i,1]],(frf[[i,2]]+I*frf[[i,3]])},{i,1,401}];
(*Next line applies the calibration constants of the accelerometer and SLDV and also converts the
acceleration to velocity and the units to Hz.*)
REIM=Table[{reim[[i,1]],N[I*2*Pi*reim[[i,1]]*reim[[i,2]]*
(1/7.620)/(386.4/.1005)]},{i,20,401}];
(*Fits a line to the data*)
FIT[w_]=Fit[REIM,{1,w},w]
FITData=Table[FIT[w],{w,38,800,2}];

(*Calculates the residuals*)
RESID=Table[FITData[[i]]-REIM[[i,2]],{i,1,382}];
(*Calculates the mean residual*)
MR=Mean[RESID];Print["Mean Residual = ",MR]
(*Calculates the Variance of Residuals *)
VR[1]=Variance[RESID];Print["Variance of Residual = ",VR[1]]
(*Calculates the Sum Square Error*)
SSE=SumSquareError=(Sum[RESID[[i]]^2,{i,1,382}])^.5;
Print["Sum Square Error = ",SSE]
(*Creates a table of the magnitudes for the fit data*)
MagFIT=Table[{w,Abs[FIT[w]]},{w,38,800,2}];
(*Creates a table of the phases for the fit data*)
PhaseFIT=Table[{w,Arg[FIT[w]]*180/Pi},{w,38,800,2}];
(*Creates a table of the phases for the actual data*)
phasedat=Table[{REIM[[i,1]],Arg[REIM[[i,2]]]*180/Pi},{i,1,382}];
```

```
(*Creates a table of the magnitudes for the actual data*)
magdat=Table[{REIM[[i,1]],Abs[REIM[[i,2]]]},{i,1,382}];
(*Creates a table of the phase residuals*)
Residphase=Table[{phasedat[[i,1]],phasedat[[i,2]]-PhaseFIT[[i,2]]},
{i,1,382}];
(*Creates a table of the magnitude residuals *)
Residmag=Table[{magdat[[i,1]],magdat[[i,2]]-MagFIT[[i,2]]},
{i,1,382}];
(*Prepares a Plot of the fit phase*)
FitPhase=Plot[Arg[FIT[w]]*180/Pi,{w,0,800},PlotRange->All,
DisplayFunction->Identity,
Frame->True,FrameLabel->{"Frequency, hz","Phase Angle, degress",
FontForm["Phase for the Fitted Equation",
{"Times-BoldItalic",14}]," " },AxesOrigin->{0,0}];
(*Prepares a plot of the actual phase*)
DataPhase=ListPlot[phasedat,PlotStyle->RGBColor[1,0,0],
Frame->True,FrameLabel->{"Frequency, hz","Phase Angle, degress",
FontForm["Phase for Actual Data",
{"Times-BoldItalic",14}]," " },DisplayFunction->Identity,
AxesOrigin->{0,0}];
(*Prepares a plot of the overlay of the fit and data for the phase.*)
P1=Show[{DataPhase,FitPhase},PlotRange->All,
DisplayFunction->Identity,
FrameLabel->{"Frequency, hz","Phase Angle, degress",
FontForm["Actual Data and Fitted Equation for Phase",
{"Times-BoldItalic",14}]," " },AxesOrigin->{0,0}];
(*Prepares a plot of the phase residuals*)
P2=ListPlot[Residphase,PlotStyle->RGBColor[1,0,1],
PlotRange->All,
DisplayFunction->Identity,
Frame->True,FrameLabel->{"Frequency, hz","Residual, degress",
FontForm["Phase Residuals for the Linear Fit",
{"Times-BoldItalic",14}]," "},AxesOrigin->{0,0}];FitMag=Plot[Abs[FIT[w]],
{w,0,800},PlotRange->All,
DisplayFunction->Identity,
Frame->True,FrameLabel->{"Frequency, hz","Magnitude, Laser/Accel",
FontForm["Laser Accel./Accelermoeter Accel. for Fitted Equation",
{"Times-BoldItalic",14}]," " },AxesOrigin->{0,0}];DataMag=ListPlot[magdat,
PlotStyle->RGBColor[1,0,0],
Frame->True,FrameLabel->{"Frequency, hz","Magnitude, Laser/Accel",
FontForm["Laser Acceleration/Accelermoeter Acceleration for Actual Data",
{"Times-BoldItalic",14}]," " },DisplayFunction->Identity,AxesOrigin->{0,0}];
(*Prepares a plot of the overlay of the fit and data for the magnitude.*)
P3=Show[DataMag,FitMag,PlotRange->All,
DisplayFunction->Identity,
Frame->True,FrameLabel->{"Frequency, hz","Magnitude, Laser/Accel",
FontForm["Actual Data and Fitted Equation for Magnitude",
{"Times-BoldItalic",14}]," " },AxesOrigin->{0,0}];
(*Prepares a plot of the magnitude residuals*)
```

```
P4=ListPlot[Residmag,PlotStyle->RGBColor[1,0,1],
PlotRange->All,DisplayFunction->Identity,
Frame->True,FrameLabel->{"Frequency, hz","Magnitude, Laser/Accel",
FontForm["Magnitude Residuals for the Linear Fit",
{"Times-BoldItalic",14}]," " },AxesOrigin->{0,0}];
(*Create a postscript file with a graphics array showing the phase and the magnitude with both the
fit and data overlayed as well as residual plots*)
Display[Lfix[[1]],GraphicsArray[{{P1,P3},{P2,P4}}]]

(*Continues as above adding a degree to the polynomial*)
FIT[w_]=Fit[REIM,{1,w,w^2},w]
FITData=Table[FIT[w],{w,38,800,2}];

RESID=Table[FITData[[i]]-REIM[[i,2]],{i,1,382}];
MR=Mean[RESID];Print["Mean Residual = ",MR]
VR[2]=Variance[RESID];Print["Variance of Residual = ",VR[2]]
SSE=SumSquareError=(Sum[RESID[[i]]^2,{i,1,382}])^.5;
Print["Sum Square Error = ",SSE]

MagFIT=Table[{w,Abs[FIT[w]]},{w,38,800,2}];
PhaseFIT=Table[{w,Arg[FIT[w]]*180/Pi},{w,38,800,2}];
phasedat=Table[{REIM[[i,1]],Arg[REIM[[i,2]]]*180/Pi},{i,1,382}];
magdat=Table[{REIM[[i,1]],Abs[REIM[[i,2]]]},{i,1,382}];
Residphase=Table[{phasedat[[i,1]],phasedat[[i,2]]-PhaseFIT[[i,2]]},
{i,1,382}];
Residmag=Table[{magdat[[i,1]],magdat[[i,2]]-MagFIT[[i,2]]},
{i,1,382}];
FitPhase=Plot[Arg[FIT[w]]*180/Pi,{w,0,800},PlotRange->All,
DisplayFunction->Identity,
Frame->True,FrameLabel->{"Frequency, hz","Phase Angle, degress",
FontForm["Phase for the Fitted Equation",
{"Times-BoldItalic",14}]," " },AxesOrigin->{0,0}];
DataPhase=ListPlot[phasedat,PlotStyle->RGBColor[1,0,0],
DisplayFunction->Identity,
Frame->True,FrameLabel->{"Frequency, hz","Phase Angle, degress",
FontForm["Phase for Actual Data",
{"Times-BoldItalic",14}]," " },AxesOrigin->{0,0}];
P1=Show[{DataPhase,FitPhase},PlotRange->All,
DisplayFunction->Identity,
FrameLabel->{"Frequency, hz","Phase Angle, degress",
FontForm["Actual Data and Fitted Equation for Phase",
{"Times-BoldItalic",14}]," " },AxesOrigin->{0,0}];
P2=ListPlot[Residphase,PlotStyle->RGBColor[1,0,1],PlotRange->All,
DisplayFunction->Identity,
Frame->True,FrameLabel->{"Frequency, hz","Residual, degress",
FontForm["Phase Residuals for the 2nd Order Fit",
{"Times-BoldItalic",14}]," "},AxesOrigin->{0,0}];
FitMag=Plot[Abs[FIT[w]],{w,0,800},PlotRange->All,
DisplayFunction->Identity,
```

```
Frame->True,FrameLabel->{"Frequency, hz","Magnitude, Laser/Accel",
FontForm["Laser Accel./Accelermoeter Accel. for Fitted Equation",
{"Times-BoldItalic",14}]," " },AxesOrigin->{0,0}];
DataMag=ListPlot[magdat,PlotStyle->RGBColor[1,0,0],
DisplayFunction->Identity,
Frame->True,FrameLabel->{"Frequency, hz","Magnitude, Laser/Accel",
FontForm["Laser Acceleration/Accelermoeter Acceleration for Actual Data",
{"Times-BoldItalic",14}]," " },AxesOrigin->{0,0}];
P3=Show[DataMag,FitMag,PlotRange->All,DisplayFunction->Identity,
Frame->True,FrameLabel->{"Frequency, hz","Magnitude, Laser/Accel",
FontForm["Actual Data and Fitted Equation for Magnitude",
{"Times-BoldItalic",14}]," " },AxesOrigin->{0,0}];
P4=ListPlot[Residmag,PlotStyle->RGBColor[1,0,1],
PlotRange->All,DisplayFunction->Identity,
Frame->True,FrameLabel->{"Frequency, hz","Magnitude, Laser/Accel",
FontForm["Magnitude Residuals for the 2nd Order Fit",
{"Times-BoldItalic",14}]," " },AxesOrigin->{0,0}];
Display[Lfix[[2]],GraphicsArray[{{P1,P3},{P2,P4}}]]

(*Continues as above adding a degree to the polynomial*)
FIT[w_]=Fit[REIM,{1,w,w^2,w^3},w]
FITData=Table[FIT[w],{w,38,800,2}];

RESID=Table[FITData[[i]]-REIM[[i,2]],{i,1,382}];
MR=Mean[RESID];Print["Mean Residual = ",MR]
VR[3]=Variance[RESID];Print["Variance of Residual = ",VR[3]]
SSE=SumSquareError=(Sum[RESID[[i]]^2,{i,1,382}])^.5;
Print["Sum Square Error = ",SSE]

MagFIT=Table[{w,Abs[FIT[w]]},{w,38,800,2}];
PhaseFIT=Table[{w,Arg[FIT[w]]*180/Pi},{w,38,800,2}];
phasedat=Table[{REIM[[i,1]],Arg[REIM[[i,2]]]*180/Pi},{i,1,382}];
magdat=Table[{REIM[[i,1]],Abs[REIM[[i,2]]]},{i,1,382}];
Residphase=Table[{phasedat[[i,1]],phasedat[[i,2]]-PhaseFIT[[i,2]]},
{i,1,382}];
Residmag=Table[{magdat[[i,1]],magdat[[i,2]]-MagFIT[[i,2]]},
{i,1,382}];
FitPhase=Plot[Arg[FIT[w]]*180/Pi,{w,0,800},PlotRange->All,
DisplayFunction->Identity,
Frame->True,FrameLabel->{"Frequency, hz","Phase Angle, degress",
FontForm["Phase for the Fitted Equation",
{"Times-BoldItalic",14}]," " },AxesOrigin->{0,0}];
DataPhase=ListPlot[phasedat,PlotStyle->RGBColor[1,0,0],
DisplayFunction->Identity,
Frame->True,FrameLabel->{"Frequency, hz","Phase Angle, degress",
FontForm["Phase for Actual Data",
{"Times-BoldItalic",14}]," " },AxesOrigin->{0,0}];
P1=Show[{DataPhase,FitPhase},PlotRange->All,
DisplayFunction->Identity,
```

```
FrameLabel->{"Frequency, hz","Phase Angle, degress",
FontForm["Actual Data andFitted Equation for Phase",
{"Times-BoldItalic",14}]," " },AxesOrigin->{0,0}];
P2=ListPlot[Residphase,PlotStyle->RGBColor[1,0,1],PlotRange->All,
DisplayFunction->Identity,
Frame->True,FrameLabel->{"Frequency, hz","Residual, degress",
FontForm["Phase Residuals for the 3rd Order Fit",
{"Times-BoldItalic",14}]," "},AxesOrigin->{0,0}];
FitMag=Plot[Abs[FIT[w]],{w,0,800},PlotRange->All,
DisplayFunction->Identity,
Frame->True,FrameLabel->{"Frequency, hz","Magnitude, Laser/Accel",
FontForm["Laser Accel./Accelermoeter Accel. for Fitted Equation",
{"Times-BoldItalic",14}]," " },AxesOrigin->{0,0}];
DataMag=ListPlot[magdat,PlotStyle->RGBColor[1,0,0],
DisplayFunction->Identity,
Frame->True,FrameLabel->{"Frequency, hz","Magnitude, Laser/Accel",
FontForm["Laser Acceleration/Accelermoeter Acceleration for Actual Data",
{"Times-BoldItalic",14}]," " },AxesOrigin->{0,0}];
P3=Show[DataMag,FitMag,PlotRange->All,DisplayFunction->Identity,
Frame->True,FrameLabel->{"Frequency, hz","Magnitude, Laser/Accel",
FontForm["Actual Data and Fitted Equation for Magnitude",
{"Times-BoldItalic",14}]," " },AxesOrigin->{0,0}];
P4=ListPlot[Residmag,PlotStyle->RGBColor[1,0,1],
PlotRange->All,DisplayFunction->Identity,
Frame->True,FrameLabel->{"Frequency, hz","Magnitude, Laser/Accel",
FontForm["Magnitude Residuals for the 3rd Order Fit",
{"Times-BoldItalic",14}]," " },AxesOrigin->{0,0}];
Display[Lfix[[3]],GraphicsArray[{{P1,P3},{P2,P4}}]]

REIMM=Table[{reim[[i,1]]/1000,N[I*2*Pi*reim[[i,1]]*reim[[i,2]]*
(1/7.620)/(386.4/.1005)]},{i,20,401}];
FIT[w_]=Fit[REIMM,{1,w,w^2,w^3,w^4},w]/.w->w/1000
FITData=Table[FIT[w],{w,38,800,2}];
RESID=Table[FITData[[i]]-REIM[[i,2]],{i,1,382}];
MR=Mean[RESID];Print["Mean Residual = ",MR]
VR[4]=Variance[RESID];Print["Variance of Residual = ",VR[4]]
SSE=SumSquareError=(Sum[RESID[[i]]^2,{i,1,382}])^.5;
Print["Sum Square Error = ",SSE]
MagFIT=Table[{w,Abs[FIT[w]]},{w,38,800,2}];
PhaseFIT=Table[{w,Arg[FIT[w]]*180/Pi},{w,38,800,2}];
phasedat=Table[{REIM[[i,1]],Arg[REIM[[i,2]]]*180/Pi},{i,1,382}];
magdat=Table[{REIM[[i,1]],Abs[REIM[[i,2]]]},{i,1,382}];
Residphase=Table[{phasedat[[i,1]],phasedat[[i,2]]-PhaseFIT[[i,2]]},
{i,1,382}];
Residmag=Table[{magdat[[i,1]],magdat[[i,2]]-MagFIT[[i,2]]},
{i,1,382}];
FitPhase=Plot[Arg[FIT[w]]*180/Pi,{w,38,800},PlotRange->All,
DisplayFunction->Identity,
Frame->True,FrameLabel->{"Frequency, hz","Phase Angle, degress",
```

```
FontForm["Phase for the Fitted Equation",
{"Times-BoldItalic",14}]," " },AxesOrigin->{0,0}];
DataPhase=ListPlot[phasedat,PlotStyle->RGBColor[1,0,0],
DisplayFunction->Identity,
Frame->True,FrameLabel->{"Frequency, hz","Phase Angle, degress",
FontForm["Phase for Actual Data",
{"Times-BoldItalic",14}]," " },AxesOrigin->{0,0}];
P1=Show[{DataPhase,FitPhase},PlotRange->All,
DisplayFunction->Identity,
FrameLabel->{"Frequency, hz","Phase Angle, degress",
FontForm["Actual Data and Fitted Equation for Phase",
{"Times-BoldItalic",14}]," " },AxesOrigin->{0,0}];
P2=ListPlot[Residphase,PlotStyle->RGBColor[1,0,1],PlotRange->All,
DisplayFunction->Identity,
Frame->True,FrameLabel->{"Frequency, hz","Residual, degress",
FontForm["Phase Residuals for the 4th Order Fit",
{"Times-BoldItalic",14}]," "},AxesOrigin->{0,0}];
FitMag=Plot[Abs[FIT[w]],{w,38,800},PlotRange->All,
DisplayFunction->Identity,
Frame->True,FrameLabel->{"Frequency, hz","Magnitude, Laser/Accel",
FontForm["Magnitude for Fitted Equation",
{"Times-BoldItalic",14}]," " },AxesOrigin->{0,0}];
DataMag=ListPlot[magdat,PlotStyle->RGBColor[1,0,0],
DisplayFunction->Identity,
Frame->True,FrameLabel->{"Frequency, hz","Magnitude, Laser/Accel",
FontForm["Magnitude for Actual Data",
{"Times-BoldItalic",14}]," " },AxesOrigin->{0,0}];
P3=Show[DataMag,FitMag,PlotRange->All,DisplayFunction->Identity,
Frame->True,FrameLabel->{"Frequency, hz","Magnitude, Laser/Accel",
FontForm["Actual Data and Fitted Equation for Magnitude",
{"Times-BoldItalic",14}]," " },AxesOrigin->{0,0}];
P4=ListPlot[Residmag,PlotStyle->RGBColor[1,0,1],
PlotRange->All,DisplayFunction->Identity,
Frame->True,FrameLabel->{"Frequency, hz","Magnitude, Laser/Accel",
FontForm["Magnitude Residuals for the 4th Order Fit",
{"Times-BoldItalic",14}]," " },AxesOrigin->{0,0}];
Display[Lfix[[4]],GraphicsArray[{{P1,P3},{P2,P4}}]]
```

(*Continues as above adding a degree to the polynomial*)

```
REIMM=Table[{reim[[i,1]]/1000,N[I*2*Pi*reim[[i,1]]*reim[[i,2]]*
(1/7.620)/(386.4/.1005)]},{i,20,401}];
```

(*Creates a plot of the variance of the residuals as a function of polynomial order*)

```
Do[
FIT[w_]=Fit[REIMM,Table[w^i,{i,0,n}],w]/.w->w/1000;
FITData=Table[FIT[w],{w,38,800,2}];
RESID=Table[FITData[[i]]-REIM[[i,2]],{i,1,382}];
SSQE[n]=(Sum[RESID[[i]]^2,{i,1,382}])^.5;
```

```
VR[n]=Variance[RESID];,{n,0,20}];
VRorder=Table[{i,Abs[VR[i]]},{i,0,20}];
SSEorder=Table[{i,Abs[SSQE[i]]},{i,0,20}];
<<Graphics`Graphics`
<<ORD;
ORDER[1]=LogListPlot[VRorder,PlotRange->All,PlotJoined->True,
Frame->True,
FrameLabel->{"Order","Log Magnitude Variance",
FontForm["Order of Fit Determination",
{"Times-Bold",14}]," "},GridLines->{{2,4,6,8,10,12,14,16,18,20},Automatic},
FrameTicks->{{2,4,6,8,10,12,14,16,18,20},Automatic},
RotateLabel->True,DefaultFont->{"Times-Bold",10},
DisplayFunction->Identity]
Do[Display[Ord[[j]],ORDER[j]],{j,1,2}]
```

ibicrun: A Mathematica program used to create an IBIC script file "lasetest".

```
(*Begin Program ibicrun*)
(*Don't forget to enter the number of rows and columns. c= # columns and r = # rows.*)
c=4
r=20
(*reads in the angle information from the scanarea file and converts it back to voltages*)
reg = ReadList["scanarea",{Word,Number,Word,Word,Word,
Number,Word,Number,Number,Number,Number,Number,Number,
Word,Number,Number,Number,Number,Number,Number,Word,
Number,Number,Number,Number,Number,Number,Word,
Number,Number,Number,Number,Number,Number}];
regist = Table[{{
(reg[[1,13]]+.0212)/-2.4998,
(reg[[1,12]]+.0115)/-2.3988},{
(reg[[1,20]]+.0212)/-2.4998,
(reg[[1,19]]+.0115)/-2.3988},{
(reg[[1,27]]+.0212)/-2.4998,
(reg[[1,26]]+.115)/-2.3988},{
(reg[[1,34]]+.0212)/-2.4998,
(reg[[1,33]]+.0115)/-2.3988}}]
(*Reads the voltages coordinates of the four corners of the scan area tabled above in regist.*)
x1=regist[[1,1]];y1=regist[[1,2]];
x2=regist[[2,1]];y2=regist[[2,2]];
x3=regist[[3,1]];y3=regist[[3,2]];
x4=regist[[4,1]];y4=regist[[4,2]];
(*Calculates the vertical voltage increments for the scan using the top and bottom points*)
dy=(y2-y1)/(r-1);
(*Determines the equation of the line of each vertical edge as a function vertical position.*)
xside1[y_]:=(x2-x1)/(y2-y1)*(y-y1)+x1
xside2[y_]:=(x3-x4)/(y3-y4)*(y-y4)+x4
(*Determines the horizontal increments using the equations of the two edges.*)
dx[y_]:=(xside2[y]-xside1[y])/(c-1)
DX=Table[N[dx[y1+dy*i]],{i,0,r}];
(*Tables the voltage coordinates as v[i,j]*)
j=1;i=0;
Do[Do[v[i,j]=Table[{N[(xside1[y1+(j-1)*dy]+DX[[(j)]]*
(i-1))],
N[(y1+dy*(j-1))]}],{j,1,r}],{i,1,(c)}];
g=Table[v[i,j],{j,1,r},{i,1,(c)}];MatrixForm[g]
(*Creates the appropriate ConvertScans formatted file with the voltage positions*)
data = OpenAppend["scanvoltages", PageWidth->Infinity,
FormatType->TextForm];
Write[data,"SCANLABEL  0  MONTY'S FRF DATA"];
Write[data,"SCANDATE  0  Wednesday OCTOBER 26, 1995"];
Write[data,"SOFTWARE  0  STRUCTURAL IMAGING 1.0"];
Write[data,"LASERRANGE  0  LOW"];
Write[data,"DSP_RIO  0  LSQUARE  Hz 100.000000  64 1 0.0"];
Write[data,"SCANRECT  0  20 4  1.0"];
```

```
Write[data,"SIGNAL  0 0 FORCE"];
Write[data,"SIG_CAL  0 0 lbs  1.00000E-1  0.0"];
Write[data,"SIGNAL  0 1 VELOCITY"];
Write[data,"SIG_CAL  0 1 mps  2.5119E-1  0.0"];
Write[data,"SIGNAL  0 2 ANGLE"];
Write[data,"SIG_CAL  0 2 DEG  -2.4998  -0.0212"];
Write[data,"SIGNAL  0 3 ANGLE"];
Write[data,"SIG_CAL  0 3 DEG  -2.3988  -0.0115"];
Close[data];
k=0;
Do[k=k+1;
data = OpenAppend["scanvoltages", PageWidth->Infinity,
FormatType->TextForm];
Write[data,"SCA_PAIR  0  ",k,"  ",
g[[i,j,2]],"  ",g[[i,j,1]]];
Write[data,"SIGI_RIOS  0  ",k,"  0  1  0 0  0"];
Write[data,"SIGI_RIOS  0  ",k,"  1  1  0 0  0"];
Write[data,"SIGI_STATS  0  ",k,"  1  0  1 0"];
Close[data];,{i,1,20},{j,1,4}]
g=Flatten[Table[Part[Part[v[i,j]]1,1],{j,1,r},{i,1,c}]];!
Table[y[j]=Part[Part[v[1,j]]1,2],{j,1,r}];
Table[x[i]=Part[g,i],{i,1,c*r}];
```

(*Prepares the names of the data files.*)

```
Pwr={"p1.dat","p2.dat","p3.dat","p4.dat","p5.dat",
"p6.dat","p7.dat","p8.dat","p9.dat","p10.dat",
"p11.dat","p12.dat","p13.dat","p14.dat","p15.dat",
"p16.dat","p17.dat","p18.dat","p19.dat","p20.dat",
"p21.dat","p22.dat","p23.dat","p24.dat","p25.dat",
"p26.dat","p27.dat","p28.dat","p29.dat","p30.dat",
"p31.dat","p32.dat","p33.dat","p34.dat","p35.dat",
"p36.dat","p37.dat","p38.dat","p39.dat","p40.dat",
"p41.dat","p42.dat","p43.dat","p44.dat","p45.dat"
"p46.dat","p47.dat","p48.dat","p49.dat","p50.dat",
"p51.dat","p52.dat","p53.dat","p54.dat","p55.dat",
"p56.dat","p57.dat","p58.dat","p59.dat","p60.dat",
"p61.dat","p62.dat","p63.dat","p64.dat","p65.dat",
"p66.dat","p67.dat","p68.dat","p69.dat","p70.dat",
"p71.dat","p72.dat","p73.dat","p74.dat","p75.dat",
"p76.dat","p77.dat","p78.dat","p79.dat","p80.dat",
"p81.dat","p82.dat","p83.dat","p84.dat","p85.dat",
"p86.dat","p87.dat","p88.dat","p89.dat","p90.dat",
"p91.dat","p92.dat","p93.dat","p94.dat","p95.dat",
"p96.dat","p97.dat","p98.dat","p99.dat","p100.dat"};
freq={"x1.dat","x2.dat","x3.dat","x4.dat","x5.dat",
"x6.dat","x7.dat","x8.dat","x9.dat","x10.dat",
"x11.dat","x12.dat","x13.dat","x14.dat","x15.dat",
"x16.dat","x17.dat","x18.dat","x19.dat","x20.dat",
"x21.dat","x22.dat","x23.dat","x24.dat","x25.dat",
```

```
"x26.dat","x27.dat","x28.dat","x29.dat","x30.dat",
"x31.dat","x32.dat","x33.dat","x34.dat","x35.dat",
"x36.dat","x37.dat","x38.dat","x39.dat","x40.dat",
"x41.dat","x42.dat","x43.dat","x44.dat","x45.dat",
"x46.dat","x47.dat","x48.dat","x49.dat","x50.dat",
"x51.dat","x52.dat","x53.dat","x54.dat","x55.dat",
"x56.dat","x57.dat","x58.dat","x59.dat","x60.dat",
"x61.dat","x62.dat","x63.dat","x64.dat","x65.dat",
"x66.dat","x67.dat","x68.dat","x69.dat","x70.dat",
"x71.dat","x72.dat","x73.dat","x74.dat","x75.dat",
"x76.dat","x77.dat","x78.dat","x79.dat","x80.dat",
"x81.dat","x82.dat","x83.dat","x84.dat","x85.dat",
"x86.dat","x87.dat","x88.dat","x89.dat","x90.dat",
"x91.dat","x92.dat","x93.dat","x94.dat","x95.dat",
"x96.dat","x97.dat","x98.dat","x99.dat","x100.dat"};
coh={"c1.dat","c2.dat","c3.dat","c4.dat","c5.dat",
"c6.dat","c7.dat","c8.dat","c9.dat","c10.dat",
"c11.dat","c12.dat","c13.dat","c14.dat","c15.dat",
"c16.dat","c17.dat","c18.dat","c19.dat","c20.dat",
"c21.dat","c22.dat","c23.dat","c24.dat","c25.dat",
"c26.dat","c27.dat","c28.dat","c29.dat","c30.dat",
"c31.dat","c32.dat","c33.dat","c34.dat","c35.dat",
"c36.dat","c37.dat","c38.dat","c39.dat","c40.dat",
"c41.dat","c42.dat","c43.dat","c44.dat","c45.dat",
"c46.dat","c47.dat","c48.dat","c49.dat","c50.dat",
"c51.dat","c52.dat","c53.dat","c54.dat","c55.dat",
"c56.dat","c57.dat","c58.dat","c59.dat","c60.dat",
"c61.dat","c62.dat","c63.dat","c64.dat","c65.dat",
"c66.dat","c67.dat","c68.dat","c69.dat","c70.dat",
"c71.dat","c72.dat","c73.dat","c74.dat","c75.dat",
"c76.dat","c77.dat","c78.dat","c79.dat","c80.dat",
"c81.dat","c82.dat","c83.dat","c84.dat","c85.dat",
"c86.dat","c87.dat","c88.dat","c89.dat","c90.dat",
"c91.dat","c92.dat","c93.dat","c94.dat","c95.dat",
"c96.dat","c97.dat","c98.dat","c99.dat","c100.dat"};
```

(*Open and create the file lasertest.*)(*SEE CHAPTER 5.6 for details on these ibic commands*)

```
data = OpenAppend["lasertest", PageWidth->Infinity,
FormatType->TextForm];
Write[data,"ibfind dev1"];
Write[data,"ibpad 11"];
Write[data,"ibclr"];
Write[data,"ibwrtf \"frs\""];
Write[data,"ibfind dev2"];
Write[data,"ibpad 9"];
Write[data,"ibclr"];
Close[data];
Clear[k];
k=0;
```

```
Do[k=k+1;
data = OpenAppend["lasertest", PageWidth->Infinity,
FormatType->TextForm];
Write[data,"set dev2"];
Write[data,"ibwrt \"c0 p1 a0 r2 v",x[i],"x\""];
Write[data,"ibwrt \"c0 p3 a0 r2 v",y[j],"x\""];
Write[data,"set dev1"];
Write[data,"ibwait rqs timo"];
Write[data,"ibrsp"];
Write[data,"ibwrt \"VOLT1:RANG:AUTO ON;*WAI\""];
Write[data,"ibwrt \"VOLT2:RANG:AUTO ON;*WAI\""];
Write[data,"ibwait rqs timo"];
Write[data,"ibrsp"];
Write[data,"ibwrt \"ABOR;:INIT;*WAI\""];
Write[data,"ibtmo 14"];
Write[data,"ibwait rqs timo"];
Write[data,"ibrsp"];
Write[data,"ibwait rqs timo"];
Write[data,"ibrsp"];
Write[data,"ibtmo 13"];
Write[data,"ibwrt \"TRAC:DATA D1, TRAC1\""];
Write[data,"ibwrt \"TRAC:DATA D2, TRAC2\""];
Write[data,"ibwrt \"TRAC? D1\""];
Write[data,"ibrdf \"",Pwr[[k]],"\""];
Write[data,"ibwrt \"TRAC? D2\""];
Write[data,"ibrdf \"",coh[[k]],"\""];
Write[data,"ibwrt \"TRAC:X? TRAC1\""];
Write[data,"ibrdf \"",freq[[k]],"\""];
Close[data];,{j,1,r},{i,1,c}]
End Program lasertest
```

ibicprocess: - Post processes data from lasertest.

Begin Program ibicprocess

Data Processing Section I.

```
SetDirectory["/disk2/users/monty/beamnov4"];
(*Sets up the names of the data files into an array*)
Pwr={"p1.dat","p2.dat","p3.dat","p4.dat","p5.dat",
"p6.dat","p7.dat","p8.dat","p9.dat","p10.dat",
"p11.dat","p12.dat","p13.dat","p14.dat","p15.dat",
"p16.dat","p17.dat","p18.dat","p19.dat","p20.dat",
"p21.dat","p22.dat","p23.dat","p24.dat","p25.dat",
"p26.dat","p27.dat","p28.dat","p29.dat","p30.dat",
"p31.dat","p32.dat","p33.dat","p34.dat","p35.dat",
"p36.dat","p37.dat","p38.dat","p39.dat","p40.dat",
"p41.dat","p42.dat","p43.dat","p44.dat","p45.dat",
"p46.dat","p47.dat","p48.dat","p49.dat","p50.dat",
"p51.dat","p52.dat","p53.dat","p54.dat","p55.dat",
"p56.dat","p57.dat","p58.dat","p59.dat","p60.dat",
"p61.dat","p62.dat","p63.dat","p64.dat","p65.dat",
"p66.dat","p67.dat","p68.dat","p69.dat","p70.dat",
"p71.dat","p72.dat","p73.dat","p74.dat","p75.dat",
"p76.dat","p77.dat","p78.dat","p79.dat","p80.dat",
"p81.dat","p82.dat","p83.dat","p84.dat","p85.dat",
"p86.dat","p87.dat","p88.dat","p89.dat","p90.dat",
"p91.dat","p92.dat","p93.dat","p94.dat","p95.dat",
"p96.dat","p97.dat","p98.dat","p99.dat","p100.dat"};
freq={"x1.dat","x2.dat","x3.dat","x4.dat","x5.dat",
"x6.dat","x7.dat","x8.dat","x9.dat","x10.dat",
"x11.dat","x12.dat","x13.dat","x14.dat","x15.dat",
"x16.dat","x17.dat","x18.dat","x19.dat","x20.dat",
"x21.dat","x22.dat","x23.dat","x24.dat","x25.dat",
"x26.dat","x27.dat","x28.dat","x29.dat","x30.dat",
"x31.dat","x32.dat","x33.dat","x34.dat","x35.dat",
"x36.dat","x37.dat","x38.dat","x39.dat","x40.dat",
"x41.dat","x42.dat","x43.dat","x44.dat","x45.dat",
"x46.dat","x47.dat","x48.dat","x49.dat","x50.dat",
"x51.dat","x52.dat","x53.dat","x54.dat","x55.dat",
"x56.dat","x57.dat","x58.dat","x59.dat","x60.dat",
"x61.dat","x62.dat","x63.dat","x64.dat","x65.dat",
"x66.dat","x67.dat","x68.dat","x69.dat","x70.dat",
"x71.dat","x72.dat","x73.dat","x74.dat","x75.dat",
"x76.dat","x77.dat","x78.dat","x79.dat","x80.dat",
"x81.dat","x82.dat","x83.dat","x84.dat","x85.dat",
"x86.dat","x87.dat","x88.dat","x89.dat","x90.dat",
"x91.dat","x92.dat","x93.dat","x94.dat","x95.dat",
"x96.dat","x97.dat","x98.dat","x99.dat","x100.dat"};
coh={"c1.dat","c2.dat","c3.dat","c4.dat","c5.dat",
"c6.dat","c7.dat","c8.dat","c9.dat","c10.dat",
"c11.dat","c12.dat","c13.dat","c14.dat","c15.dat",
"c16.dat","c17.dat","c18.dat","c19.dat","c20.dat",
```

```
"c21.dat","c22.dat","c23.dat","c24.dat","c25.dat",
"c26.dat","c27.dat","c28.dat","c29.dat","c30.dat",
"c31.dat","c32.dat","c33.dat","c34.dat","c35.dat",
"c36.dat","c37.dat","c38.dat","c39.dat","c40.dat",
"c41.dat","c42.dat","c43.dat","c44.dat","c45.dat",
"c46.dat","c47.dat","c48.dat","c49.dat","c50.dat",
"c51.dat","c52.dat","c53.dat","c54.dat","c55.dat",
"c56.dat","c57.dat","c58.dat","c59.dat","c60.dat",
"c61.dat","c62.dat","c63.dat","c64.dat","c65.dat",
"c66.dat","c67.dat","c68.dat","c69.dat","c70.dat",
"c71.dat","c72.dat","c73.dat","c74.dat","c75.dat",
"c76.dat","c77.dat","c78.dat","c79.dat","c80.dat",
"c81.dat","c82.dat","c83.dat","c84.dat","c85.dat",
"c86.dat","c87.dat","c88.dat","c89.dat","c90.dat",
"c91.dat","c92.dat","c93.dat","c94.dat","c95.dat",
"c96.dat","c97.dat","c98.dat","c99.dat","c100.dat"};
(*sets the number of columns and rows in the scan*)
c=4;
r=20;
(*Read in all the data files*)
Do[Coh[k]=ReadList[coh[[k]], Number,401,
RecordSeparators->{","}];
Freq[k]=ReadList[freq[[k]], Number,401,
RecordSeparators->{","}];
frs=ReadList[Pwr[[k]],{Number,Character},802];
frs=Map[First,frs];
frs=Partition[frs,2];
(*Creates three columns with frequency, FRF, an coherence*)
FRF[k]=Table[{Part[Freq[k],i],Part[frs,i],Part[Coh[k],i]},
{i,1,401}];,{k,1,82}];
(*Tables the SLDV calibration correction at each specifc spectral line at which data was collected.
The SLDV frequency response equation was determined using the Mathematica notebook
"correction"*)
Vectore=Table[1.02755306422872-0.02807972496539766*I+
(0.00007059611959679348 - 0.0007700043973625048*I)*f+
(-(9.65496925789271*10^-7) + 3.296781290116684*10^-8*I)*f^2+
(5.077373156856555*10^-10+2.833493029105364*10^-10*I)*f^3,
{f,0,800,2}];
(*Reads in the angle file created by ConvertScans*)
ang = ReadList["/disk2/users/monty/beamnov4/beamnov4.meas",
{Word,Number,
Number,Number,Number,Number,Number,Number,Word,Number,Number,
Word,Number,Number,Number,Number,Number,Number,Number,Number,
Number,Number,Number}];
(*The file created by ConvertScans has more information in it than just the angles this code
seperates the required angles into a variable cosangles*)
cosangles = Table[ang[[i,23]],{i,1,80}];
```

```
(*Tables the phase angle errors using the variable "Vectore" calculated from the SLDV FRF correction*)
AngleError=Table[N[Arg[Vectore]]];
(*Tables the magnitude errors using the variable "Vectore" calculated from the SLDV FRF correction*)

MagnitudeError=Table[N[Abs[Vectore]]];

(*Corrects for the scanning angle determined by convertscans and applies the .72688 calibration factor which is the ratio of the laser's calibration factor to the force gage calibration factor to convert the FRFs to mm/s over newtons.*)
Do[Vectorm[j]=Table[
(FRF[j][[i,2,1]]+I*FRF[j][[i,2,2]])*cosangles[[j]]*(.72688),
{i,1,401}];
(*Tables the phase angles that were measured*)
Anglemeas[j]=Table[N[Arg[Vectorm[j]]]];
(*Tables the magnitudes that were measured*)
Magnitudemeas[j]=Table[N[Abs[Vectorm[j]]]];
(*Determines the true magnitude and true phase angle using the correction factor determined using the frequency response of the SLDV*)
TrueMagnitude[j]=Magnitudemeas[j]/MagnitudeError;
TrueAngle[j]=Anglemeas[j]-AngleError;
(*Forms a vectore using the corrected (TRUE) angles above*)
z[j]=TrueMagnitude[j]*Exp[I*TrueAngle[j]];
(*Tables the corrected FRF magnitudes from the Vector, z, above*)
fmagnitude[j]=Table[{FRF[j][[i,1]],Abs[z[j][[i]]]},
{i,1,401}];
(*Tables the coherences*)
Coher[j]=Table[{FRF[j][[i,1]],FRF[j][[i,3]]},
{i,1,401}];
(*Tables the corrected FRF phase angles from the Vector, z, above*)
Phas[j]=Table[{FRF[j][[i,1]],Arg[z[j][[i]]]*180/(Pi)},
{i,1,401}],
{j,1,c*r}];
(*iomega is an array contain 2 PI I frequency*)
iomega=Flatten[Table[{{100000*Pi*I},
{Table[2*Pi*I*i,{i,2,800,2}]}}]];
(*FRF 81 and 82 for this test were driving point FRFs collected using a Force gage and an accelerometer. The 23137.6225 is the ratio of the calibration factors to convert the FRS to mm/s^2 over Newtons. Dividing through iomega converts the ratio to mm/s over Newton or velocity over Force (mobility) This section could probably be eliminated unless this is how the Driving point measurement will be taken. In this thesis one of the laser FRFs were used as the Driving point measurement*)
Do[z[j]=Table[(23137.6225/iomega[[i]])*
(FRF[j][[i,2,1]]-I*FRF[j][[i,2,2]]),{i,1,401}];
fmagnitude[j]=Table[{FRF[j][[i,1]],
Abs[z[j][[i]]]},
{i,1,401}];
Coher[j]=Table[{FRF[j][[i,1]],FRF[j][[i,3]]},
```

```
{i,1,401}];
Phas[j]=Table[{FRF[j][[i,1]],N[Arg[z[j][[i]]]*
180/(Pi)]},{i,1,401}],{j,81,82}];
```
(*RIC is a sub program that creates four ASCII files FrfI, FrfR, Frfcohe, and Freq that can then be manipulate in Matlab and prepared for MODHAN*)
```
<<RIC
```
Data Processing Section II. Creation of the postscript files of the plots.
(*Opens the graphics package*)
```
<<Graphics`Graphics`
```
(*Call in each of the files below each of which have the titles for the plots or the name of the files for the plots to be saved*)
```
<<Plots;
<<Label;
<<LabelC;
<<LabelP;
<<CPlots;
<<CurveF;
<<CurveFR;
<<Curvep;
<<CurvepR;
<<PlotsEPS;
```
(*The Groups of commands that follow create the magnitude, phase, and coherence plots*)
```
Do[frfunc[j]=LogListPlot[fmagnitude[j],PlotRange->All,
PlotJoined->True,
Frame->True,
FrameLabel->{"Frequency, Hz","Log Magnitude, (mm/s)/N",
FontForm[Lable[[j]],
{"Times-Bold",12}],"  "}
,GridLines->{{100,200,300,400,500,600,700},Automatic},
FrameTicks->{{100,200,300,400,500,600,700,800},Automatic},
RotateLabel->True,DefaultFont->{"Times-Bold",10},
DisplayFunction->Identity],{j,1,82}]

Do[Cohfunc[j]=ListPlot[Coher[j],PlotStyle->RGBColor[1,0,0],
PlotRange->All,PlotJoined->True,
Frame->True,
FrameLabel->{"Frequency, Hz","  ",FontForm[LableC[[j]],
{"Times-Bold",12}],"  "},
GridLines->{{100,200,300,400,500,600,700},Automatic},
FrameTicks->{{100,200,300,400,500,600,700,800},Automatic},
RotateLabel->True,DefaultFont->{"Times-Bold",10},
DisplayFunction->Identity],{j,1,82}]

Do[Phasfunc[j]=ListPlot[Phas[j],
PlotRange->All,PlotJoined->True,Frame->True,
FrameLabel->{"Frequency, Hz","Angle, Degree",
FontForm[LableP[[j]],
{"Times-Bold",12}],"  "},
GridLines->{{100,200,300,400,500,600,700},Automatic},
```

```
FrameTicks->{{100,200,300,400,500,600,700,800},Automatic},
RotateLabel->True,DefaultFont->{"Times-Bold",10},
DisplayFunction->Identity],{j,1,82}];

(*This group of commands overlays the coherence on top of the FRFs*)
Do[cohfrf[j]=Show[{frfunc[j],Cohfunc[j]},
FrameLabel->{"Frequency, Hz","Log Magnitude, (mm/s)/N",
FontForm["Coherence FRF Overlay",
{"Times-Bold",12}],"Coherence (red)"},
DisplayFunction->Identity],{j,1,82}];

(*Creates postscript files with plot arrays of FRF magnitude, phase, coherence, and coherence/FRF
overlay.*)
Do[Display[PL[[j]],GraphicsArray[{{frfunc[j],Cohfunc[j]},
{Phasfunc[j],cohfrf[j]}}]];
Print[j];,
{j,1,82}];

Data Processing Section III. (*This section post processes the data from MODHAN*)
(*Reads in the pole data which are seperated into real and imaginary values*)
p2i=ReadList["pole2I.txt",Number];
p2r=ReadList["pole2r.txt",Number];
p1i=ReadList["pole1I.txt",Number];
p1r=ReadList["pole1r.txt",Number];
p3i=ReadList["pole3I.txt",Number];
p3r=ReadList["pole3r.txt",Number];
(*Combines the real and imaginary poles in to one tomake the pole tables*)
PL3=Table[.01*p3r[[i+(j*82)]]+p3i[[i+(j*82)]]*I,
{j,0,5},{i,1,82}];
PL2=Table[.01*p2r[[i+(j*82)]]+p2i[[i+(j*82)]]*I,
{j,0,3},{i,1,82}];
PL1=Table[.01*p1r[[i+(j*82)]]+p1i[[i+(j*82)]]*I,
{j,0,9},{i,1,82}];

(*Forms the FRF from the pole tables*)
H[f_,point_]=
Sum[((2*Pi*f*I)*
(PL1[[j]][[point+1]]/((I*2*Pi*f)-(PL1[[j]][[1]])))),
{j,1,10}]+Sum[((2*Pi*f*I)*
(PL2[[j]][[point+1]]/((I*2*Pi*f)-(PL2[[j]][[1]]))))
,{j,1,4}]+Sum[((2*Pi*f*I)*
(PL3[[j]][[point+1]]/((I*2*Pi*f)-(PL3[[j]][[1]]))))
,{j,1,6}];
Do[
(*Forms a table of the magnitude of the FRF*)
Hmagnitude[j]=Table[{i,Abs[N[H[i,j]]]},
{i,0,800,2}];
(*Forms a table of the phase angles of the FRF*)
HPhas[j]=Table[{i,N[Arg[N[H[i,j]]]*180/Pi]},{i,0,800,2}];
```

```
Print[j];,
{j,1,81}];
(*Creates FRF magnitude plots*)
Do[Curve[j]=LogListPlot[Hmagnitude[j],
PlotRange->All,PlotStyle->RGBColor[0,0,1],
PlotJoined->True,Frame->True,
FrameLabel->{"Frequency, Hz","Log Magnitude, (mm/s)/N",
FontForm[CurveF[[j]],
{"Times-Bold",12}]," "},
GridLines->{{100,200,300,400,500,600,700},Automatic},
FrameTicks->{{100,200,300,400,500,600,700,800},Automatic},
RotateLabel->True,DefaultFont->{"Times-Bold",10},
DisplayFunction->Identity],{j,1,81}]

(*Creates FRF phase plots*)
Do[CurveP[j]=ListPlot[HPhas[j],
PlotRange->All,PlotRange->All,PlotStyle->RGBColor[0,0,1],
Frame->True,PlotJoined->True,
FrameLabel->{"Frequency, Hz","Angle, Degree",
FontForm[Curvep[[j]],
{"Times-Bold",12}]," "},
GridLines->{{100,200,300,400,500,600,700},Automatic},
FrameTicks->{{100,200,300,400,500,600,700,800},Automatic},
RotateLabel->True,DefaultFont->{"Times-Bold",10},
DisplayFunction->Identity],{j,1,81}]

(*Creates overlay Plots of the curve fit FRF magnitude and collected FRF magnitude*)
Do[Comp[j]=Show[{frfunc[j],Curve[j]},
FrameLabel->{"Frequency, Hz","Log Magnitude, (mm/s)/N",
FontForm["Curve Fit Comparison",
{"Times-Bold",12}]," "},
DisplayFunction->Identity],{j,1,81}];


(*Creates overlay plots of the curve fit FRF phase angles and collected FRF phase angles*)
Do[Compp[j]=Show[{Phasfunc[j],CurveP[j]},
FrameLabel->{"Frequency, Hz","Angle, Degree",
FontForm["Curve Fit  Phase Comparison",
{"Times-Bold",12}]," "},
DisplayFunction->Identity],{j,1,81}];

(*Calculates the residuals of the phase and magnitude*)
Do[
residM[j]=Table[{Hmagnitude[j][[i,1]],
(Hmagnitude[j][[i,2]]-fmagnitude[j][[i,2]])},
{i,1,401}];
residP[j]=Table[{HPhas[j][[i,1]],
(HPhas[j][[i,2]]-Phas[j][[i,2]])},{i,1,401}];,
{j,1,81}]
```

```
(*Creates plots of the phase residuals*)
Do[CurvePR[j]=ListPlot[residP[j],
PlotRange->All,PlotRange->All,PlotStyle->RGBColor[0,1,0],
Frame->True,
FrameLabel->{"Frequency, Hz","Angle, Degree",
FontForm[CurvepR[[j]],
{"Times-Bold",12}]," "},
GridLines->{{100,200,300,400,500,600,700},Automatic},
FrameTicks->{{100,200,300,400,500,600,700,800},Automatic},
RotateLabel->True,DefaultFont->{"Times-Bold",10},
DisplayFunction->Identity],{j,1,81}]

(*Creates plots of the magnitude residuals*)
Do[CurveR[j]=ListPlot[residM[j],
PlotRange->All,PlotStyle->RGBColor[0,1,0],
Frame->True,
FrameLabel->{"Frequency, Hz","Magnitude, (mm/s)/N",
FontForm[CurveFR[[j]],
{"Times-Bold",12}]," "},
GridLines->{{100,200,300,400,500,600,700},Automatic},
FrameTicks->{{100,200,300,400,500,600,700,800},Automatic},
RotateLabel->True,DefaultFont->{"Times-Bold",10},
DisplayFunction->Identity],{j,1,81}]

(*Creates postscript files of plots containing an array of all the plots in this data section*)
Do[Display[CPL[[j]],GraphicsArray[{{Curve[j],CurveP[j]},
{frfunc[j],Phasfunc[j]},{Comp[j],Compp[j]},
{CurveR[j],CurvePR[j]}}]];
Print[j];,
{j,1,81}];
End Program ibicprocess
```

Appendix B Users Manual

The following manual is not intended to be an all inclusive step by step manual, but the basic procedures required to setup and use the data acquisition software.

Hardware Setup

- The GPIB should already be connected and mounted to the SGI, redbaron.
- Connect the HP35665A frequency analyzer and the DAC to the GPIB controller via GPIB cables.
- The IBIC script software, "lasertest" requires that the x deflection mirror be connected to channel one of the DAC and the y deflection mirror be connected to channel three of the DAC.
- In order to form the FRF(mobility) channel one of the frequency analyzer must be connected to the force transducer and channel two of the frequency analyzer connected to the laser velocity output.
- The HP35665A frequency provides the excitation source. The source is connected to an amplifier then to the shaker.

Note: The connections to the shaker and force transducer should be made after the structure is setup.

Registration

- Setup
  1. Lay out the registration points on the structure and record the coordinates of these points relative to a chosen origin. The more registration points the better, but the time associated with each registration point can be up to ten minutes. *Note: It is important that this be done before the structure is hung. It is also important to measure the location of the registration points as accurately as possible so that the registration will be accurate.*
  2. Hang the structure and connect the shaker to the structure as well as all other connections as instructed in Hardware setup.
- **ESDM**

  Note: It is important that the next step in the registration process be the last thing done before data is acquired. The purpose of the registration is to locate the structure in the laser coordinate system. If the structure or laser is moved after the registration process has been completed then the points have moved relative to the laser and the registration is poor.

  If the structure is completely setup, use ESDM to register the structure.

1. Start ESDM by typing ESDM at the UNIX prompt.
2. Move the laser to the first registration point using the ESDM button bars. Get as close to the previously marked points as possible. The closer the laser beam is to the points the better the registration.
3. Enter the coordinates of the registration point.
4. Click on register point.
5. Continue 2-4 until all points have been registered.
6. Click on Done and save the file with a name that can be easily identified later. Example: beam.reg An example of a registration file is shown in Fig. 5-7.

Defining the Scan Area

- Start ESDM.
- Use ESDM to move the laser to the first corner of the scan area and register this point. The coordinates can be left as zero since this area of the file is not used for defining the scan area. The locations and order of the points used to define the area are crucial. The first two points define the first edge and the second two points define the second edge. The "ibicrun" requires that the points are registered in the order shown in the following figure. The IBIC program uses the "scanarea" file to divide the scan into a rectangular grid.

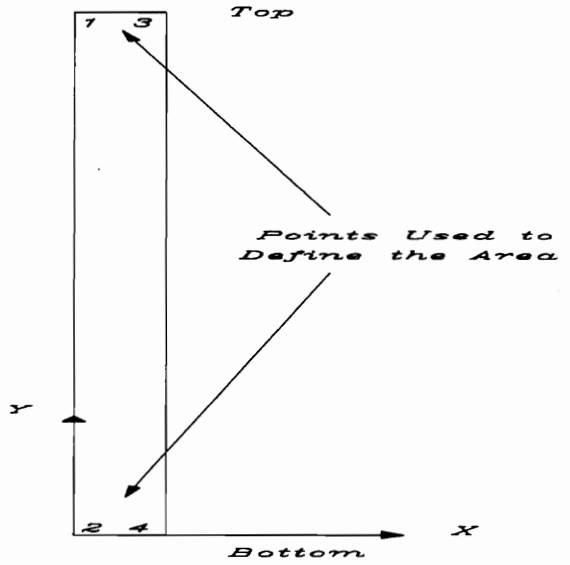

- Using ESDM to manipulate the laser beam move to the remain three corners of the beam and register each of them.

- Save the file as "scanarea". The IBIC script file "lasertest" requires this name. The "scanarea" file looks exactly like the registration file in Fig. 5-7 except it only has four registered points and the spatial coordinates have been left as zeros.

Note: Points one and two define the position of the top and bottom of the scan area edges, respectively. The sides of the scan area are defined using all four points.. This means that the sides of the scan area don't necessarily have to be parallel. However, in extreme cases since points three and four are not used to define the top and bottom edges of the scan area, it is possible that the laser beam will go off the structure if the horizontal line of the laser and structure are not equal. This problem can be solved if points three and four are incorporated into the definition of the scan area edges by solving for the slopes of the upper and lower lines. This incorporation was already done for the vertical edges.

Determining the Proper Excitation Power Level

- Manually turn on the excitation source.
- Choose the source type.
- With the amplifier on but the speaker systems turned off adjust the excitation source until the limiting power level of the shaker on the amplifier is reached. Write down the excitation voltage level of the source. This voltage level should not be exceeded or the shaker will blow.
- With laser and the excitation source on, use ESDM to control the laser and scan the structure while adjusting the voltage level of the excitation source. Be sure not exceed the previously recorded input power level of the shaker. Adjust the excitation source so that the chosen dynamic range of the laser is optimized. This means that at areas of peak response the level meter on the SLDV should reach at least 90%. However, do not set it too high because when the structure is being scanned areas of higher response might be found causing the range to be exceeded.
- Write down the voltage level of the excitation source determined from the above procedure. Make sure the voltage type is known (V_{rms},V_{peak}, etc.). The excitation voltage level will be entered into the HP35665A frequency analyzer setup file "frs".

Editing the Frequency Analyzer Setup File "frs"

- Chapter 3.4 discusses the frequency analyzer setup file. However, the changes that are probably of most interest include the source level, source type, trigger type, frequency span and the number of averages.

- Edit the frequency analyzer setup file "frs" and enter the appropriate settings including the source level and type that was noted in "Determining the proper excitation power level". For additional information on The HP35665A commands see the HP reference manuals in the lab. Note: A copy of the file "frs" is located on snoopy /disk2/users/monty/Program.

Creating the IBIC script file "lasertest" using the Mathematica notebook "ibicrun". (All files are located on snoopy /disk2/users/monty/Program)

- Create a working data directory on the SGI, redbaron, for saving the data files.
- Create a working directory on the HP server snoopy and change the default directory to the directory that was just made. Copy "ibicrun" and "scanarea" into this directory
- Open the "ibicrun" Mathematica notebook on the HP server snoopy from the default directory. Enter the number of rows and columns of the scanning grid. Make sure the default directory includes the file scanarea. Run the notebook. The notebook creates the files "scanvoltages" and "lasertest" to be used by ConvertScans and IBIC, respectively.
- Copy the files "frs", "lasertest", and "scanvoltages" into the working data directory on the SGI, redbaron.

Note: Just in case "ibicrun" is run more than once, the files "lasertest" and "scanvoltages" must be deleted from the working directories. Otherwise, the program "ibicrun" appends the new commands on to the end of the old commands.

Starting the Data Collection

- Change the directory to the working data directory on the SGI, redbaron,. Start the IBIC program by typing ibic at the UNIX prompt.
- Start the ibic script file "lasertest" by typing "$ lasertest". Note if you get an error at this point it might be caused by one of the following:
    1. The files "lasertest" and "frs" are not present in the current directory.
    2. Careful with the syntax "$ lasertest" it requires a space after the $.
    3. The GPIB hardware and program are not setup correctly.
- At this point the system is running and it will automatically setup the analyzer and download the data to the current directory.

Data Processing

- Copy all the data from the working directory on the SGI to a working directory on snoopy. This has to be done because Mathematica is not installed on Redbaron.
- Run ConvertScans. Copy the file containing the angle information to the working directory.
- Copy all the files from snoopy /disk2/users/monty/Program to the working directory on snoopy.
- Open the Mathematica notebook "ibicprocess". Change the line ang=Readlist["/disk2/users/monty/beamnov4/beamnov4.meas etc to indicate the path name of the file containing the angle information produced by ConvertScans.
- Run Data processing sections I and II. The result of these two sections gives a set of files all corrected for the frequency response of the laser and for the scan angles. It creates a postscript files for each spatial location with the corresponding FRFs and coherences. The plots will be saved as Plot1, Plot2, Plot3, etc. corresponding to each spatial location in the order the data was collected. The processing also creates four ASCII files, Freq, FrfI, FrfR, and Frfcohe for importing into the curve fitting routine MODHAN. The "Freq" file is a column of numbers representing the spectral lines where data was taken. The files FrfR and FrfI represent the real and imaginary portions of the FRFs, respectively. The file "Frfcohe" provides the coherences.
- The data processing section three is only used after data is returned from MODHAN. This section creates plots to compare the experimental FRFs and curve fit FRFs calculated using MODHAN.

Vita

Monty Moshier was born March 30, 1966 in Santa Maria, California. After living in Oregon from 1972-1976, He and his family returned to California to settle in Bakersfield, where he graduated from West High School in June of 1984. In 1988, after representing the Church of Jesus Christ of Latter-day Saints as a missionary in Brazil, he married Kelly Hart. Shortly after his marriage, He started college at California State University Fresno. In 1990 he transferred to California Polytechnic State University in San Luis Obispo where he graduated Summa Cum Laude in Mechanical Engineering June of 1994. In August of 1994 he began a Masters degree in Mechanical Engineering at Virginia Tech. He is now pursuing a Ph.D. in Mechanical Engineering at Purdue University.